University of Trento
University of Padova

Paolo Zampieri

SEMPLIFIED SEISMIC VULNERABILITY ASSESSMENT OF MASONRY ARCH BRIDGES

Tutor: Prof. Claudio Modena
Co-Tutor: Dr. Francesca da Porto

2014

UNIVERSITY OF TRENTO
Civil and Mechanical Structural Systems Engineering
XXVI Cycle

Final Examination 10/04/2014

Board of Examiners
Prof. Maurizio Piazza (Università di Trento)
Prof. Andrea Prota (Università di Napoli Federico II)
Prof. Carmelo Gentile (Polytechnic of Milan)
Prof. Helmut Wenzel (Universität für Bodenkultur Wien)

SUMMARY

This study concerns seismic vulnerability assessment of masonry arch bridges with common typologies in Europe. Bridges are, in most cases, the most vulnerable elements in the transportation network during an earthquake; therefore, their seismic vulnerability assessment is necessary for a proper planning of the emergency phase and to define a priority for retrofit interventions.

Masonry arch bridges were subdivided into homogeneous classes of single span and multi-span structures, according to the result of a statistical analysis made up of a large stock of 757 railway bridges located in high seismic areas.

All the different collapse mechanisms for seismic action were studied for each class of masonry arch bridges with application of limit analysis and the calibration with FEM. In particular, limit analysis methods for the seismic assessment of single and multi spans bridges were developed. A innovative limit analysis approach was proposed for the assessment of the global transverse seismic capacity of multi-span masonry bridges with slender piers.

Envelope curves representing the seismic capacity expressed in terms of limit horizontal acceleration were derived by parametrical analysis by means of simplified limit analysis. These curves can be used for a simplified vulnerability assessment of masonry arch bridges and for a simple calibration of the judgment obtained by BMS through inspection visits to bridges.

In the second part of the study, a new simplified approach for the fast calculation of seismic fragility curves of numerous masonry arch bridge clusters is proposed.

The aim of this thesis is to propose a quickly procedure to estimate the seismic vulnerability of extended roadway and railway bridge networks in emergency conditions and to optimize the retrofit interventions.

DEDICATION

A Laura e a tutta la mia Famiglia

“Chiunque è un genio, ma se tu giudichi un pesce per la sua abilità di salire su un albero vivrà eternamente con la sensazione di essere uno stupido.”

- Albert Einstein -

ACKNOWLEDGMENTS

Ringrazio chi mi ha dato l'opportunità di compiere questo lavoro, chi mi ha seguito e supportato, chi mi ha trasmesso le proprie conoscenze e chi mi è stato vicino. I vostri nomi rimarranno sempre impressi nella mia memoria.

INDEX

1 INTRODUCTION 10
2 MASONRY ARCH BRIDGES 15

2.1 Masonry Arch bridges 15
2.2 Methods of analysis 19
2.2.1 Limit analysis 19
2.2.2 Finite element analysis 22
2.2.3 Discrete element analysis 23
2.2.4 Discontinuous Deformation Analysis 24
2.3 Main structural assessment method of masonry bridges 24
2.3.1 MEXE method 24
2.3.2 “SMART” method 24
2.4 Typical deficiencies in masonry arch bridges 24
2.5 Rehabilitation and retrofit strategies for masonry arch bridges: innovative vs. traditional 26

3 ITALIAN RAILWAY MASONRY BRIDGE STOCK 28

3.1 Introduction 28
3.1.1 Survey of the Italian railway masonry bridge stock 28

4 TRANSVERSE SEISMIC CAPACITY OF MULTISPAN MASONRY BRIDGES 36

4.1 Introduction 36
4.2 Limit analysis for seismic assessment of transverse capacity 38
4.3 Numerical calibration of simplified kinematic approach 45
4.3.1 Numerical analyses 45

4.3.2 Calibration of k-parameter 48
4.3.3 Safety check for shear failure of piers 51
4.4 Parametric analyses of multi-span railway bridges 52
4.4.1 Parametric analyses 52
4.5 Example 57
4.6 Conclusion 59

5 VULNERABILITY ASSESSMENT OF MASONRY BRIDGES CLASSES BY LIMIT ANALYSIS 61

5.1 Introduction 61
5.1.1 Influence of bridge type and geometry on the behaviour 61
5.1.2 Classification of masonry bridge structures 64
5.2 Limit analysis for seismic assessment of masonry arch bridges 66
5.2.1 Single-span bridges in longitudinal direction 67
2.1.1 Single-span bridges in transverse direction 70
5.2.2 Multi-span bridges in longitudinal direction 71
5.2.3 Multi-span bridges in transverse direction 73
5.3 Parametric analyses 73
5.3.1 Single span bridges with squat abutments (SS_sa, 1.1) 76
5.3.2 Single span bridges with high abutments (SS_ha, 1.2) 79
5.3.3 Two-Three span (TS_sl, 2.2) and multi-span (MS_sl, 3.2) bridges with slender piers 81
5.4 Simplified seismic verification procedure 88
5.4.1 Example of Single-Span, high abutments bridge 89
5.4.2 Example of Multi-Span, slender piers bridge 90
5.5 Consideration about seismic vulnerability in the formulation of judgement of structures state of maintenance. 91
5.6 Conclusions 93

6 SEMPLIFIED SEISMIC FRAGILITY CURVES FOR SINGLE-SPAN MASONRY BRIDGES CLASS 95

6.1 Introduction 95
6.2 Non-linear Kinematic analysis of masonry arch bridges 96
6.3 Seismic Performance levels of masonry bridges 100
6.4 Fragility curves construction 101
6.4.1 Reduction of Demand Spectrum 105
6.5 Simplified fragility curves for single-span masonry arch bridges 106
6.6 Conclusions 116

7 CONCLUSION 118

7.1 Future development 119

REFERENCES 121

1 INTRODUCTION

The European railway network is characterised by the presence of thousands of masonry arched structures (about 200000, SB-ICA, 2007), and the majority of them are more than one hundred years old (over 60%, Melbourne, 2007). The condition of Italian railway network is not better than the European one. We have more than 11250 masonry bridges of medium-long span (L>5m, see Fig. 1.1) and if we consider also the secondary structures, i.e. shorter bridges with span length L<5m, the amount of masonry bridges reaches a total of 56370 units. This means that in Italy there is a total length of over 427 km of railway lines on masonry arches (Cocciaglia and Mosca, 1998).

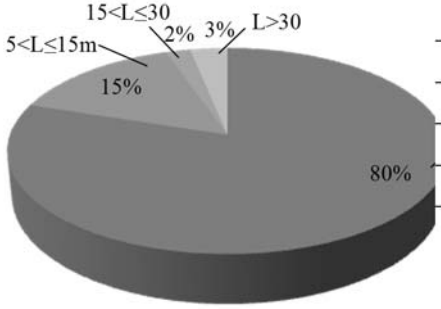

L (m)	No.	No. (%)	Ltot (km)
≤5	45.118	80.0	139.12
5<L≤15	8308	14.7	68.58
15<L≤30	1164	2.1	22.08
L>30	1783	3.2	197.57
	56373	100	427.35

Fig. 1.1 Masonry arch bridges of Italian railway network (Cocciaglia and Mosca, 1998)

Many of these structures are located on major railway lines in medium-high seismic areas. It is evident that suitable methods are required for preliminary seismic vulnerability assessment of masonry bridges, to understand when more detailed analyses are necessary and to know the priority of interventions.

A preliminary evaluation has to be based only on data gathered by bridge inventories and safety analyses have to be planned on a large-scale for thousands of structures, so the use of quick simplified procedures is predominant.

Most of currently available Bridge Management Systems (BMS) are based on information obtained by visual inspections (BRIME 2001), including Pontis (Thompson et al., 1998), BRIDGIT (Hawk and Small, 1998), the Danish DANBRO (Gharib, 2002) and others, as well as the inspection procedures (FS, Istruzioni 44C, 2013) used by the Italian Railway Network Authority (RFI).

It seems reasonable and quite inexpensive for the managing authority that simple geometric data can be integrated in the Masonry Bridge Database (MBD).

These information represent a sufficient set of input data to be applied in the proposed graphical iterative procedure based on limit analysis approach for the preliminary seismic assessment of masonry bridges.

A large stock of 757 railway bridges located in high seismic areas are selected as representative of the typological characteristics of masonry bridges.

Masonry arch bridges were subdivided into homogeneous classes of single span and multi-span structures, according to the result of a statistical analysis of the stock.

All the different collapse mechanisms for seismic action of each class of masonry arch bridges were studied, with the application of limit analysis and the calibration with FEM . In particular we developed limit analysis methods for the seismic assessment of single and multi spans bridges.

In this study the analysis of global (in-plane) collapse mechanisms of multi-spans bridges and an iterative procedure for the design of thrust line were proposed and developed.

Moreover an innovative limit analysis approach was proposed for the assessment of the global transverse seismic capacity of multi-span masonry bridges with slender piers. This approach derived from the association of some typical aspects of the limit analysis and some concepts of the pushover analysis.

Subsequently a parametrical analysis using simplified limit analysis was performed for each class, to calculate the seismic capacity of the bridges. Appropriate ranges for geometrical and mechanical parameters, i.e. span length, arch thickness, span-to-rise ratio, pier height, etc. were considered, and the limit horizontal load multiplier was calculated for each relevant seismic collapse mechanism. Envelope curves representing the seismic capacity expressed in terms of limit horizontal acceleration were derived. These curves can be used for a simplified vulnerability assessment of railway masonry arch bridges. The input data necessary for the use of envelope curves are easily detectable from geometric parameters of the bridges.

A simple calibration of the judgment obtained by BMS through inspection visits to bridges was presented in order to considered the intrinsic seismic vulnerability of some masonry bridges located in high seismic risk area.

In this way is possible to guarantee a priority of intervention at those bridges that have in the same time an evident state of degrade and/or a high seismic vulnerability.

In the second part of the study, a new simplified approach for the fast calculation of seismic fragility curves of numerous masonry arch bridge clusters is proposed. The aim of this proposal is to provide useful information for the fast seismic vulnerability assessment of single-span masonry arch bridges in the context of territorial scale analyses. This is possible through the grouping of bridges in classes characterised by similar structural features.

These guidelines allow to quickly estimate the seismic vulnerability of extended roadway and railway bridge networks in emergency and to optimize the retrofit intervention. Considering the high percentage of bridges characterised by single span in European transportation infrastructural networks, the results of this study should be interesting.

This methodology can be applied at regional level for the vulnerability assessment of transportation networks with regard to the specific scenario earthquakes formulated.

It would allow us to better manage the phase after the main shock so that it should be possible to rationalise resources for the assessment of bridges in the post-seismic, to close the most vulnerable railway network or road network and to maintain the use of the most secure one.

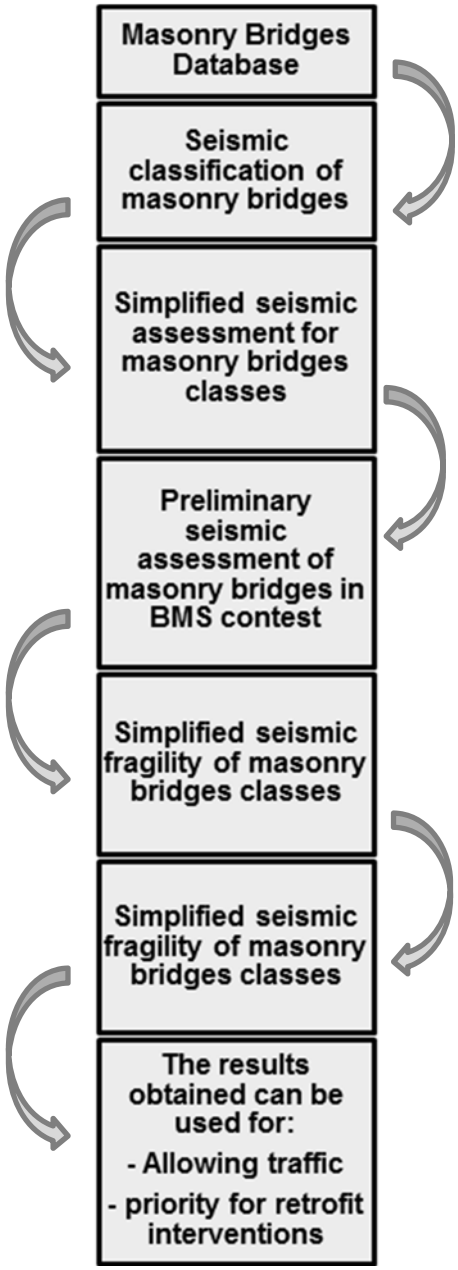

Fig. 1.2 - Thesis flowchart

2 MASONRY ARCH BRIDGES

2.1 Masonry Arch bridges

Old masonry and stone arch bridges currently represent a large proportion of the Europe road and railway bridge stock. Most modern masonry arch bridges are part of the historical heritage of the 19th century and the most important were built between the second half of the nineteenth century and the first half of the twentieth. In the same period the actual railway network was also built in the most part of Europe.

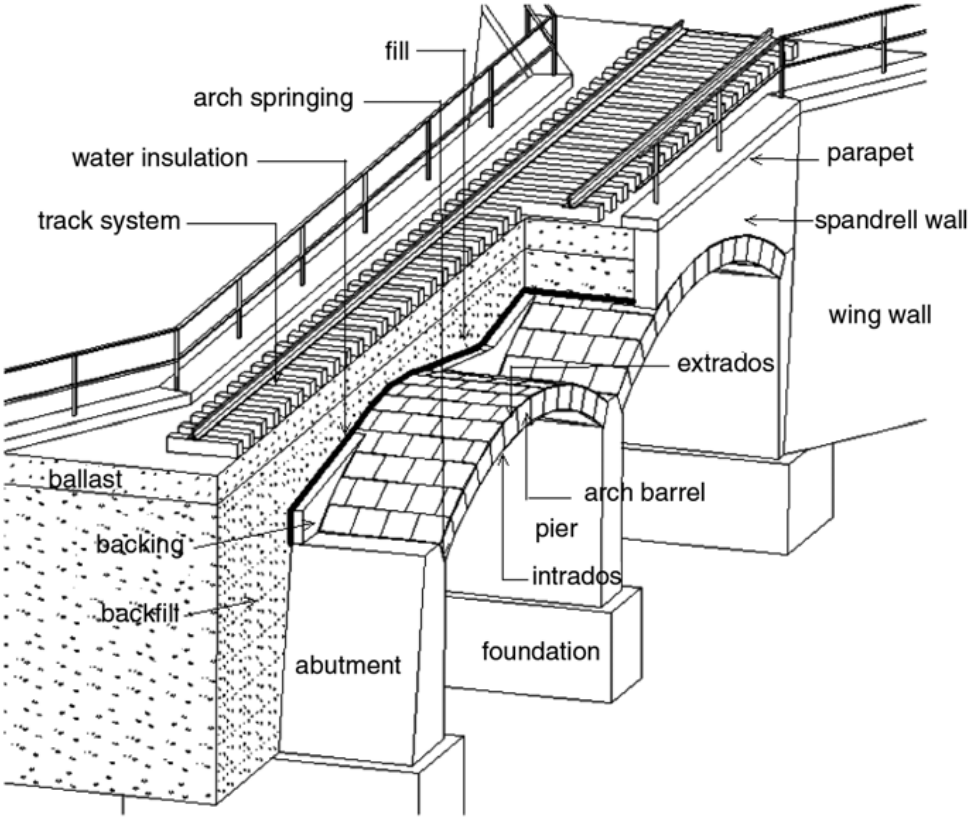

Fig. 2.1 Typical structures of a multi-span railway arch bridge (Orbán & Gutermann, 2009).

The main elements of a masonry railway arch bridge are:

Arch barrel:
The arch barrel is the main element for the load bearing capacity of an arch bridge. It transfers death and live loads to the abutments and then to the foundations.
The vault can be designed with various shapes distinct by the rise to span ratio r/s; the most common shapes are: semi-circular, parabolic, segmental, elliptical, gothic pointed.
The semi-circular arch was largely used especially in the case of viaducts. During the construction, the vaults are not built all at the same time: semi-circular arch pushes less than other configurations, so it induces the minimum bending stress in the pier in which the work was stopped.
The gothic pointed shape is usually realised when there is a concentrated force on the key stone. It transfers less pressure to the piers but it needs more space in height.
Materials depend on the age of construction and the geographic location: they can include stone voussoirs, random rubble and individual or bonded brickwork or concrete rings.

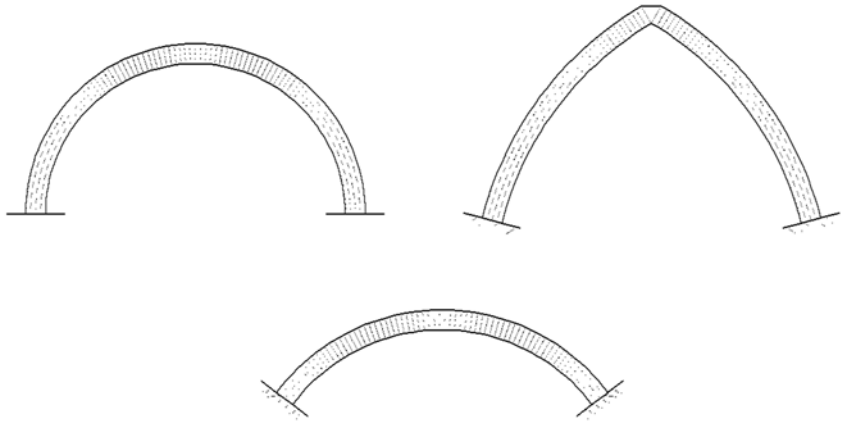

Fig. 2.2 Masonry vault shapes

Spandrel wall and wing wall:
Spandrel wall contain the fill and the backfill material over the arches. In addition it provides additional stiffness for the structures, which sometimes may be increased with an internal spandrel wall that can also reduce the horizontal soil pressures on the external spandrel walls.

Wing walls restrain the fill behind the abutments and may also increase their stability. They are usually inclined between 60 and 80 degrees from the axis of the bridge. Like in spandrel wall also in wing walls there may be an internal wall with the function to decrease the pressure of the ground.

Backfill:
The fill above the vault distributes live loads and gives stability to the arch due to its weight; in addition it provides passive reaction against large movements hindering the collapse mechanism.

Backing:
The backing is usually made up of a high quality soil or a poor masonry and it is located between arches over the piers and the abutment. Generally, backing increases the load-bearing capacity because it resists to the collapse mechanism activated by horizontal loads.
A waterproofing membrane is usually placed between backing and backfill, but often it is deteriorated and no longer effective.

Abutments:
Abutments provide horizontal and vertical resistance for the arch or arches in multi-span bridges and transfer loads to the foundations. They have the function of containing the soil and this is the reason why they usually have a considerable size. Due to the large amount of material required, low quality masonry is often used except for the area under the springing. There may be a change of the arrangement of the masonry under the springing to allow a better load transfer from the arch to the abutment.

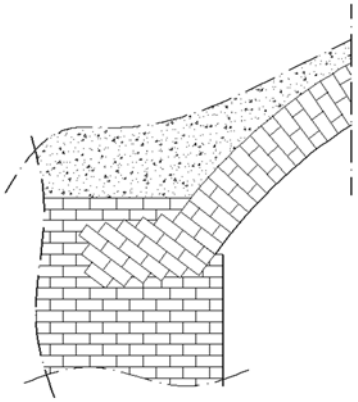

Fig. 2.3 Arrangement of masonry between arch and abutment

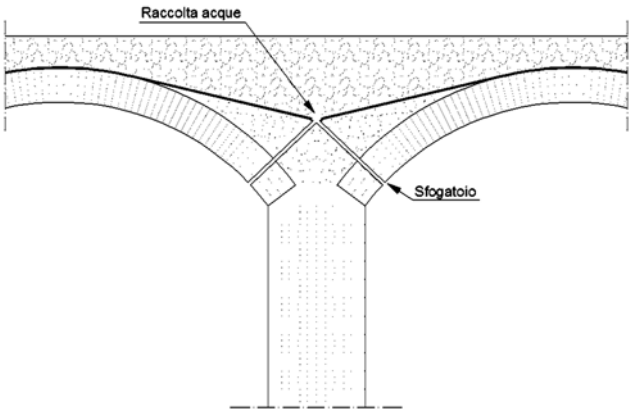

Fig. 2.4 Water drainage system in masonry arch bridges

Piers:

Arches in multi-span bridge are supported by piers. The cross section of piers may be homogeneous, hollowed or filled with lighter material. For heights greater than 15 meters they are often tapered to lighten and to reduce the amount of materials used. Long bridges with many spans have often a pier (or piers) with a greater section used as an abutment. This pier may resist to the horizontal pressure which arises in case of vault collapse; it resists also to the actions arising during the construction of the bridge.

Deep foundations:

Deep foundations on timber piles have been used since Roman times. Usually the diameter was between 20 and 30 cm and length till 10 m. Piles were driven into the ground with a regular pattern of 80 - 150 cm. In the presence of water cofferdams made of wood formworks can be used, to go deeply under the river bed and provide a dry working area. Tender stones and mortar were placed between the upper side of the piles to connect and lock themselves; a wood boarding was built over the heads to spread loads.

Shallow foundations:

When the load bearing soil is near to the ground level it is common to find spread footing foundations. In general, they were made with big block of stones to guarantee the required stiffness. If it was possible to dig the bottom of the watercourse until the bedrock, concrete was used.

2.2 Methods of analysis

2.2.1 Limit analysis

It is well known that the arch structures behaviour is not governed by materials strength but by their geometry. This characteristic is the basis of limit analysis method. This approach generally does not require materials and mechanical properties for the bearing capacity assessment because the evaluation is done only considering arch geometry and acting load (Clemente, et al., 1995).
Simplicity and speed have made limit analysis suitable for a preliminary estimation of the load-carrying capability of masonry arches and multi-span bridges but this method is not accurate for a structure with complex geometry, boundary conditions and redundancy.
The theoretical bases derive from plastic theory formulated for steel structures. In the mid-20th century many authors (Kooharian, 1952; Heyman, 1966) provided that it could be applied to masonry gravity structures such as masonry arch bridge.
The hypotheses made by Heyman to simplify the problem were:

- the masonry in the arch has infinite compressive strength ;
- the masonry in the arch has no tensile strength;
- sliding between masonry units cannot occur.

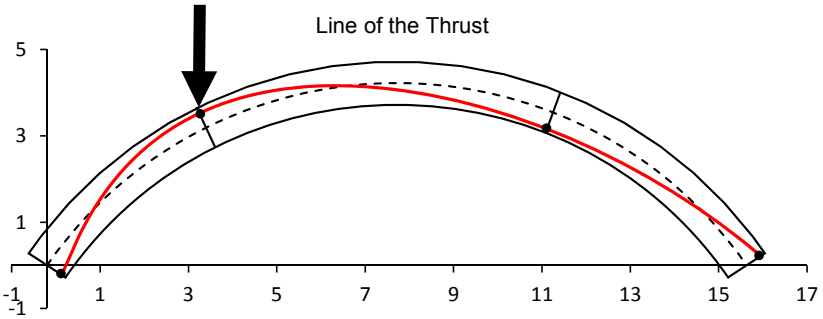

Fig. 2.5 Trust line at collapse

The first statement may be considered correct because the actual stresses, generally in masonry bridges, are one or two orders of magnitude lower than compressive strength of the material itself. Anyway this assumption should be checked at the end of the analysis. The second statement in some cases is conservative; actually, the

joints between voussoirs may be dry or made with a weak mortar. The last assumption is related with the high coefficient of friction of masonry (μ = 0,6 - 0,7).

In the context of masonry gravity structures, for ultimate collapse the following conditions may be used to test:

- Equilibrium condition: Computed internal actions must represent a state of equilibrium between the internal and external loads.
- Mechanism condition: Sufficient releases must be made to transform the structure into a mechanism; this happens when the line of thrust touches exterior faces of the masonry blocks.
- Yield condition: The stresses in the material must be everywhere less than or equal to the material strength (e.g. shear, crushing and tensile strength limits must all be respected).

The possibility to find an exact solution is provided from the three fundamental theorems of plastic analysis, which can be stated in an easier way inserting the load factor λ, multiplier of the agent load on the structure. The theorems are:
Static or lower bound theorem If at any load factor λ the equilibrium and yield conditions are everywhere satisfied, then $\lambda = \lambda_l$ which is less than or equal to the failure load factor λ_p.
Kinematic or upper bound theorem If at any load factor λ is equal to the work done in plastic energy dissipation, then $\lambda = \lambda_u$ which is greater than or equal to the failure load factor λ_p.
Uniqueness theorem if at any load factor λ, the internal stress state is such that the three conditions of equilibrium, mechanism, and yield are satisfied then that load factor is the collapse load factor λ_p.

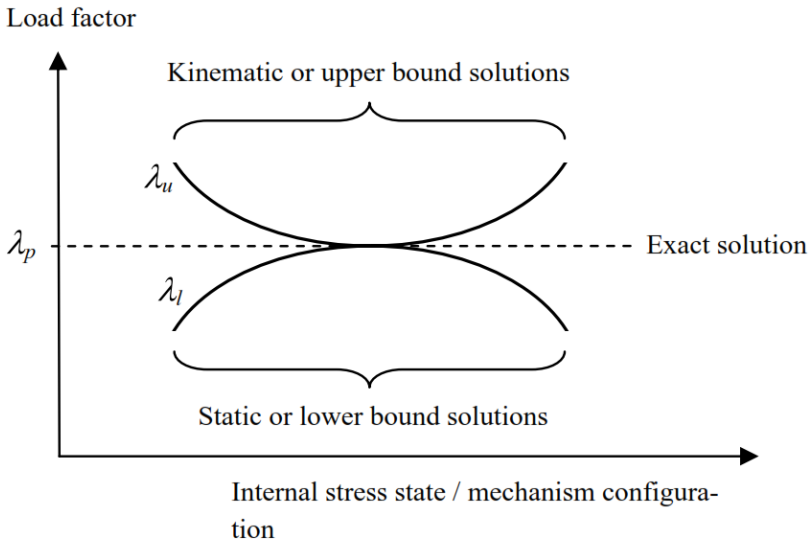

Fig. 2.6 The relationship between upper and lower bound solutions (Gilbert, 2007)

Under these hypotheses, the arch collapses only when a certain number of hinges transform the structure into a mechanism (Sinopoli, et al., 1998). For a single arch generally the collapse occurs when four hinges are formed and three are aligned.
Under these hypotheses the yield surface is bounded between two straight lines with equations:

$$M = \pm h \cdot N \tag{2.1}$$

h is the half thickness of an arch brick and M is the product of the normal force N by the eccentricity e. The eccentricity must satisfy the condition to not form a hinge between blocks:

$$-h \leq e \leq +h \tag{2.2}$$

In reality, the material has a finite strength, so the yield surface is individuated by two curves, but, since the normal agent force is much smaller than the critic normal force, the two boundary conditions can be considered equal near the origin (Hayman, 1982).

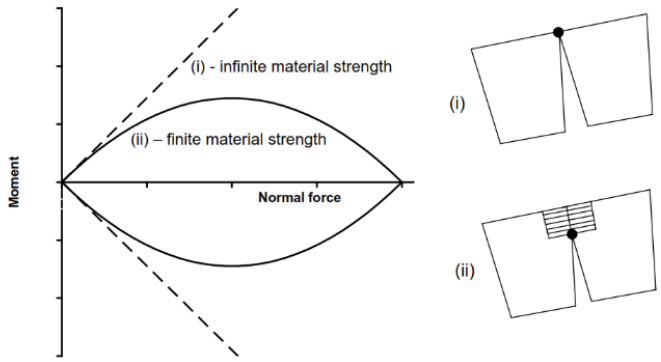

Fig. 2.7 Contact surface moment vs. normal force failure envelopes (Gilbert, 2007)

Many studies have followed the work of Heyman to include the effective resistance of the masonry and to consider the sliding failure mechanism (Livesley, 1978; Gilbert & Melbourne, 1994), but, as Drucker pointed out (Drucker, 1954), the inclusion of these invalidate the bounding theorems and lead to unsafe load factor.
The interaction with the soil surrounding the arch barrels has also been taken into account, including the effect of live load spreading through the fill and of passive fill thrust with different load spreading models (Cavicchi & Gambarotta, 2005; 2007).

2.2.2 Finite element analysis

Since the birth of the finite element method, much research has been done in the field of masonry arches bridges and nowadays it is the common analysis method for this kind of structures.
The Finite Element Method is based on stress analysis. An adequate research on materials properties and especially on existing damage, environmental factors and lack of maintenance must be done to determinate the input parameters and to develop a realistic simulation. This estimation is often difficult because of the unavailability of certain data due to the lack of knowledge of such ancient structures. The characterisation of historic materials is important to know the initial stress state. It may be evaluated through tests in situ such as load test and the measurement of the relative displacement (e.g. flat-jack test (Binda & Tiraboschi, 1999; Oliveira, et al., 2007)) or in laboratory such as mechanical tests on specimens picked up from the bridges (Hughes & Pritchard, 1998; Orbán & Gutermann, 2009).

Moderns techniques allow to investigate the internal geometry of the bridge with non-destructive methods. The external appearance may be different from the real bearing structure e.g. internal spandrel walls, different thickness of the barrel from the keystone to the springing, different materials in piers and backfill. In addition to this, it is important to know if there is the presence of defects such as ring separation, empty space in the backfill or cracking in the arch extrados. The main non-destructive tests are Ground Penetrating Radar (GPR), infrared thermography and sonic methods (Orbán & Gutermann, 2009).
When it is not possible to characterise materials properties, a sensitivity analysis with stochastic method (Schlegel & Will, 2007; Brencich, et al., 2007) is usually required. This one is used after an investigation of particular common properties of bridges in a specific geographical area (Oliveira, et al., 2010).
Recently new modelling strategies have been developed for a deeper understanding of the structures as a whole. Therefore the interaction between soil and arch (Cavicchi & Gambarotta, 2005; Gilbert, et al., 2007; Wang & Melbourne, 2007), and the influence of spandrel walls (Cavicchi & Gambarotta, 2007; Harvey, et al., 2007) were studied with 2-D or 3-D finite elements.
In addiction 1-D models have been developed, which allowed to have a limited computational effort, making the proposed strategy suitable for practical applications. Analysis done using fibre beam elements (de Felice, 2009) offers also a good compromise between simplicity and accuracy. The method takes into account the backfill and it considers the interaction between normal force and bending moment in the non-linear behaviour.

2.2.3 Discrete element analysis

Masonry peculiarity is that the joints between bricks form natural predefined planes of weakness and, in some cases, the assumption of homogenous and continuous material properties may not be valid.
The first application of the method was proposed by Cundall (Cundal, 1971). He considered the material as a group of distinct rigid blocks linked together by joints.
DEM analysis may assume rigid or deformable blocks. In addition, for the evaluation of masonry structures, there are two main features that must be undertaken (Al-Heib, 2012). The first is that large displacement and rotations between blocks must be allowed, and the second is that the detection of new contacts must be automatic during the calculation. For these reason DEM method can simulate progressive failure because of crack propagation.

The calculation procedure used by DEM, in its basic application, uses both force/displacement law at all contacts and Newton's second law at all blocks.

2.2.4 Discontinuous Deformation Analysis

It is based on an assumed deformation field within distinct domains and a rigorous imposition of contact constraints (Shi, 1988), and it has been applied to stone arches in (Ma et al., 1995) to represent the possibility of sliding between blocks.

2.3 Main structural assessment method of masonry bridges

2.3.1 MEXE method

The MEXE method (Military Engineering eXperimental Establishment) is a simple method for the load carrying capacity assessment of historical arch bridges. It was originated from Pippard in the 1930s and it is based on the assumption of linear-elastic behaviour of the material. It was widely used during the World War II for the load-bearing assessment under military loads. The method was modified several times during the years (Hughes & Blackler, 1997) till the current version given by the Department of Transport of UK. It can be quickly applied because it is based on empirical rules that depend from the arch span, arch thickness and the fill depth. In recent years, the method was criticised in particular with respect to load carrying capacity evaluation of short span bridges: the current version of MEXE overestimates the load carrying capacity of short span bridges, but for spans over 12m it becomes increasingly conservative (Melbourne, et al., 2009).

2.3.2 "SMART" method

The Sustainable Masonry Arch Resistance Technique or "SMART" method (Melbourne, et al., 2007) is a relatively new approach for the assessment of masonry arch bridge. Its purpose is to estimate the long-term service life, permissible loading limits and residual life.
It is based on the analysis of the geometry, of material properties, of loads and of the modes of failure. In addition to the Ultimate Limit State (ULS) that define the collapse load it introduces the Permissible Limit State (PLS).

2.4 Typical deficiencies in masonry arch bridges

The main deficiencies in masonry arch bridges are broadly classified as damage to foundations and to superstructure.
The most common defects in foundations include local undermining, differential settlements, and masonry dislocations due to loss of mortar joints. The main problem in identifying foundation damage is the difficulty of inspecting underground structures. Therefore, the first step in detecting problems in faulty foundation systems implies the observation and the analysis of how the superstructure behaves, i.e., the consequence of rotational or differential movements at foundation level. Due to their high stiffness and brittle structural behaviour, masonry bridges cannot generally absorb foundation settlements without structural damage.

Fig. 2.8 Typical defects of masonry arch bridges. Loss of bricks, longitudinal cracking in barrel vault; opening of arch joints, salt efflorescence in bricks; penetration by vegetation.

Superstructure defects (Fig. 2.8) are easier to detect by visual inspection. The main deficiencies are:

- deterioration of materials, such as degradation and loss of bricks, loss of mortar joints, and salt efflorescence in bricks, all often due to inadequate rainwater drainage, freeze-thaw cycles and penetrating vegetation;
- arch barrel deformations, with longitudinal or transverse cracking; opening of arch joints, and separation between brick rings in multi-barrel vaults;
- spandrel wall movements: sliding, bulging, or detachment from the barrel. Spandrel walls have little inertia and are generally weak elements with respect to out-of-plane behaviour (pressures orthogonal to spandrel walls are due not only to the weight of infill and traffic but also to horizontal transverse seismic action);
- fractures in piers and wing walls; cracking.

2.5 Rehabilitation and retrofit strategies for masonry arch bridges: innovative vs. traditional

Two main general approaches can be identified for masonry arches retrofitting:
- strengthening, to recover and increase the load-bearing capacity of the original structure (by improving material properties and connections, thickening the old structure with the same materials, etc.);
- resistant systems creation, that act in parallel with the old structure or directly increase the strength of original members (e.g., by adding tensile reinforcements in the original masonry section).
The various techniques can often be used in combination; design choices also can be influenced by construction phases and requirements regarding possible closure to road traffic. For example, methods requiring work on the extrados may be considered for road bridges but cannot be countenanced for railway bridges, to avoid traffic interruptions.
The most common techniques used for strengthening old masonry barrel vaults are:
- old masonry arch thickening with new layers of bricks;
- FRP strips application at the extrados of the barrel vault;
- methods of masonry restoration, such as grout injections, repointing of stone joints with good-quality hydraulic lime mortar, crack stitching and patch repairs by manual methods;
- internal brick spandrel walls construction, connected to the extrados of the vault. The new walls are stiff elements which tend to oppose antimetric deformation of vaults, contribute to bearing some of the loads, and enhance seismic resistance. Lateral spandrel walls have the same effects, since they work as rigid load-bearing

walls after rehabilitation and retrofitting of connections with arches (Tecchio et al., 2012).

Some common applications which introduce resistant systems are:

- saddling (laying of a new rc slab) at the extrados of the vault; rc jacketing at the vault intrados; anchorage with (usually high-strength) steel bars;
- prefabricated steel liners at the intrados, to support the vaults.

Spandrel walls are generally critical in masonry bridges, because of their high vulnerability to out-of-plane actions. A significant increase in resistance can be obtained by the simple insertion of transversal stainless steel ties, which prevent them from overturning (Oliveira and Lourenço, 2004).

For the rehabilitation of piers and abutments, in addition to traditional methods for masonry restoration, masonry post-tensioning techniques and jacketing works can be applied. Improved safety levels of foundations, underpinning and new foundations on micro-piles are often used.

3 ITALIAN RAILWAY MASONRY BRIDGE STOCK

3.1 Introduction

Masonry bridges of the Italian railway system were mostly built over a century, in the period 1840-1930, according to typologies and design rules given by the Railway Manual of Practice in use (Italian State Railways, 1907). This led to the use of recurrent dimensions and to a repetitive design (excluding singular cases due to the particular local topography), with geometrical properties varying within specific ranges (Italian State Railways, 1924). A typological approach is particularly suitable for a seismic vulnerability study on a large scale: the entire stock of masonry arch bridges can thus be subdivided into homogeneous classes. In this work, the classification is based on the typological features of the bridges and on the collapse mechanisms expected under seismic action.

3.1.1 Survey of the Italian railway masonry bridge stock

The effective ranges of the main geometric parameters affecting the seismic capacity of bridges were obtained from a preliminary survey of a large stock of existing structures still in use. In particular, the considered parameters are: number of spans, span length (L), arch rise (f), arch thickness (s), pier height (H), pier longitudinal width (B), bridge transverse width (P), abutment height (h). Some values, such as (f/L), (s/L), (H/B), are also given as non-dimensional ratio of two parameters, as those ratios are characteristic of the bridge type.

The structural evaluation campaign and archival research regarded 757 masonry bridges belonging to the Italian railway network. This set is significantly representative of the Italian masonry bridge stock, and the structures are located along various railway lines throughout the country (see Fig. 3.1). These lines were chosen because they pass through areas classified as Zone 2 and 1 in the Italian seismic zoning map: the maximum PGA value of the reference stiff soil for Zones 2 and 1 is 0.25-0.35g (expected peak ground acceleration with a 10% probability of being exceeded in 50 years).

The main results of the preliminary statistical analysis are shown in Fig. 3.2-Fig. 3.5, in which histograms summarise the main geometric parameters and their percentage

distribution (reported data do not include very short bridges, with span length L<3m). The set of histograms of Fig. 3.2 is related to the whole stock of structures, while Fig. 3.3 refers to single-span bridges and Fig. 3.4 to multi-span bridges only.

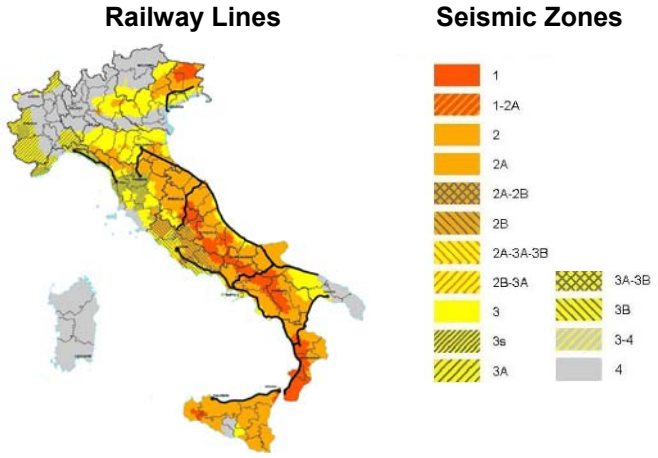

Fig. 3.1 Italian railway lines where are located the masonry bridges of the stock

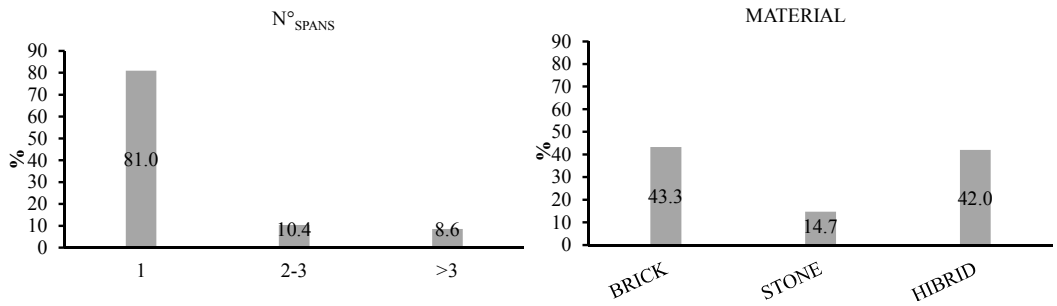

Fig. 3.2 Statistical analysis of railway masonry bridge stock, general data.

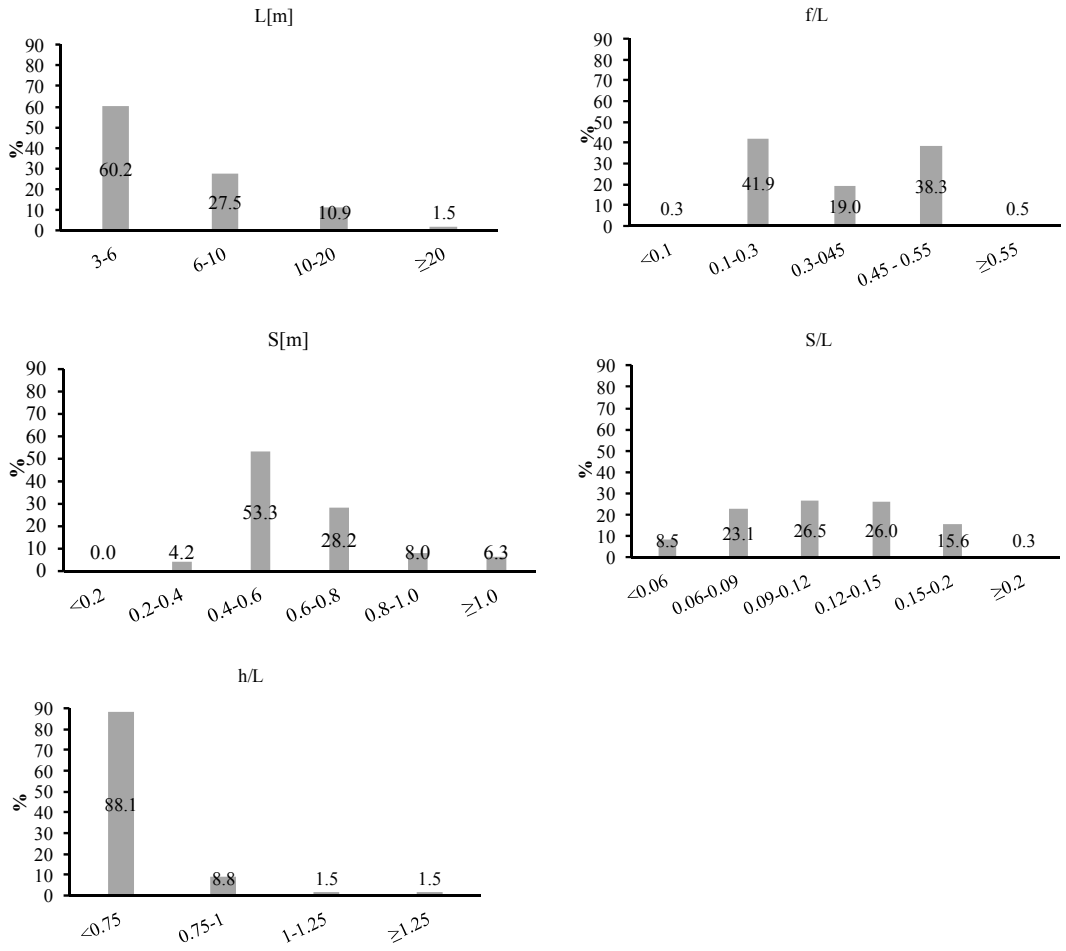

Fig. 3.3 Statistical analysis of railway masonry bridge stock, single-span structures.

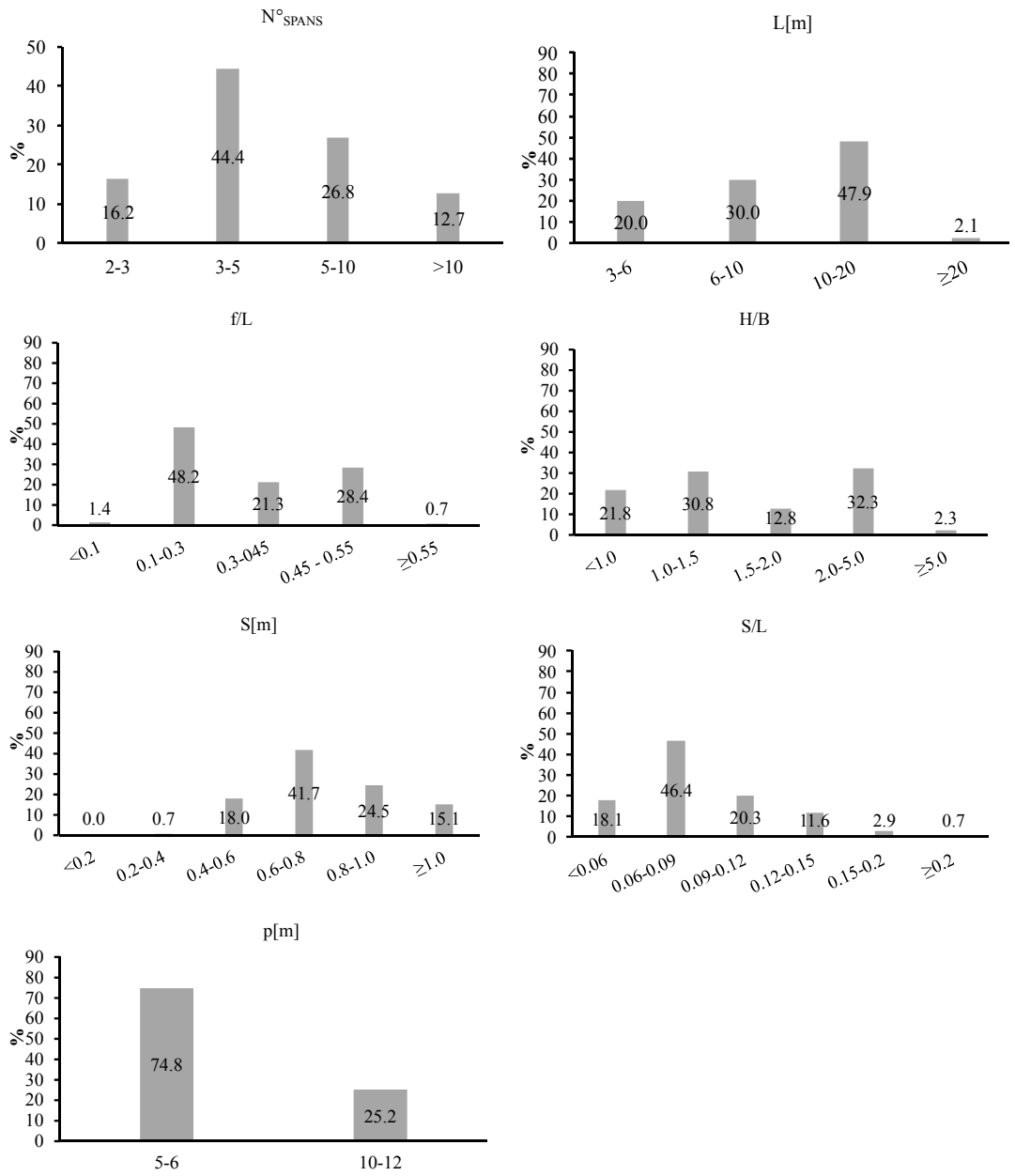

Fig. 3.4 Statistical analysis of railway masonry bridge stock, multi-span structures.

As can be seen in Fig. 3.2 most bridges are single span (81%). The span length is variable, with predominance of short (3≤*L*<6) and medium (6≤ *L*<10) spans in single-span bridges (Fig. 3.3), while almost half (48%) of multi-span structures have longer

spans ($10 \leq L < 20$, Fig. 3.4). Only a small percentage of structures, around 1-2%, has span length greater than 20m.

A great number of arches is semi-circular (38 and 28% for single- ad multi-span structures) or depressed (42 and 48% for single- ad multi-span structures) with medium span to rise ratio ($0.1 < f/L < 0.3$) (Fig. 3.3-Fig. 3.4); flattened arch shapes were predominantly used in medium or long span bridges.

The non-dimensional arch ratio s/L is generally higher (0.12-0.15) in case of short to medium-span than for longer spans (0.06-0.09).

Among single-span bridges, arches with high abutments ($h/L > 0.75$) represent a not negligible portion (13%, Fig. 3.3), particularly within the range of short spans ($L < 6$m).

In most cases, the bridge platform hosts one or two railway lines: in case of single-track bridge, the width (P) is generally in the range 4.80-6.50m, while for a double-track bridge, the width is about 10.0-12.0m or more.

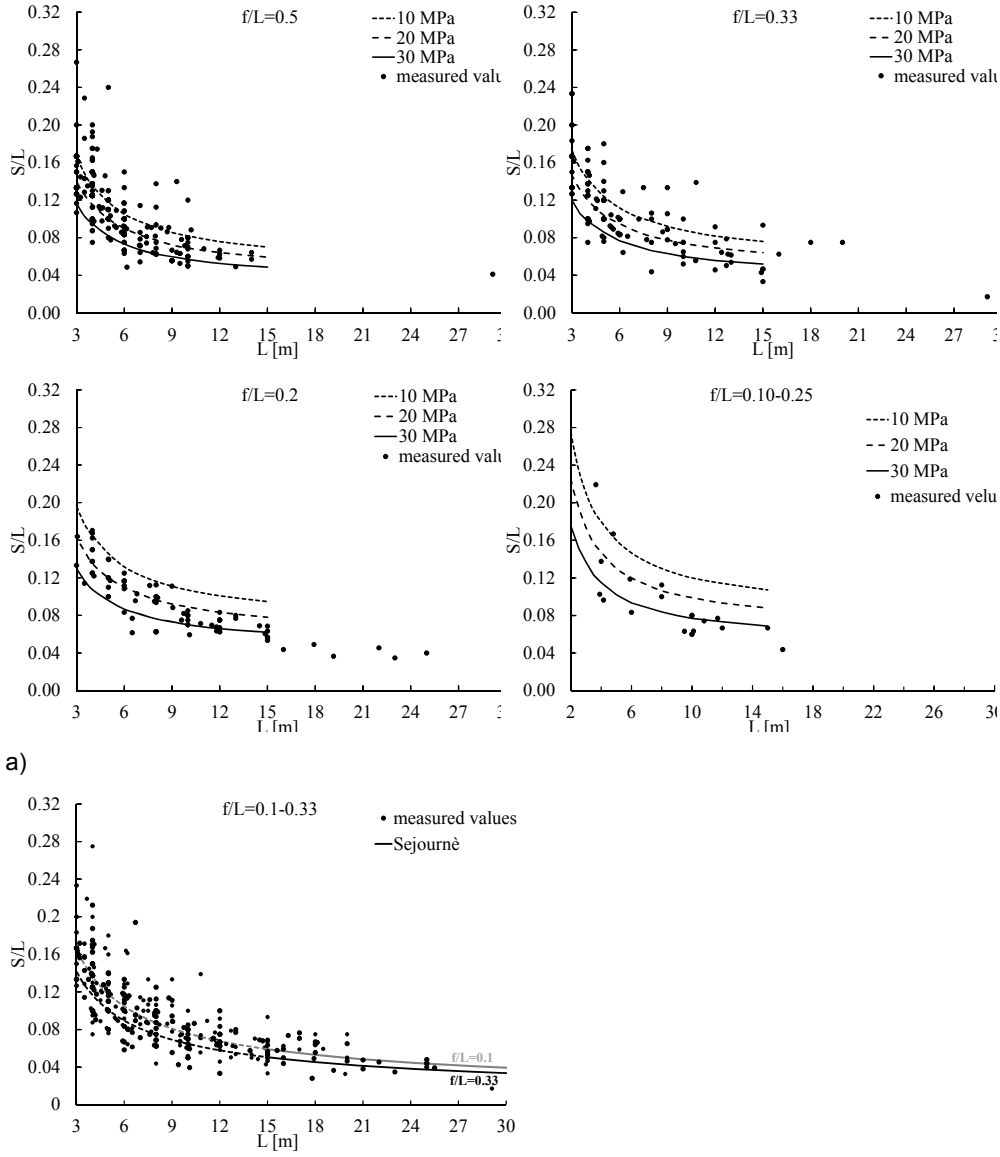

a)

b)

Fig. 3.5 Design curves of s/L parameter versus on-site measured values: a) short-medium span bridges (L≤15m); b) medium-long span bridges (L>15m).

To check the validity of the on-site measured values, these data were compared with geometric dimensions obtained by design rules in use at the beginning of the 20th Century.

In the Italian State Railways (1907) Manual of Practice, parameters are tabulated for short and medium span bridges (span length *L*≤15m), considering different values of

the rise-to-span ratio, (*f/L)*, and three possible values of the compressive strength f_c of bricks (10MPa, 20MPa and 30MPa). Design curves are plotted in Fig. 3.5 against parameters of actual masonry bridges of the analysed stock. Fig. 3.5a shows that the design curves represent quite well the medium trend of the measured (*s/L)* parameter, for both circular and depressed arches, although a major dispersion characterises short-span bridges.

For medium and long span masonry bridges (*L*≥15m), which are not reported in the above-mentioned Manual, the arch thickness can be calculated according to Sejournè (1916):

$$s = 0.15 + 0.15\sqrt{L} \qquad \text{semi-circular arches} \qquad (3.1)$$

$$s = 0.15\left(1+\sqrt{L}\right)\frac{4}{3}\left(1-\frac{f}{L}+\left(\frac{f}{L}\right)^2\right) \qquad \text{depressed arches} \qquad (3.2)$$

As already demonstrated by Cocciaglia and Mosca (1998), these equations are well representative of dimensions measured on actual structures (Fig. 3.5b), particularly in the case of flattened arches, which are the most typical solution for longer structures.

Considering the good match between simple measures obtained on site and design values in use at the beginning of the 20th Century, other curves extrapolated from the Italian railway Manual of Practice (Italian State Railways, 1907) were used to define parameter *s'/L* (where *s'* is the abutment thickness) and *t* (thickness of spandrel wall). Their values are shown in Fig. 3.6 and Fig. 3.7. *s'* and *t* are necessary for evaluating the behaviour of spandrel walls and abutments, but they cannot be measured by visual surveys.

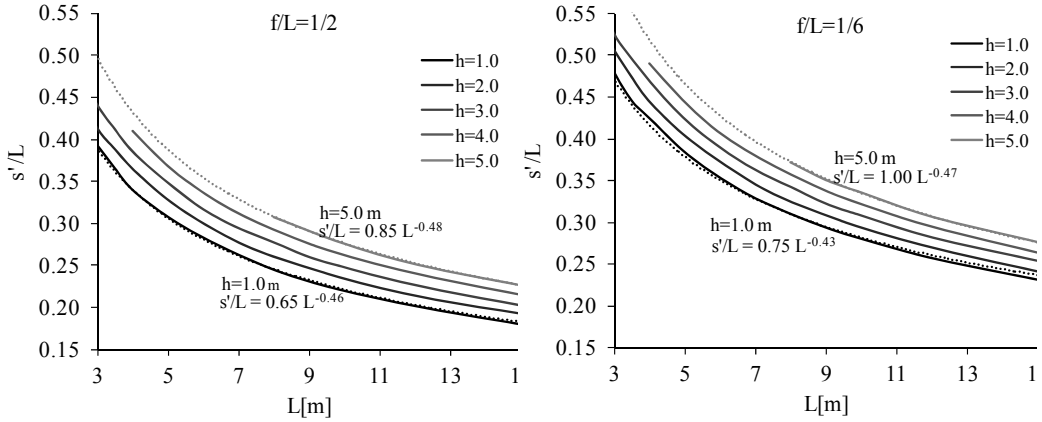

Fig. 3.6 Short-medium span masonry bridges (L≤15m): design curves for s'/L.

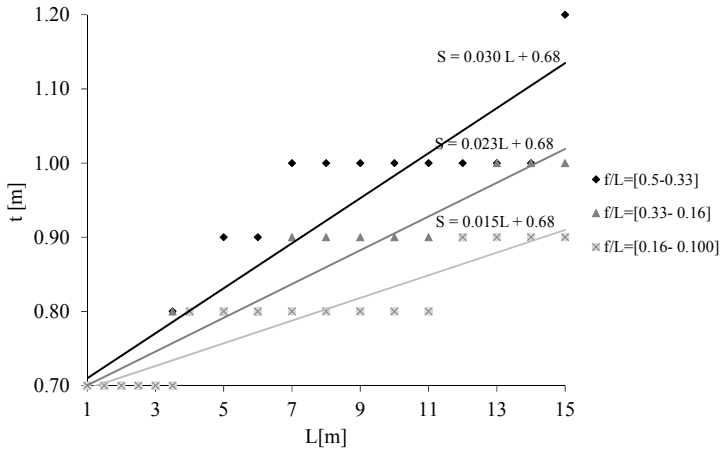

Fig. 3.7 Design curves for t (Italian State Railways, 1907)

4 TRANSVERSE SEISMIC CAPACITY OF MULTISPAN MASONRY BRIDGES

4.1 Introduction

The kinematic method, based on an adaptation of limit design for masonry structures, has proved to be a conceptually simple and robust procedure to verify the safety of masonry arch bridges under vertical loads. The method can also be applied for seismic assessment, providing a limit of bridge capacity under horizontal loads.

Since Heyman (1966, 1972) noted that the plastic theory, initially formulated for steel structures, could also be applied to masonry structures, many studies have focused on limit analysis to assess the vertical load-bearing capacity of single- and multi-span masonry arches (Gilbert, 2007).

Heyman (1982) adopted some simplifying assumptions to perform the above analyses:

i) absence of sliding between voussoirs,

ii) infinite compressive strength,

iii) no tensile resistance of masonry.

With these hypotheses, arch failure occurs when a thrust line can be found, lying wholly within the masonry and representing an equilibrium state for the structure under acting loads, which allows the formation of a sufficient number of plastic hinges to transform the structure into a mechanism. Following Heyman's assumptions, iterative methods to find the geometric safety factor, related to minimum arch thickness under dead and live loads, were proposed by Clemente et al. (1995).

Several authors have incorporated crushing of masonry, which cannot sustain infinite compressive stresses. A rectangular stress block carrying the compressive force at the edge of the hinge section was assumed, among others, by Gilbert (1998). Alternatively, to go beyond the assumption of infinite compressive strength, Bufarini et al. (2010) used a procedure based on reducing the design thickness of masonry.

Sliding between adjacent blocks was introduced and evaluated by Gilbert and Melbourne (1994), who successfully modelled multi-span brickwork arch bridges.

Interactions with the soil surrounding the arch barrels were also taken into account, including the effect of live load spreading through the fill and passive fill thrust with various load spreading models. Gilbert (2001) incorporated uniaxial line elements in

RING software to ensure that soil pressures were mobilised in the correct direction. Cavicchi and Gambarotta (2005, 2007) implemented a finite element limit analysis model, in which infill material was modelled with a special triangular finite element to evaluate the arch-fill effect on the ultimate load-bearing capacity under vertical loads.
Relatively little research has been carried out on the application of limit analysis for assessing masonry arches under horizontal (seismic) loads. In particular, research has focused on the longitudinal behaviour of arched structures. Some researchers have studied the dynamic response of a single masonry arch under base motion. Clemente (1998) provided the horizontal acceleration factor inducing the onset of motion, and analysed the subsequent first half-cycle of vibration in free and forced conditions according to Heyman's hypotheses. De Lorenzis et al. (2007) used discrete element modelling to predict the combinations of impulse magnitudes and durations which lead unreinforced masonry arches to collapse, and analysed the impact of rigid blocks over several cycles of motion. Other studies (De Luca et al., 2004, da Porto et al., 2007) have examined the activation of semi-global and global mechanisms involving not only local arch failure but also the simultaneous formation of hinges in the arch and at the base of piers (or abutments).
To date, little attention has been paid to the seismic capacity of masonry arch bridges in the transverse direction and their susceptibility to out-of-plane collapse.
It has been shown that local out-of plane overturning of spandrel walls may make the entire bridge inoperational (Resemini and Lagomarsino, 2004), since collapse does not involve the failure of the main structural elements but compromises ballast supports and rail tracks or road paving (Tecchio et al., 2012). Rota et al. (2005) applied limit analysis to a set of arch bridge types to evaluate the multiplier of the horizontal loads activating the out-of-plane mechanism of the spandrel walls, including the effect of infill material.
Despite these researches, appraisal of the overall transverse seismic capacity of multi-span bridges has not been comprehensively addressed. The overall deformed shape at collapse, involving transverse deflection of piers was obtained by Pelà et al. (2009, 2013) with numerical simulations according to Non-linear Static Analysis (NSA) and Non-linear Dynamic Analysis (NDA).
Within the framework of limit analysis approaches, the present work applies the mechanism method to assess the overall transverse seismic capacity of multi-span masonry bridges with slender piers. On the basis of the procedure developed, a parametric study was carried out on a set of multi-span railway masonry bridges. Typical geometric and mechanical parameters were examined in order to create a series of charts providing the lateral capacity of masonry bridges in terms of resistant

horizontal acceleration. The input data for the simplified assessment are geometric parameters only, which are easily revealed by visual inspection.

4.2 Limit analysis for seismic assessment of transverse capacity

The seismic vulnerability of masonry arch bridges is due to collapse mechanisms, depending on geometric and mechanical factors, which affect the structure both longitudinally and transversely. Local mechanisms are generally more easily activated in squat structures and overall mechanisms are more likely to occur in slender ones.

Longitudinal collapse under horizontal loads is activated by the formation of four skew-symmetric hinges. The local mechanism is characterised by failure of the arch only, whereas in the semi-global or global mechanisms, one or two hinges are located at the base of the piers (De Luca et al., 2004).

When an arch bridge is subjected to transverse seismic excitation, local collapse is due to failure of the spandrel walls, as noted above. In the case of regular multi-span bridges with slender piers, the overall transverse collapse mechanism involves flexural failure at the base of the piers and failure of the arches in the areas of maximum tensile stress, leading to complete loss of resistance and stiffness. The collapse configuration can be represented by a 3D kinematic model in which the structure is transformed into a mechanism when spherical hinges form at the base of the piers and in the arch crown sections, where the maximum compressive stresses are located (Fig. 4.1).

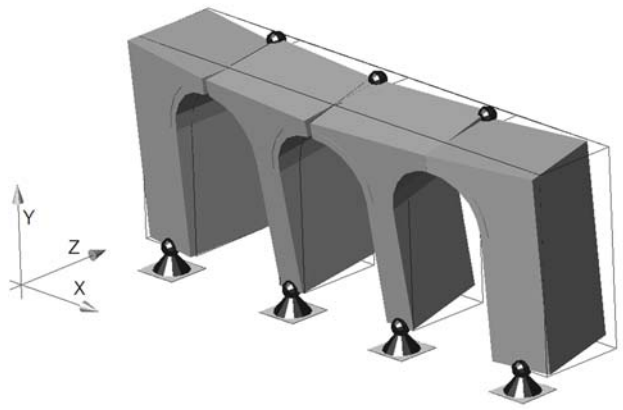

Fig. 4.1 Overall transverse collapse mechanism

In this work, limit analysis was used to estimate the horizontal seismic load multiplier which triggers overall transverse failure of the structure. The procedure was developed for multi-span bridges with spans of equal length; effects due to possible arch skewness were not taken into account.
The analysis applies the kinematic theorem to rigid macro-blocks subjected to dead loads - and live loads when required - and to distribution of horizontal seismic loads proportional to structural masses. The bridge is discretised into rigid voussoirs, the centroid virtual displacement of which is determined. The filling material is exclusively viewed as applied mass. Heyman's simplifying hypotheses are taken into account but, due to the compressive strength of materials, plastic strains are also taken into account by moving the location of the plastic hinges forming along the height of critical cross-sections (Clemente et al., 2010).
The procedure consists of an iterative application of the Principle of Virtual Work (PVW). Collapse multiplier α_0 is calculated according to the following steps:
(a) definition of a Cartesian coordinate system and subdivision of the structure into blocks;
(b) identification of the collapse mechanism;
(c) definition of the force system applied to the structure;
(d) application of the PVW.

A Cartesian coordinate system is defined and the procedure starts by subdividing the structure into n+1 macro-blocks (Fig. 4.2), in which n is the number of spans. Two macro-blocks represent the bridge portions, including the abutments and half the external spans; the remaining n-1 macro blocks are those centred on the piers. The point of separation between adjacent blocks is the arch crown and is perpendicular to the vault plane. This simplified collapse configuration is functional to the direct application of the kinematic approach, and is identified according to the crack patterns obtained by numerical simulation (see 4.3).
The PVW is then written, after definition of the transverse virtual displacement profile of the bridge, $\Delta z(x)$, which varies according to the properties (geometry and degree of lateral restraint provided at abutments) of the lateral resisting system. Part of the seismic inertia force is directly transmitted to the pier footings, as higher piers determine greater displacements in the central portion of the bridge. The remaining inertial force is transferred by lateral bending of the deck to the abutments, when the deck is effectively restrained at the abutments.
It is assumed that displacement is zero at the abutments and pier base, and increases linearly along the height of the bridge (vertical axis y), the peak value being at deck

level. The total transverse displacement is obtained as the sum of two contributions (Fig. 4.2)

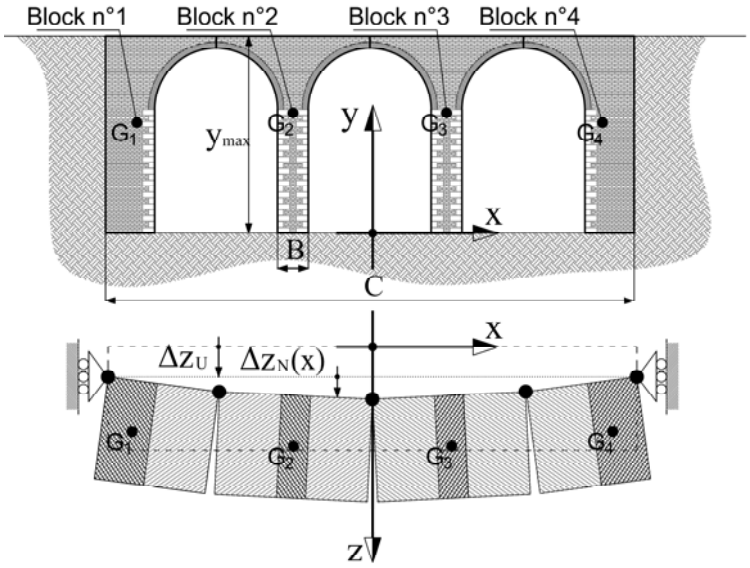

Fig. 4.2 Coordinate system and macro-blocks of a three-span bridge

$$\Delta z\left(x\right) = \Delta z_U + \Delta z_N\left(x\right) \tag{4.1}$$

where:

Δz_U is the uniform component of transverse displacement (when abutments are completely unrestrained; see Fig. 4.3, left);

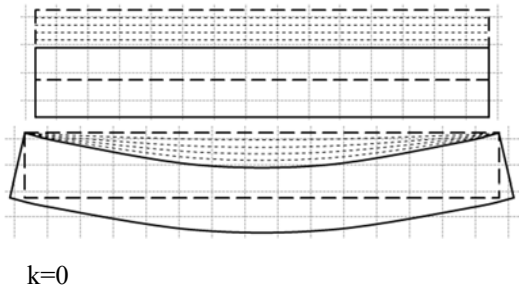

Fig. 4.3 Deck transverse displacement profiles and limit values of abutment restraint: k=0 (free abutments), k=1 (fixed abutments)

$\Delta z_{N(x)}$ is the non-uniform component of transverse displacement, expressed as a function of coordinate x.
Under the assumption that the shape of the non-uniform transverse displacement is circular, the generic point of the deck at coordinate x in the undeformed configuration moves to position x' (see Fig. 4.4), with total transverse displacement expressed by:

$$xx' = r - \sqrt{\left(x\right)^2 + \left(r - \Delta z_{N_{max}}\right)^2} \tag{4.2}$$

where:

xx' is the distance from x to x';
r is the radius of the shape of the circular displacement, expressed as:

$$r = \frac{C/2}{\sin\left(2\beta\right)} \qquad \tan(\beta) = \frac{\Delta z_{N_{max}}}{C/2} \tag{4.3}$$

C being the total length of the bridge;
ΔzNmax is maximum transverse non-uniform displacement.
Consequently, the transverse non-uniform displacement of generic point x is given by:

$$\Delta z_N\left(x\right) = xx_1 = x'x\cos\left(\delta\right) \tag{4.4}$$

where xx1 is the non-uniform displacement along axis z and δ is the angle with axis z defined in Fig. 4.4, with:

$$\tan\left(\delta\right) = \frac{x}{\left(r - \Delta z_{N_{max}}\right)} \tag{4.5}$$

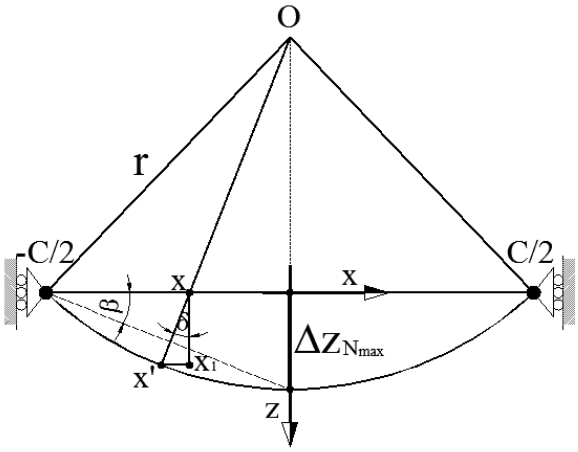

Fig. 4.4 Geometric relations of overall transverse displacement of bridge.

Parameter k is then introduced to represent the restraint effect of the abutments. It is defined as the ratio between maximum transverse non-uniform displacement Δz_{Nmax} and total maximum transverse displacement at midspan Δz_{max}.

$$k = \frac{\Delta z_{N_{max}}}{\Delta z_{\max}} \quad (0<k<1) \tag{4.6}$$

The values representing the two limit conditions, k=1 for fully restrained abutments and k=0 for completely unrestrained ones, are shown in Fig. 4.3, together with the relative deck displacement profiles. Uniform transverse displacement is expressed as:

$$\Delta z_U = \left(\frac{1}{k} - 1\right)\Delta z_{N_{max}} \tag{4.7}$$

Parameter k enables the equation of the PVW, which otherwise could not be made explicit directly, to be written in closed form. If a displacement field is normalised to $\Delta z_{Nmax} = 1$ and parameter k is fixed, the corresponding virtual displacements Δz(x) can be expressed as:

$$\Delta z(x) = 1 - k + \Delta z_N(x) \tag{4.8}$$

Introducing Eq. (4.1) into Eq. (4.6), in the case of small displacements, ($\cos(\delta) \cong 1$), Eq. (4.6) may be rewritten as:

$$\Delta z\left(x\right)=1-k+\left[r-\sqrt{x^2+\left(r-k\right)^2}\right] \tag{4.9}$$

and, inserting Eq. (4.2a) into Eq. (4.7), expression of total transverse displacement becomes:

$$\Delta z\left(x\right)=1-k+\left[\frac{C}{2\sin\left(2\arctan\left(\frac{C}{2k}\right)\right)}-\sqrt{x^2+\left(\frac{C}{2\sin\left(2\arctan\left(\frac{C}{2k}\right)\right)}-k\right)^2}\right] \tag{4.10}$$

Once the total length of bridge C and abutment restraint parameter k are known, total transverse displacement can be calculated with Eq. (4.8).

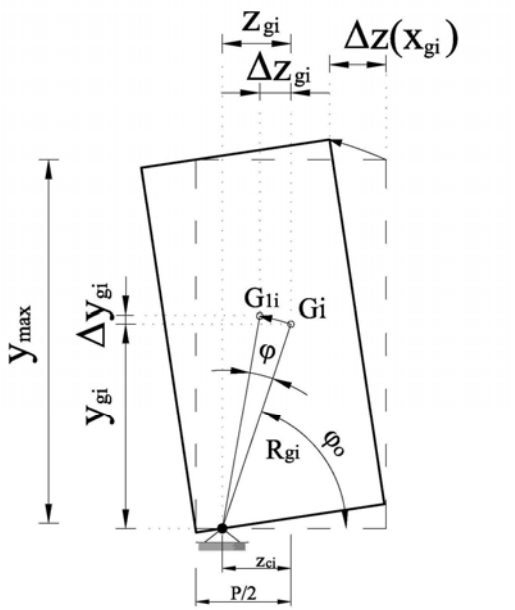

Fig. 4.5 Out-of-plane rotation and displacement of macro-block i

If (xgi, ygi, zgi) are the coordinates of barycentre Gi (Fig. 4.5) of macro-block i, angle φ of rotation may be written as:

$$\sin\varphi \cong \frac{\Delta z\left(x_{gi}\right)}{\sqrt{\left(\frac{P}{2}+z_{ci}\right)^2 + {y_{\max}}^2}} \tag{4.11}$$

where:

$\Delta z(x_{gi})$ is the transverse displacement of the block at barycentre G_i;

P is the transverse width of the pier;

z_{ci} is the distance between the vertical barycentre axis and the position of the plastic hinge;

y_{max} is the maximum height of macro-block i.

The condition of equilibrium expressed by the PVW equation requires virtual transverse and vertical displacements of barycentre G_i of macro-block i, defined as follows:

$$\Delta y_{gi} = R_{gi}\sin\left(\varphi+\varphi_0\right) - y_{gi} \tag{4.12}$$

$$\Delta z_{gi} = z_{gi} - R_{gi}\cos\left(\varphi+\varphi_0\right) \tag{4.13}$$

where:

φ_0 is the angle between segment R_gi and axis z;

$R_{gi} = \sqrt{z_{ci}^2 + y_{gi}^2}$ is the distance between the position of the plastic hinge and the barycentre of macro-block i.

The location of plastic hinge z_{ci} is determined from the value of compressive strength f_M of masonry, the hinge being located at the pier base section where compression forces occur.

If vertical load P_i acting on the macro-block is known, depth a of the compression zone at the pier base section can be calculated. In the failure condition, an equivalent uniform stress diagram (stress-block diagram) can be assumed for masonry:

$$a = \frac{\gamma_M P_i}{2 f_M B} \tag{4.14}$$

where B is the pier width in the longitudinal direction of the bridge and γ_M is the partial safety coefficient of masonry. Location z_c of the hinge is easily shown by:

$$z_c = \frac{p}{2} - a \tag{4.15}$$

where p is the transverse width of the pier.

Once external forces (vertical load P_i and horizontal seismic force $\alpha_0 P_i$, proportional to the bridge masses) are applied and the transverse virtual displacement components are calculated in barycentre G_i of each (n+1) macro-blocks, seismic load multiplier α_0 can be calculated with the PVW equation:

$$L_e = L_i = \alpha_0 \sum_1^{n+1} P_i \Delta z_{gi} - \sum_1^{n+1} P_i \Delta y_{gi} = 0 \tag{4.16}$$

Collapse trigger acceleration a_0^* can then be obtained with the following equation (NTC, 2008), multiplying α_0 by gravity acceleration g and dividing it by e^*, the fraction of the mass participating in the kinematic mechanism:

$$a_0^* = \frac{\alpha_0 \sum_1^{n+1} P_i}{M^*} = \frac{\alpha_0 g}{e^*} \tag{4.17}$$

where e^* is:

$$e^* = \frac{gM^*}{\alpha_0 \sum_1^{n+1} P_i} \tag{4.18}$$

and M^* represents the participating mass, calculated as:

$$M^* = \frac{\left(\sum_1^{n+1} P_i \Delta z_{gi}\right)^2}{g \sum_1^{n+1} \Delta z_{gi}^2 P_i} \tag{4.19}$$

4.3 Numerical calibration of simplified kinematic approach

4.3.1 Numerical analyses

The simplified kinematic approach for appraisal of global transverse capacity was calibrated according to the results of a numerical study, with benchmark responses obtained from a comprehensive set of Non-linear Static Analyses carried out by computer code Midas FEA v2.9.6, 2009. Finite Element (FE) models were developed

in order to verify the collapse mechanism in terms of the location of the plastic hinges in the kinematic chain and correct subdivision of the bridge into macro-blocks, and to calibrate the value of parameter k taking into account the abutment restraint.

3-D models implementing a macro-modelling approach were adopted for FE discretisation, in which masonry was modelled as a homogeneous continuum with eight- and six-node elements. The numerical model was characterised by material and geometric non-linearity: the Total Strain Crack Model implemented in Midas FEA was used as a constitutive law for masonry. In detail, the Smeared Crack Fixed Model developed from the modified compression field theory of Vecchio and Collins (1986) and later developed by Selby and Vecchio (1993) was used as a damage model for cracking. The masonry material exhibits isotropic properties prior to cracking and anisotropic properties after cracking, the cracks being orthogonal to the directions of the main strains.

Seismic performance, i.e., limit acceleration a_0^*[g] triggering the collapse mechanism, was evaluated by pushover analyses. Transversal forces proportional to the mass distribution (according to the assumptions adopted for the kinematic approach) were applied in a two-step sequence: first, only vertical loads were applied; lateral forces were then monotonically increased, following a displacement-controlled procedure. The transverse capacity of the bridge (limit horizontal acceleration prior to failure) corresponds to the condition in which a further increase in lateral displacement causes a significant decrease in stiffness, with an unchanged total global reaction, when limit equilibrium is reached (Fig. 4.6).

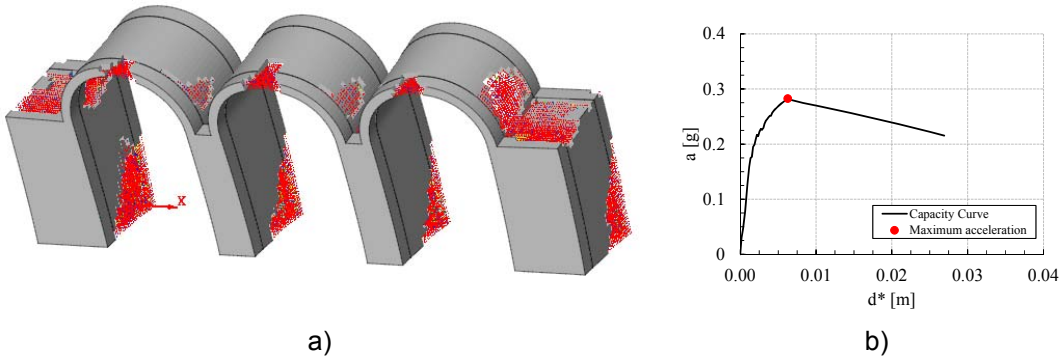

a) b)

Fig. 4.6 FE model of a three-span arch bridge: a) crack pattern with plastic hinges; b) capacity curve

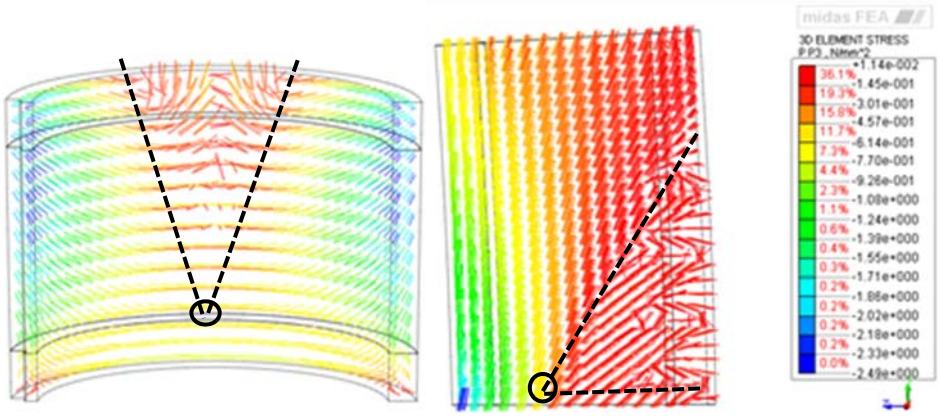

a) *b)*

Fig. 4.7 Principal stress vectors, with location of plastic hinges: a) plane view of deck (central span), b) lateral view of pier

The models required definition of the parameters listed in Tab.4.1.
Average material properties were assessed according to the usual values defined in the literature on the basis of laboratory tests (compression on cores) and in situ tests (flat-jack, sonic, Schmidt Hammer and dynamic tests) conducted on masonry bridges (Pelà et al., 2009, Brencich et al., 2008). The compressive strength of masonry adopted for bridges is generally considered to be 5-7 MPa and the corresponding tensile strength as 0.1-0.2 MPa, with an elastic modulus of E=5000-6000 MPa, valid for masonry composed of bricks and lime mortar.

Young's Modulus E[MPa]	5000
Compression behaviour	Costant
Tensile behaviour	Linear-Brittle
Tensile Fracture Energy Gft[N/m]	0.01
Compressive Strength fc [MPa]	5.0
Tensile Strength ft [MPa]	0.1

Tab. 4.1 Mechanical properties of masonry in FE models

In our analyses, backfill was also taken into account as a material of poor quality, characterised by density γ=1800 kg/m^3 and linear behaviour, with a very low value for Young's modulus (E=60 MPa).
Especially in railway masonry bridges, the repetitive design according to manuals of practice in use in the early 20th century (Italian State Railways, 1907) generally

produced good-quality masonry, in terms of both mechanical properties and type of block-laying, with well-organised joints of adequate thickness. For this reason, the variable range of mechanical properties of masonry is quite narrow and does not significantly affect ultimate behaviour. Conversely, ultimate resistance under horizontal forces is greatly affected by geometric parameters (number of spans, maximum span length L; arch rise f; arch thickness s; pier height H, longitudinal width B).

Three- and five-span bridges with round arches (f/L=0.5) were therefore examined, with transverse dimension of decks (and piers) of 5.0 m, corresponding to the average width of a single-track masonry railway bridge. Various slenderness ratios of piers (height/width ratio, H/B) and span lengths (L) were adopted. Tab.4. 2 lists the geometric characteristics in parametric analyses.

Span		3	5	
L [m]		6	12	18
f/L=0.5	→ f [m]	3	6	9
s/L=0.08	→ s [m]	0.48	0.96	1.44
H/B =4		7.2	9.6	12
H/B =2	→ B [m]	3.6	4.8	6
H/B =1		1.8	2.4	3

Tab. 4.2 Geometric properties of FE models

The crack pattern of Fig. 6 clearly shows that the transverse global collapse of multi-span bridges with slender piers is generally due to the development of non-dissipative hinges at the base of the piers and the crown of the vaults.

4.3.2 Calibration of k-parameter

Parameter k was calibrated by comparing the value of a_0^* obtained from kinematic analysis, corresponding to five values of k (0, 0.25, 0.5, 0.75, 1), with the maximum acceleration obtained from pushover analyses.

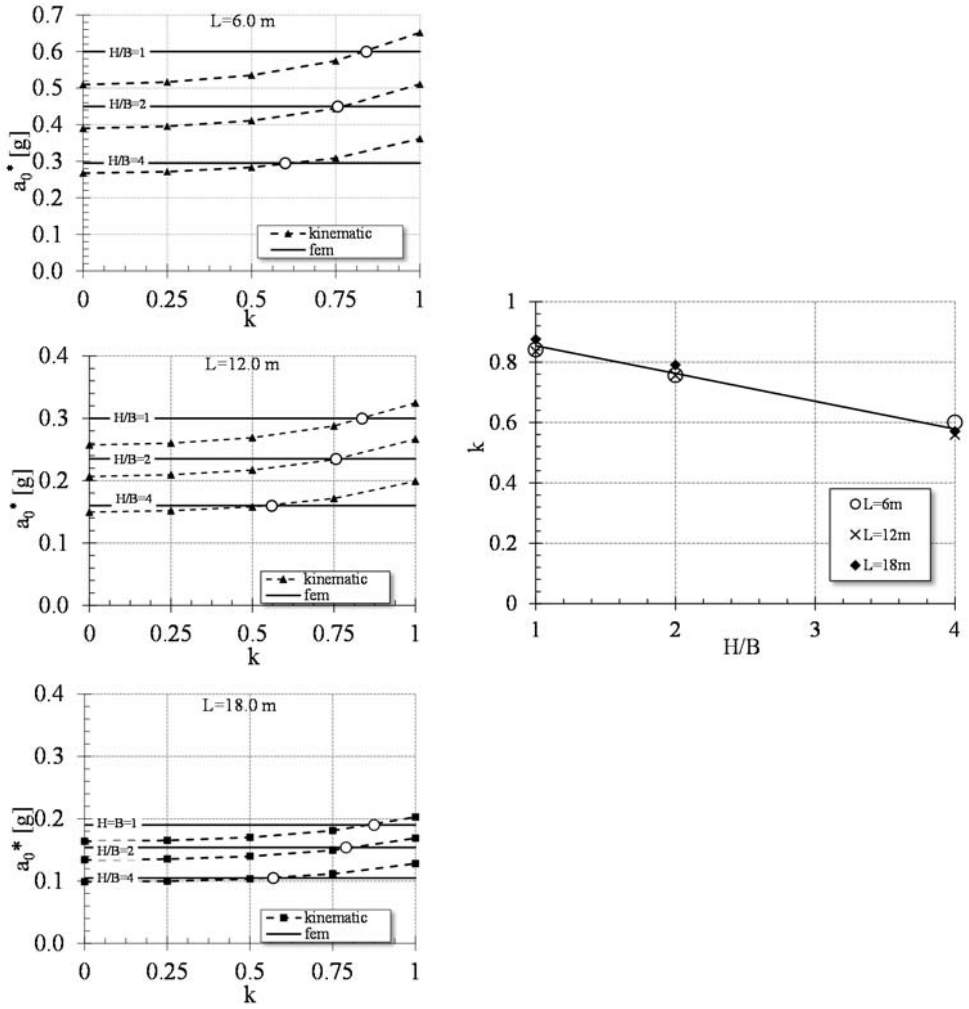

a) *b)*

Fig. 4.8 Calibration of parameter k for 3-span bridges

Fig. 4.8 describes the calibration process for a sample set of three-span bridges. The dotted curves represent the trend of a_0^* as a function of k obtained from limit analysis, and continuous lines represent maximum resisting acceleration from FE analyses. Their intersection represents the optimum value of k, which reduces to zero the error between the simplified kinematic approach and numerical FE results. As a final result, parameter k is expressed as a linear function of pier slenderness (H/B), almost independently of span length L (Fig. 4.8b).

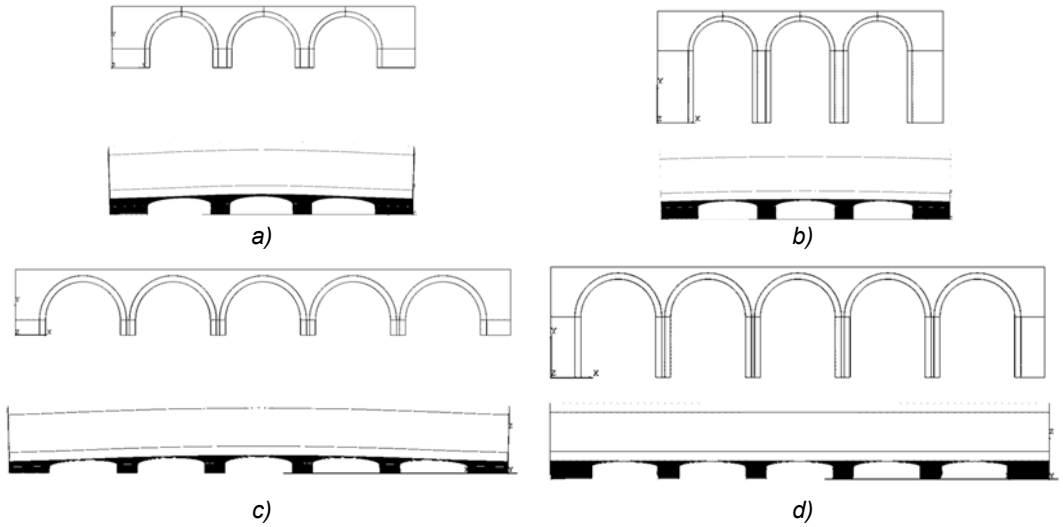

Fig. 4.9 Transverse overall deformed shape at collapse: a) three-span bridge with H/B=1 b) three-span bridge with H/B=4 c) five-span bridge with H/B=1 d) five-span bridge with H/B=4

Qualitatively, when the number of spans increases, lateral restraint at abutments is less effective (Fig. 4.9). When the calibration process was repeated for the set of five-span bridges, the value of k does decrease, showing that it depends on the number of spans, Nspan (see Fig. 4.10).
Thus, the following expression can be adopted as a general law:

$$k = -0.09\frac{H}{B} + \lambda \tag{4.20}$$

where:
λ=0.95 when Nspan=3
λ=0.75 when Nspan=5.
Different values can be obtained by interpolation or extrapolation, to an upper limit of Nspan $=7$. In long multi-span masonry viaducts, the typical sequence of arch and piers is repeated up to five or seven times, and is then interrupted by stiffer structures (‘pier-abutments’) which exert a lateral restraint similar to that of the abutments.

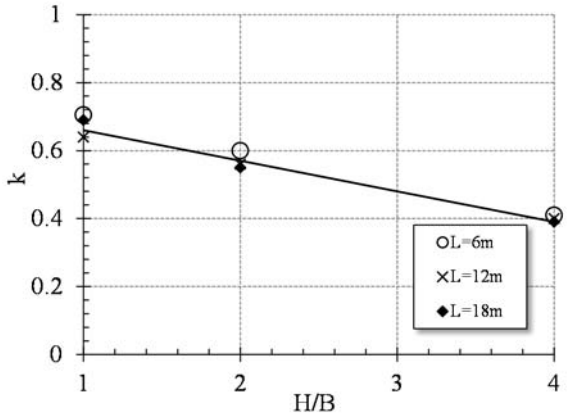

Fig. 4.10 Definition of parameter k for five-span bridges

4.3.3 Safety check for shear failure of piers

The proposed collapse mechanism and the application of the PVW equation to evaluate limit acceleration a_0* lead to overestimation of structure capacity if pier collapse is governed by shear failure. This may occur for squat or medium-slender piers, and also depends on ratio f/L.
In order to exclude this condition, a simplified safety check is recommended for shear verification. The procedure is based on the calculation of shear capacity V_{Rd} of the section at the pier base:

$$V_{Rd} = aBf_{vd} \tag{4.21}$$

where:
A_c=aB is the compressed area of the pier base section, as previously described, and f_{vd} is the shear strength, calculated as follows:

$$f_{vd} = f_{vk} / \gamma_M \tag{4.22}$$

$$f_{vk} = f_{vk0} + 0.4\sigma_n \tag{4.23}$$

where f_{vk} represents the characteristic shear resistance, which must be divided by the partial safety coefficient of masonry γ_M.
Term σ_n is the uniform compressive stress in the compressed area:

$$\sigma_n = \frac{P_i}{aB} \tag{4.24}$$

Once $\Delta z(x_{gi})$ is derived by Eq. 4.8, the maximum shear acting at the pier base can be estimated directly:

$$V_{sd} = a_0^* P_i \Delta z(x_{gi}) \tag{4.25}$$

The ratio between shear resistance V_{Rd} and acting shear V_{Sd} can then be obtained:

$$SF_s = \frac{V_{Rd}}{V_{Sd}} \tag{4.26}$$

and, if $SF_s>1$, the pier collapse mechanism occurs due to rocking or compressive-bending failure, so that limit acceleration can be calculated by the proposed kinematic method.

Conversely, if $SF_s<1$, value a_0^*, calculated with the limit analysis approach, overestimates effective transverse capacity, and maximum resistant acceleration can be evaluated as:

$$a_{sf} = \frac{V_{Rd}}{P_i} \tag{4.27}$$

4.4 Parametric analyses of multi-span railway bridges

4.4.1 Parametric analyses

For the purposes of this work, only bridges with slender piers were examined. In bridges with squat piers (H/B≤1), the overall transverse mechanism is not relevant to seismic vulnerability, and only local effects (due to overturning of spandrel walls) must be verified, longitudinal behaviour generally being more vulnerable.

L [m]=4-6-8-10-12-14-16-18
f/L=0.5-0.4-0.3-0.2-0.1
s/L=0.06-0.08-0.1
H/B=1-2-4-6
p[m]=5

Tab. 4.3 Range of geometric properties values in parametric analyses

Parametric analysis was implemented by varying geometric parameters L, f/L, S/L, H/B and P. All parametric values are listed in Tab. 4.3, and are representative of the ranges identified in the statistical survey. As regards material properties, masonry compressive strength f_M adopted in the kinematic model was assumed to be 5.0 MPa in all cases.

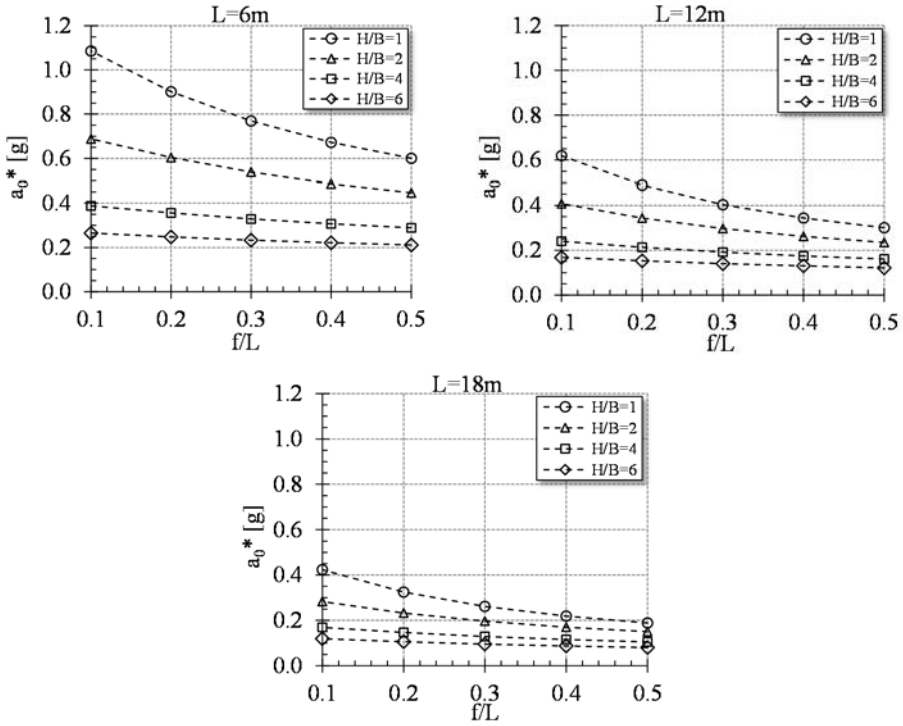

Fig. 4.11 Transverse capacity of multi-span bridges: influence of f/L

The main results of the parametric study are reported below and shown in Fig. 4.11-Fig. 4.13 shows that transverse capacity is sensitive to pier slenderness (ratio H/B), as well as to arch span-to-rise ratio f/L. In particular, the most vulnerable structures are bridges with very slender piers, as expected (H/B=4-6). Bridges with semi-circular arches are more vulnerable than those with depressed arches, limit acceleration value a_0* being minimum for f/L=0.5.

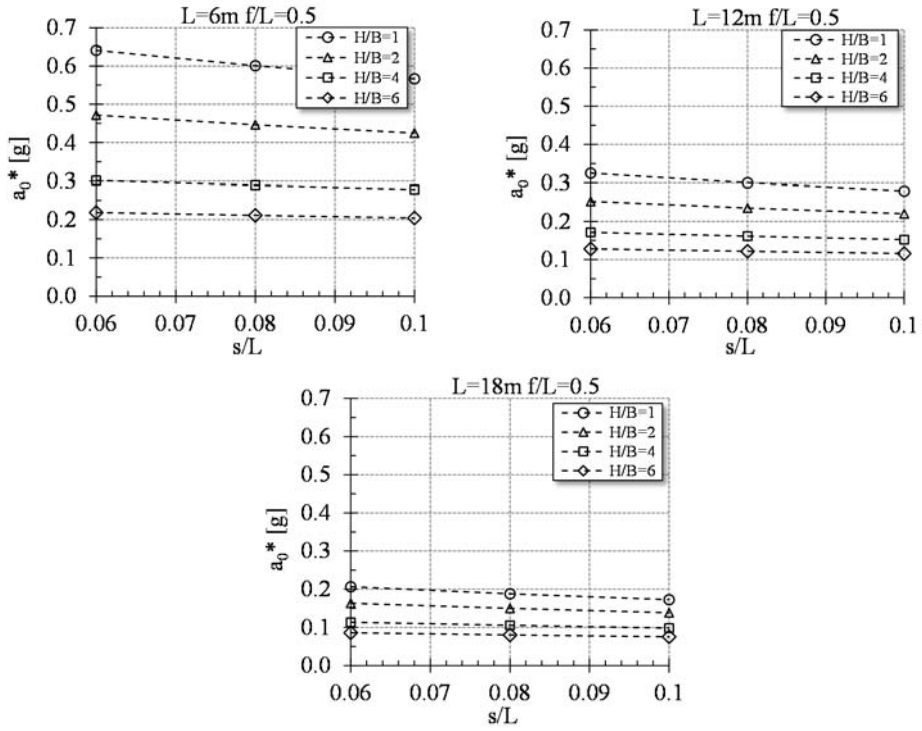

Fig. 4.12 Transverse capacity of multi-span bridges: influence of S/L

Arch thickness, characterised by the adimensional parameter s/L, significantly affects the longitudinal response (Clemente et al., 1995, Tecchio et al., 2012), but has less influence on transverse capacity, as Fig. 4.12 shows. Conversely, a parameter which greatly influences the transverse seismic response is absolute span length L (Fig. 4.13), collapse acceleration a0* decreasing greatly as span length increases.

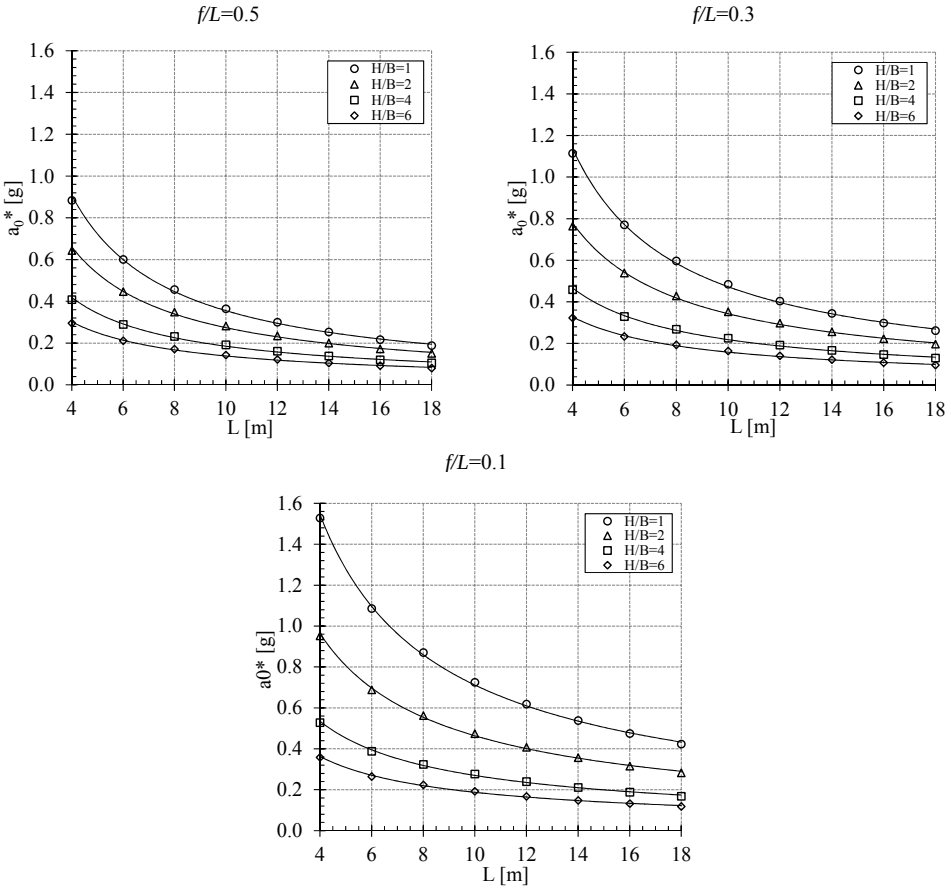

Fig. 4.13 Transverse capacity of multi-span bridges: influence of span length L

Fig. 4.13 also shows that, for fixed values of the parameters f/L and H/B, the limit acceleration a_0* of the overall transverse response can be approximated by power functions. Once these functions have been analytically defined, iso-acceleration curves, representing limit horizontal acceleration a_0^* of the bridge as a function of two geometric parameters, H/B and L, can be plotted. These curves are shown in Fig. 4.14-Fig. 4.16 for values of ratio f/L, corresponding to bridges with semi-circular arches (f/L=0.5), medium depressed arches (f/L=0.3) and depressed arches (f/L=0.1).

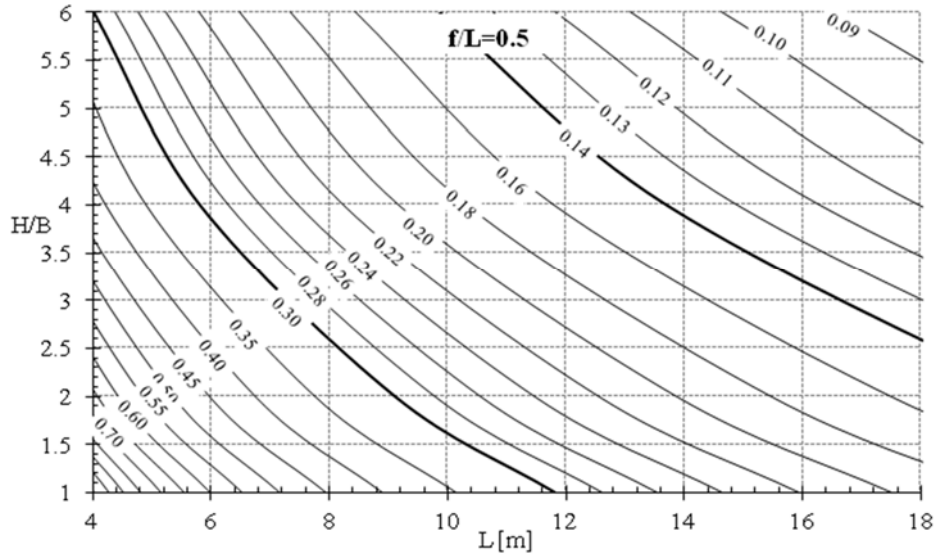

Fig. 4.14 Iso-acceleration curves for three-span bridges with semi-circular arches (f/L=0.5)

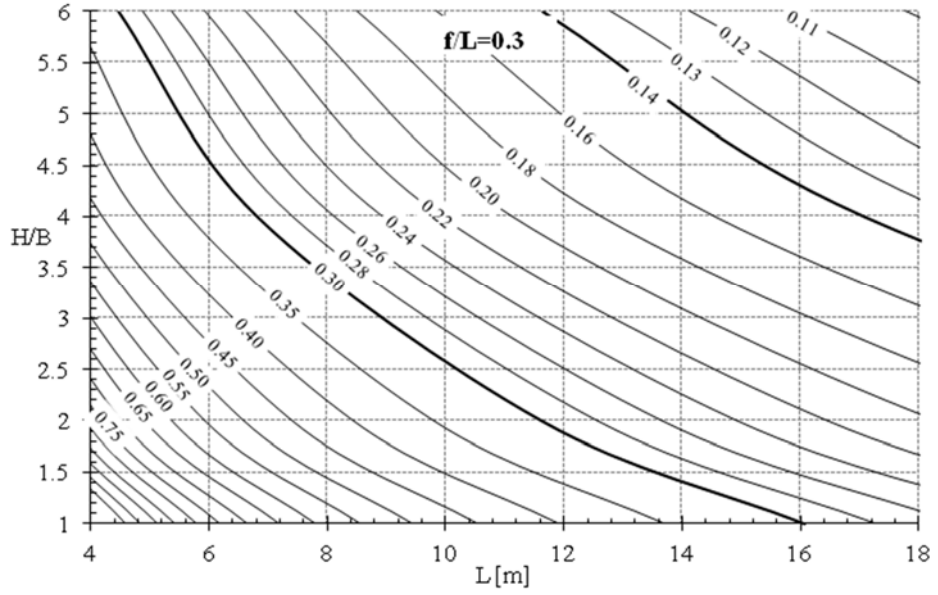

Fig. 4.15 Iso-acceleration curves for three-span bridges with medium depressed arches (f/L=0.3).

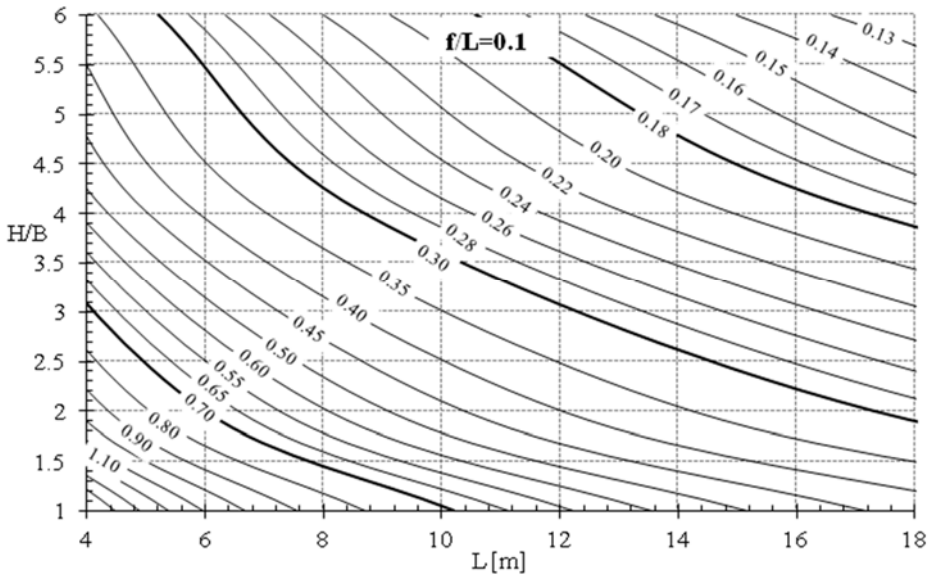

Fig. 4.16 Iso-acceleration curves for three-span bridges with very depressed arches (f/L=0.1)

These graphs can be used for preliminary evaluation of the overall transverse seismic capacity of a multi-span bridge, once the main geometric parameters characterising it are known (e.g., by simple visual inspection of the bridge and a geometric survey).

4.5 Example

According to current codes for the safety assessment of existing constructions (e.g., NTC, 2008), local mechanisms in masonry structures can be simply checked by linear kinematic analysis. At the Serviceability Limit State, seismic verification is accomplished by comparing acceleration a^*_0 triggering the collapse mechanism with the expected value of elastic spectral acceleration (corresponding to period T=0 s):

$$a_0^* \geq a_g S \tag{4.28}$$

where ag is peak ground acceleration expected in reference period PVR on a type A soil (rock soil), and S is the amplification coefficient for other soil categories and specific topographic conditions (S=1 for soil A).

At the Ultimate Limit State, a preliminary safety check can also be carried out with the linear kinematic approach, adopting an appropriate behaviour factor q (value q=2 is suggested for masonry structures; NTC, 2008). In this case, the expected spectral acceleration must be reduced in proportion to the q-factor:

$$a_0^* \geq \frac{a_g S}{q} \tag{4.29}$$

The above verification procedure is applied to an existing three-span railway masonry bridge (RB1), adopted as reference. The main geometric parameters are shown in Fig. 4.17: compressive strength f_M= 5MPa is adopted for masonry, with γ_M=1800 kg/m^3. The structure is located on a type D soil.

The limit values of horizontal acceleration were derived from the iso-acceleration curves previously obtained, as shown in Fig. 4.18, according to the geometric parameters of Fig. 4.17.

Overall safety factors SF were obtained from the corresponding peak ground acceleration value, a_g[g], computed for a rock soil with a probability of being exceeded by 10% in 50 years at the Ultimate Limit State (ULS) and 63% in 50 years at the Serviceability Limit State (SLS). The ag values listed in Tab. 4 are compatible with those expected for Zone 1 of the Italian seismic zoning map.

The shear failure safety check is carried out at the end at the ULS. Macro-block 2 (Fig. 4.2) is used as an example, with x_{g2}=3.9 m, y_{g2}=5.643 m, z_{i2}=0 m. Shear capacity V_{Rd} of the section at the pier base is directly evaluated by Eq. (4.17), VRd= 691 kN. Maximum shear V_{sd} acting at the moment of collapse at the pier base can be estimated once transverse displacement $\Delta z(x_{gi})$ and limit resistant acceleration a_0*are known:

P2=1607 kN

a^*_0=0.285g

$\Delta z(x_{gi})$= 0.947 is given by Eq. (4.8), where C=26 m, and parameter k=0.59 is obtained from Eq.(4.16), with λ=0.95.

	ULS	**SLS**
a_g [g]	0.345	0.118
S	1.683	1.800
a_gS [g]	0.581	0.212
q	2.000	1.000
a_gS/q	0.290	0.212
a^*_0 [g]	0.285	0.285
SF	0.98	1.34

Tab. 4.4 Spectral acceleration values; a^*_0[g]: limit horizontal acceleration for overall mechanism; SF: corresponding safety factor

V_{sd} at the pier base can be thus estimated from Eq. (20), V_{sd}= 433 kN, so that the ratio between shear resistance V_{Rd} and acting shear V_{Sd} is SFs= 1.59. The pier collapse mechanism occurs due to rocking or compressive-bending failure, and the overall safety factor is that given in Tab.4.4.

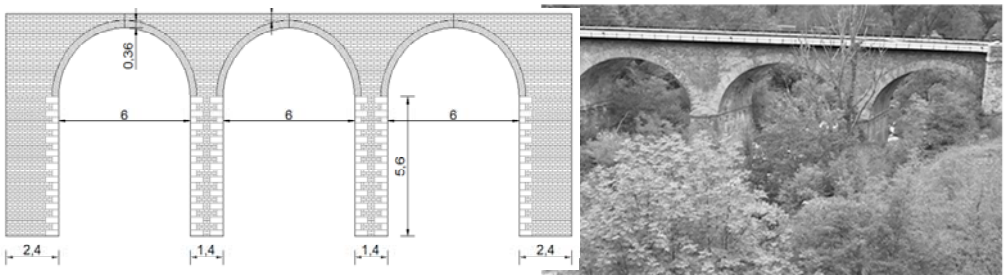

Fig. 4.17 RB1 bridge: L=6.0m; f=3.0m; S=0.36m; H=5.6m; B=1.4m; f/L=0.5; H/B=4; S/L=0.08; p=5m

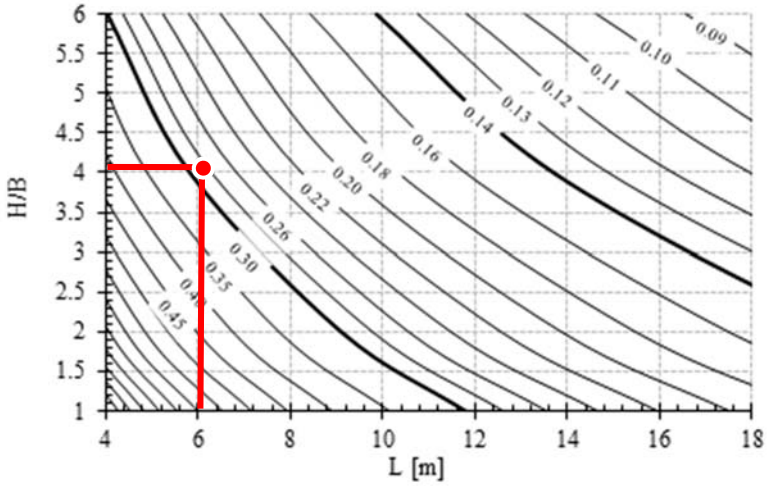

Fig. 4.18 Resistant horizontal acceleration a^*_0 of RB_1

4.6 Conclusion

Of the simplified approaches which may be used for vulnerability assessment of masonry bridges, limit analysis is highly effective in verifying the safety of this class of structures, providing a limit of horizontal seismic capacity. This thesis presents a limit analysis procedure to evaluate the overall transverse seismic capacity of multi-span masonry bridges.

In the first part, seismic load multiplier α_0 is calculated for the global transverse mechanism by definition of virtual displacements and applying the Principle of Virtual Work to the kinematic chain.
Non-linear Static Analyses were also carried out to validate the envisaged collapse mechanism and to calibrate the restraint effect of the abutment.
In the second part of the work, the simplified kinematic method is extensively used in a parametric study on multi-span railway masonry bridges, evaluating the influence of geometric parameters on the transverse response under horizontal loads. The final result is a series of graphs, providing the value of overall transverse collapse acceleration a_0^* for multi-span bridges, on the basis of easily calculated geometric parameters only.
The proposed model could be misleading in the case of squat piers, when pier collapse does not occur due to rocking or compressive-bending failure. A simplified safety check is proposed to evaluate whether shear failure at the pier base is induced by lower collapse acceleration than the previously determined a_0^*.

5 VULNERABILITY ASSESSMENT OF MASONRY BRIDGES CLASSES BY LIMIT ANALYSIS

5.1 Introduction

The bridge seismic safety can be thus verified with limit analysis, provided that local and overall collapse mechanisms, in longitudinal and transversal direction, are analysed.
In this work, as innovative contribution, a comprehensive parametric study based on limit analysis procedure is developed, aimed at supplying a direct tabular procedure for the preliminary seismic assessment of single-and multi-span masonry bridges. The kinematic method is applied for evaluating the structural capacity under horizontal seismic forces, which could affect the structure in longitudinal or transverse direction and activate local or global collapse mechanisms.
On the basis of an initial statistical survey on a large stock of about 750 units (see 3.1.1), railway masonry bridges are classified into homogeneous classes accounting for both the typological characteristics and the expected collapse mechanism. Once the simplified kinematic procedure is set for all possible collapse mechanisms of single- and multi-span structures, a parametrical study using limit analysis is performed for each class, for appropriate ranges of relevant geometrical parameters. Finally, a complete set of iso-acceleration curves representing the seismic capacity in terms of limit horizontal acceleration a_0^* is derived Input data are simple geometric parameters directly detectable by visual inspections and geometric survey.

5.1.1 Influence of bridge type and geometry on the behaviour

Single-span masonry arch bridges are generally characterised by massive abutments, which in most cases can be schematised as infinitely rigid constraints. The most vulnerable element, under seismic excitation in the longitudinal direction, is the masonry arch, which exhibits an antimetric collapse mechanism by means the formation of three rigid voussoirs and four hinges (Fig. 5.1a), located where the thrust line crosses the arch ring (Clemente, 1998). This collapse mechanism is referred herein as A-L (Arch mechanism in Longitudinal direction, see Table 5.1).

Single-span masonry viaducts have often high abutments: in this case, the longitudinal mechanism may involve arch and abutments, which becomes an overall mechanism, activated by the presence of two hinges at the base of the abutments and two hinges in the arch (da Porto et al., 2007 and De Luca et al., 2004; Fig. 9b). This mechanism is called herein as Arch-Abutment mechanism in Longitudinal direction (AA-L). In some cases, it is also possible that one abutment remains fixed and only the other one participates to the mechanism (semi-global mechanism).

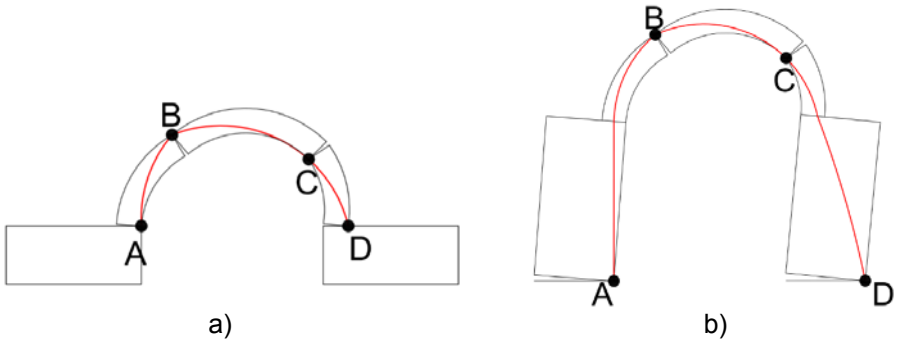

Fig. 5.1 Single-span bridges: a) collapse mechanism of arch with squat abutments (A-L); b) collapse mechanism of arch with high abutments (AA-L).

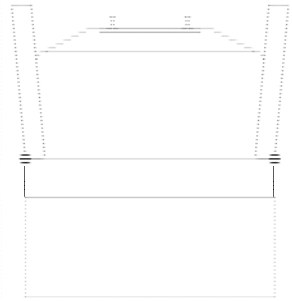

Fig. 5.2 Out-of-plane overturning of spandrel walls (SW-T mechanism).

In single span bridges, due to the high inertia of the abutment wall, the spandrel wall, which can easily rotate out-of-plane, is the most vulnerable element in transverse direction (Spandrel Wall Transverse mechanism, SW-T, Fig. 5.2). This collapse does not generally involve the structural safety of the arched structure, but it compromises ballast support and rail tracks (Tecchio et al., 2012), making the entire bridge useless (Resemini and Lagomarsino, 2004).
In squat multi-span bridge structures, spandrel walls at the arch springing constitute fixed restraints for the arch, thus each span can be considered as independent. The expected collapse mechanisms are thus the same as those listed for single-span

bridges with squat abutments (A-L for any of the arches in longitudinal direction, Fig. 5.1a, or SW-T for spandrel walls in transverse direction, Fig. 5.2).

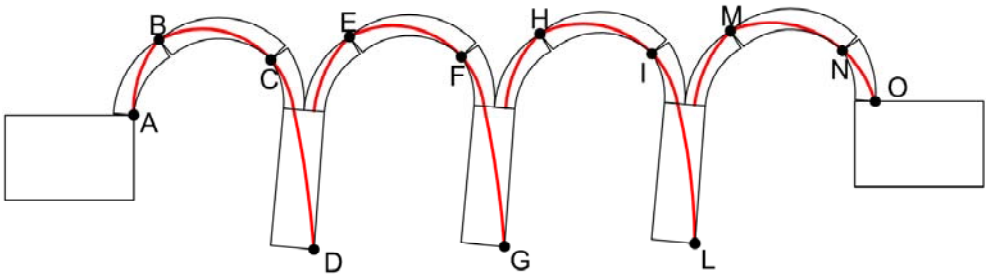

Fig. 5.3 Multi-span bridges: overall collapse mechanism in longitudinal direction (AP-L).

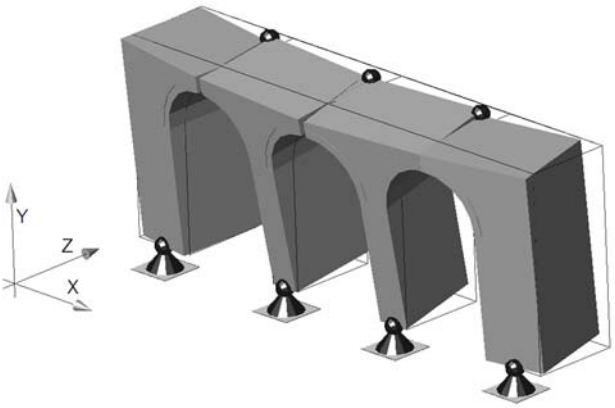

Fig. 5.4 Multi-span bridges: overall mechanism under transverse seismic action (AP-T).

In the case of multi-span structures with slender piers, the kinematic chain in longitudinal direction may involve arches only (local mechanism A-L), or the whole series of arches and piers (overall Arch-Pier Longitudinal mechanism, AP-L, Fig. 5.3), with formation of plastic hinges at the pier bases. For these structures, local (A-L) and overall (AP-L) collapse mechanisms are both possible in case of piers of medium slenderness ($1<H/B<4$). Unfortunately, a single geometric parameter characterising pier or abutment behaviour for a slender structure cannot be provided to define the specific local or overall longitudinal mechanism. Some authors (Clemente et al., 2010), tried to supply diagrams relating several ratios (*B/L*, *f/L*, *H/L*, P/*L* etc.).
When this type of bridge is subjected to transverse seismic excitation, local collapse of the spandrel walls (SW-T) may happen, but also an overall collapse mechanism, involving both arches and piers (AP-T mechanism) can occur. The overall transverse mechanism causes flexural failure at the base of the piers and tensile failure of the arches at the arch crowns. This mechanism is influenced by pier slenderness and lateral restraint degree provided at the abutments, which is generally higher in case

of shorter bridges. The collapse configuration is represented by the 3-D kinematic model of Fig. 5.4.

5.1.2 Classification of masonry bridge structures

The proposed classification of masonry arch bridges relies only on typological characteristics and geometrical parameters, easily detectable by visual inspections and geometrical survey. The ranges of parameters were defined on the basis of the statistical survey and its comparison with the design rules described in 3.1.1.

CLASS	**SUB-CLASS**				
N. of spans	*Collapse mechanisms*	*Abutment/ Pier parameter*	*Arch parameter*		
		h/L, H/B[-]	*L[m]*	*f/L[-]*	*s/L[-]*
1) SINGLE-SPAN BRIDGES (SS)	**1.1)** SQUAT ABUTMENT (sa) Long.: **A-L** Transv: **SW-T**	*h/L*≤0.75	3≤ *L*<6	0.1≤*f/L*<0.3 0.3≤*f/L*<0.45 *f/L*≥0.45	0.06≤*s/L*<0.09 0.09≤*s/L*<0.15 *s/L*≥0.15
			6≤ *L*<10 10≤ *L*<20	*f/L*≤0.1 0.1≤*f/L*<0.3 0.3≤*f/L*<0.45 *f/L*≥0.45	*s/L*<0.06 0.06≤*s/L*<0.09 0.09≤*s/L*<0.15 *s/L*≥0.15
			L≥20	*f/L*≤0.1 0.1≤*f/L*<0.3 0.3≤*f/L*<0.45	*s/L*<0.06 0.06≤*s/L*<0.09
	1.2) HIGH ABUTMENT (ha) Long.: **A-L, AA-L** Transv: **SW-T**	*h/L*>0.75	3≤*L*<6 6≤*L*<10	0.3≤*f/L*<0.45 *f/L*≥0.45	0.06≤*s/L*<0.09 0.09≤*s/L*<0.15 *s/L*≥0.15
2) 2-3 SPAN BRIDGES (TS)	**2.1), 3.1)** SQUAT PIERS (sp) Long.: **A-L** Transv: **SW-T**	*H/B*≤1	3≤ *L*<6	*f/L*≤0.1 0.1≤*f/L*<0.3 0.3≤*f/L*<0.45 *f/L*≥0.45	0.06≤*s/L*<0.09 0.09≤*s/L*<0.15 *s/L*≥0.15
			6≤ *L*<10 10≤ *L*<20		*s/L*<0.06 0.06≤*s/L*<0.09 0.09≤*s/L*<0.15 *s/L*≥0.15
3) MULTI-SPAN BRIDGES (MS)	**2.2), 3.2)** SLENDER PIERS (sl) Long.: **A-L, AP-L** Transv: **SW-T, AP-T**	*H/B* >1	*L*≥20	*f/L*≤0.1 0.1≤*f/L*<0.3 0.3≤*f/L*<0.45	*s/L*<0.06 0.06≤*s/L*<0.09

Tab. 5.1 Proposed classification of arch masonry bridges.

The parameters chosen for the classification were: number of spans, span length (L), arch rise (f), arch thickness (s), pier (H, B) and abutment (h) dimensions. These data are functional to the individuation of the collapse mechanisms characterising each subclass. According to this scheme, for the proposed simplified tabular procedure, those data will be sufficient to assess the correspondent horizontal limit acceleration a_0^*.

The bridge classification is reported in Table 5.1, and examples of structures representative of each sub-class are reported in Fig. 5.5. Classes are based on the number of spans; sub-classes are identified on the basis of pier/abutment characteristics and related to collapse mechanisms. For each subclass, different combination of arch parameters (L, f/L, s/L) can be considered.

In this work, only bridges with very squat abutment and piers belonging to classes 1.1, 2.1, and 3.1 (SS_sa, TS_sp, and MS_sp) are supposed to be subjected only to local collapse mechanisms (A-L and SW-T). Structures belonging to other classes are assessed for both local and overall mechanisms, according to a conservative approach.

a) single-span, squat abutments (SS_sa)

b) single-span, high abutments (SS_ha)

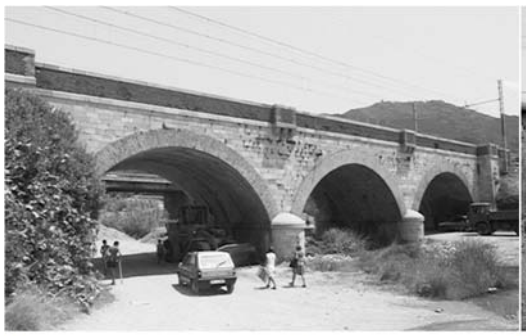

c) three-span, squat piers (TS_sp)

d) two-span, slender piers (TS_sl)

e) multi-span, squat piers (MS_sp)

f) multi-span, slender piers (MS_sl)

Fig. 5.5 Example of masonry arch bridges of the analysed stock.

5.2 Limit analysis for seismic assessment of masonry arch bridges

The limit behaviour of masonry structures is usually a matter of equilibrium of rigid blocks, rather than a problem of material strength (Clemente et al 1995). Hence, the type of collapse mechanism depends on geometric parameters and external loads. In limit analysis it is possible, however, to take into account also material strength, e.g. by the reduction of the design effective thickness of the section, as proposed by Harvey (1988). This reduction is applied in this study.

In this work, limit analysis is used to estimate the load multiplier α_0 triggering the collapse mechanism of the arch bridge under horizontal seismic loads. The procedure consists of an iterative application of the Principle of Virtual Work (PVW). Collapse multiplier α_0 is calculated according to the following steps:

(i) definition of a Cartesian coordinate system and subdivision of the structure into blocks;

(ii) identification of the collapse mechanism;

(iii) definition of the force system applied to the structure;
(iv) application of the PVW.
Once external forces (vertical load P_i and horizontal seismic force $\alpha_0 P_i$, proportional to the bridge masses) are applied and virtual displacements are calculated in the centre of the mass G_i of each macro-blocks, seismic load multiplier α_0 can be calculated with the PVW equation, according to the collapse mechanism and to the related force system.
Collapse trigger acceleration a_0^* can then be obtained with the following equation (NTC, 2008), multiplying α_0 by gravity acceleration g and dividing it by e^*, the fraction of the mass participating to the kinematic mechanism:

$$a_0^* = \frac{\alpha_0 \sum_1^{n+1} P_i}{M^*} = \frac{\alpha_0 g}{e^*} \tag{5.1}$$

where e^* is:

$$e^* = \frac{gM^*}{\alpha_0 \sum_1^{n+1} P_i} \tag{5.2}$$

and M^* represents the participating mass, calculated as:

$$M^* = \frac{\left(\sum_1^{n+1} P_i \Delta x_{gi}\right)^2}{g \sum_1^{n+1} \Delta x_{gi}^2 P_i} \tag{5.3}$$

5.2.1 Single-span bridges in longitudinal direction

The procedure is first presented in relation to the longitudinal mechanism of a single-span bridge with squat abutment (A-L, Fig. 5.1a). Fig. 5.6 shows the force system acting at the centre of mass $G_i(x_i, y_i)$ of the *i*-block: weight of the block P_i, weight of infill material above the i-block P_j (that is exclusively taken into account as applied mass), seismic action $\alpha(P_i+P_j)$ proportional to the masses. The infill material is assumed to be homogenous, and the arch thickness is considered to be constant.
Coordinates of the generic *i*-block are defined on the basis of the arch shape (circular, in our case) and dimensions, loads P_i and P_j are calculated on the basis of the arch geometry, infill height, and specific weight of masonry and infill material.

The inertia forces in Fig. 5.6, are defined according to the work of Clemente, (1995; 1998). Centre of the funicular polygon, position of plastic hinges and thrust line shape are calculated with an iterative procedure (Block et al., 2006). Cross sectional forces N_i and N_{i+1} applied at the i-block are defined once the resultant R_i of the applied forces is known, and each hinge *j* is located at a distance from the arch intrados/extrados, corresponding to half-depth of the cross section necessary to transfer axial force N_i without exceeding the yield stress f_c (masonry stress-block).

In the hypothesis of small displacements, virtual displacements of the antimetric mechanism can be calculated for the three rigid segments (AB, BC, CD), which the arch is divided into, according to the following relations (see Fig. 5.6):

$$\frac{AB}{\theta_{AB}}=\frac{BO}{\theta_{OB}};\frac{OC}{\theta_{OB}}=\frac{CD}{\theta_{DC}} \tag{5.4}$$

$$\text{AB}\quad \begin{cases}\delta x_i=(y_i-y_A)\delta\theta_{AB}\\ \delta y_i=(x_i-x_A)\delta\theta_{AB}\end{cases};\qquad \text{BC}\quad \begin{cases}\delta x_i=(y_O-y_i)\delta\theta_{OB}\\ \delta y_i=(x_O-x_i)\delta\theta_{OB}\end{cases};$$

$$\text{CD}\quad \begin{cases}\delta x_i=(y_i-y_D)\delta\theta_{DC}\\ \delta y_i=(x_i-x_D)\delta\theta_{DC}\end{cases} \tag{5.5}$$

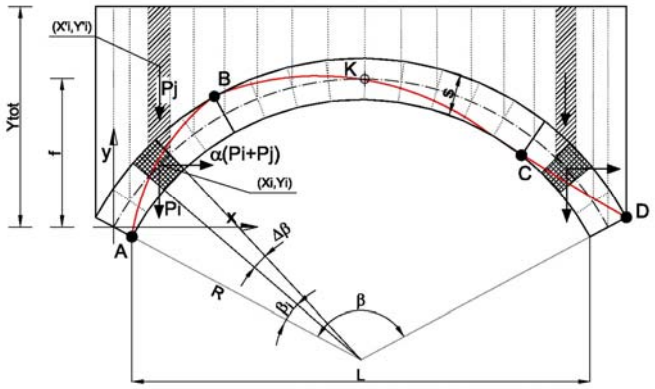

a)

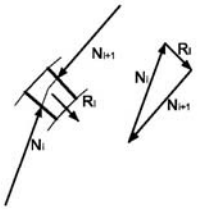

b)

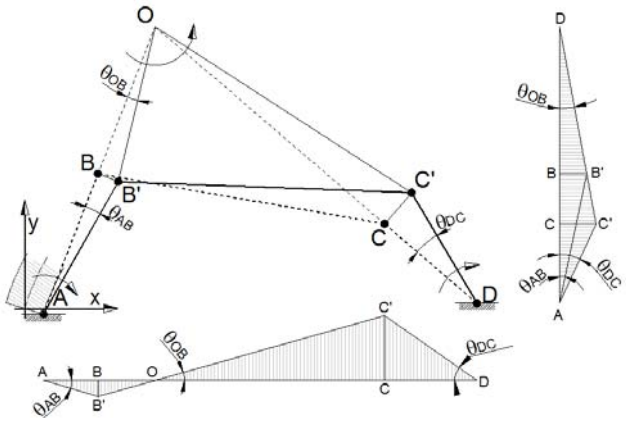

Fig. 5.6 A-L mechanism: a) force system and thrust line, b) equilibrium of each block, c) vertical and horizontal virtual displacements.

Hence, from the PVW, seismic load multiplier α_0 can be calculated:

$$\alpha_0 \sum_i \left(P_i + Q_i \right) \delta_{x,i} - \sum_j Q_j \delta_{y,j} - \sum_i P_i \delta_{y,i} = 0 \tag{5.6}$$

For A-L mechanism, the main geometric parameters influencing the value of α_0 are: span length *L*, span rise *f*, arch thickness *s*.

When collapse in longitudinal direction involves the abutments too, an overall mechanism of AA-L type is activated (see Fig. 5.1b). Virtual displacements are still obtained by Eqs. 5.6-5.77; the structure is also divided by the formation of plastic hinges into 3 rigid blocks rotating around the centre O (see Fig. 5.7). Two central hinges, B and C, are always located in the arch, while the other two (one or both), locate at the base of the abutments. In the implemented procedure, hinges A and D can be placed at different heights from the ground.

The earth wedges behind the abutments may develop significant lateral forces, thus also soil (*Ss*) left and right pressure acting on AB and CD blocks were taken into account in the PVW equation (da Porto et al 2007):

$$\alpha_0 \sum_i \left(P_i + Q_i \right) \delta_{x,i} - \sum_j Q_j \delta_{y,j} - \sum_i P_i \delta_{y,i} + S_s \delta_{s_L} - S_s \delta_{sR} = 0 \tag{5.7}$$

In AA-L mechanism, the load multiplier α_0 is affected not only by span length *L*, span rise *f*, and arch thickness *s*, but also by height *h* and thickness *s'* of abutments.

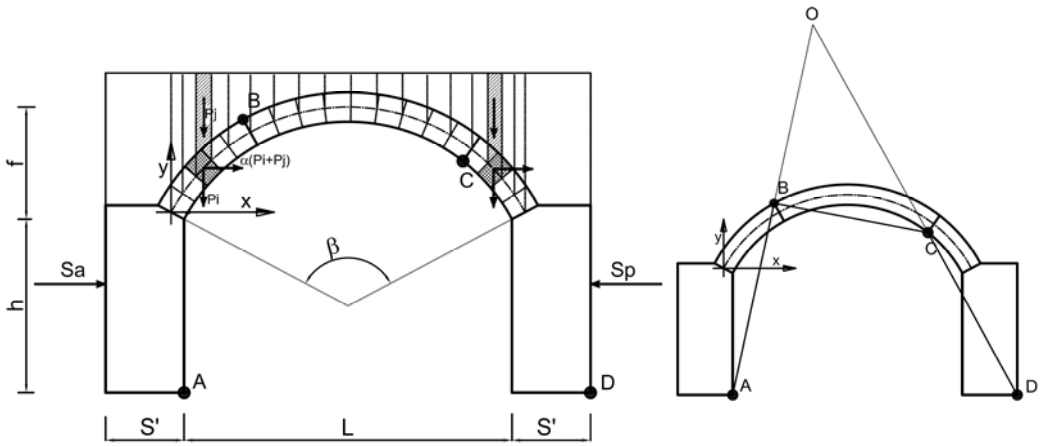

Fig. 5.7 Kinematic model of AA-L mechanism of single-span bridge.

2.1.1 Single-span bridges in transverse direction

In transverse direction, the spandrel wall mechanism (SW-T) develops with the formation of a cylindrical hinge at the base of the wall. Simplified verification can be performed per unit length, considering a rectangular wall with average height *Z*. The load multiplier α_0 is derived by the momentum equilibrium, once virtual displacements are calculated:

$$\eta_P = \eta_N = \theta \frac{(t-a)}{2},\ \xi_P = \vartheta \frac{z}{2},\ \xi_S = \vartheta b,\ \xi_N = \vartheta z \tag{5.8}$$

$$\alpha_0 (P\xi_P + N\xi_N) - P\eta_P - N\eta_N + S\xi_S = 0 \rightarrow \quad \alpha_0 = \frac{\frac{(t-a)}{2}(P+N) - Sb}{Z(P/2+N)} \tag{5.9}$$

where *P* is the wall weight, *S* is the infill material thrust, *N* is the vertical force acting at the top of the wall (e.g. the weight of the parapet), *t* is the wall thickness, *Z* is the wall height and *a* is half-depth of the masonry stress-block (Rota et al., 2005).

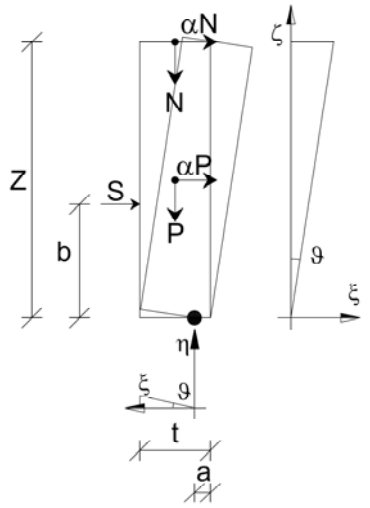

Fig. 5.8 Kinematic model of SW-T mechanism

5.2.2 Multi-span bridges in longitudinal direction

In multi-span bridges with slender piers, subjected to seismic excitation in longitudinal direction, the overall collapse of the arch-pier system (AP-L) has to be analysed. The simplified anti-metric mechanism assumes that a plastic hinge is placed at the base of each pier (D and G in Fig. 5.8), and the ultimate hinge is located at the arch springing of the last span (L). The location of other hinges is derived iteratively with the thrust line method. Fig. 5.8 shows the case of a three-span bridge: 10 hinges and 7 blocks are defined. The centers of rotation are equal to the number of arches, and the lagrangian coordinate system is shown in Fig. 5.8. In the hypothesis of small displacements the following relations are valid:

$$\frac{AB}{\theta_{AB}} = \frac{BO_1}{\theta_{O1B}} = \frac{CD}{\theta_{DC}} = \frac{O_2E}{\theta_{O2E}} = \frac{FG}{\theta_{FG}} = \frac{O_3H}{\theta_{HO3}} = \frac{IL}{\theta_{IL}} \tag{5.10}$$

For each macro-block the virtual displacements can be computed as:

AB $\begin{cases} \delta x_i = (y_i - y_A)\,\delta\theta_{AB} \\ \delta y_i = (x_i - x_A)\,\delta\theta_{AB} \end{cases}$; BC $\begin{cases} \delta x_i = (y_i - y_A)\,\delta\theta_{AB} \\ \delta y_i = (x_i - x_A)\,\delta\theta_{AB} \end{cases}$;

CDE $\begin{cases}\delta x_i = (y_i - y_D)\,\delta\theta_{DC} \\ \delta y_i = (x_i - x_D)\,\delta\theta_{DC}\end{cases}$; EF $\begin{cases}\delta x_i = (y_{O2} - y_i)\,\delta\theta_{O2E} \\ \delta y_i = (x_{O2} - x_i)\,\delta\theta_{O2E}\end{cases}$;

FGH $\begin{cases}\delta x_i = (y_i - y_G)\,\delta\theta_{GF} \\ \delta y_i = (x_i - x_G)\,\delta\theta_{GF}\end{cases}$; HI $\begin{cases}\delta x_i = (y_{O3} - y_i)\,\delta\theta_{O3H} \\ \delta y_i = (x_{O3} - x_i)\,\delta\theta_{O3H}\end{cases}$;

$$\text{LI}\begin{cases}\delta x_i = (y_i - y_L)\,\delta\theta_{LI} \\ \delta y_i = (x_i - x_L)\,\delta\theta_{LI}\end{cases} \tag{5.11}$$

and, at this point, the PVW can be written in the form of Eq. 5.6.

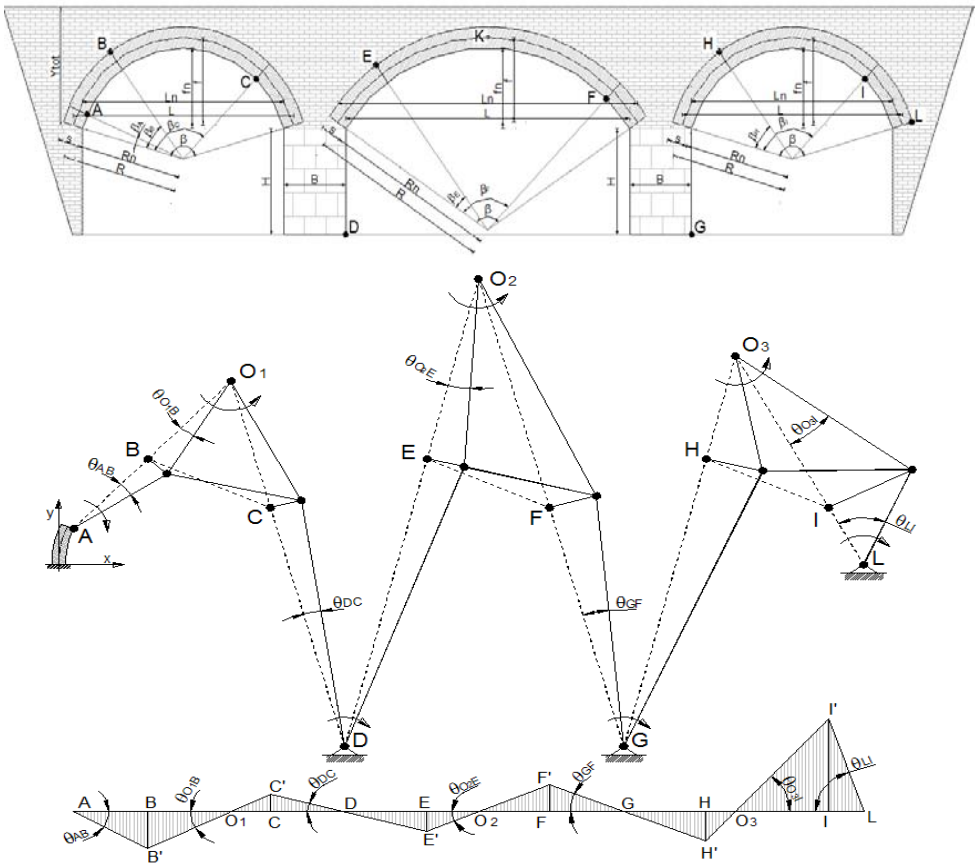

Fig. 5.9 Kinematic model of AP-L mechanism of three-span bridge.

The geometric parameter involved in the AP-L mechanism are: span length *L*, arch rise *f*, piers height *H*, pier longitudinal width *B*, arch thickness *s*, and infill height y_{tot}. Extension of the overall AP-L kinematic mechanism to a different number of span is immediate. In the case of very long multi-span bridges, the study of the overall AP-L mechanism can be limited to a reduced number of spans. In fact, a typical feature of these railway bridges is the presence of larger piers, called *pier-abutments,* every five (or maximum seven) spans, which have the function to stabilise the sequence of arches during construction phase, and to avoid the extension of the kinematic chain at collapse to neighboring spans (Tecchio et al., 2012).

5.2.3 Multi-span bridges in transverse direction

Multi-span bridges with slender piers may present an overall transverse mechanism (AP-T). The kinematic approach to evaluate AP-T is summarised hereafter with reference to the study by Zampieri et al., 2013. The transverse displacement profile at collapse depends on the bridge geometry (higher piers determine larger displacements in the central part of the bridge), and on the degree of lateral restraint provided by the abutments. The total transverse displacement Δz(x), expressed as a function of coordinate x (longitudinal axis of the bridge), can be obtained as the sum of a uniform component (Δz_U, when abutments are completely unrestrained), and the non-uniform transverse displacement $\Delta z_N(x)$, which is assumed to be of circular shape.

When parameter $k = \Delta z_{N_{max}} / \Delta z_{\max}$, with $0<k<1$, is introduced to represent the restraint effect of the abutments, the total transverse displacement can be easily derived as in 4.2.

5.3 Parametric analyses

Parametric study was carried out on a comprehensive set of bridges, according to the classification of Section 2. Geometric parameters *L*, *s*, *f/L*, *s/L*, *H/B*, *P*, number of spans, thickness *t* and height *Z* of spandrel walls (see Tab. 5.2-5.6) were varied according to the range of values of actual bridge subclasses in Tab. 1.

Limit acceleration a_0^* was calculated for each collapse mechanism with the analysis procedures described in 5.2. A complete set of curves representing the seismic

capacity of bridges in terms of horizontal acceleration a_0^* triggering a specific collapse mechanism, as a function of simple geometric parameters, was derived.

All the analyses were performed considering an average value of masonry compressive strength, f_c=5.0 MPa, and a value γ=1800 kg/m^3 for brick masonry and backfill specific weight, according to the usual values defined in literature (laboratory and *in situ* tests conducted on masonry bridges from Pelà et al., 2009, and Brencich et al., 2008). Especially for railway masonry bridges, the repetitive design generally produced good-quality masonry, in terms of both mechanical properties and type of block-laying. For this reason, the variable range of mechanical properties of masonry is quite narrow, and it does not significantly affect the ultimate behaviour.

Iso-acceleration curves, which represent limit horizontal acceleration a_0^* of the bridge as a function of two geometric parameters, were derived for each of the aforementioned collapse mechanism and bridge subclass. The procedure for the construction of iso-acceleration curves can be summarised in the following basic steps:

(i) bridge samples are defined for various subclasses (SS_sa, SS_ha, TS_sl, MS_sl), combining the parameters presented in each of the Tables from 5.2 to 5.6;

(ii) kinematic analysis of the collapse mechanisms relative to each bridge sample is carried out, according to PVW equations, and limit a_0^* values are calculated;

(iii) regression laws of the calculated a_0^* values are obtained with least squares approximation, assuming one representative parameter as a constant, e.g. the *f/L* parameter for the subclass of (SS_sa) bridges;

(iv) for a pre-fixed value of limit acceleration a_0^*, the corresponding iso-acceleration curve is plotted by interpolating with cubic splines the values derived by the regression law.

Automatic routines purposely developed in Visual Basic for Applications (VBA) environment, were used to solve iteratively the PVW equations of the various collapse mechanisms (A-L, AA-L, SW-T, AP-L, AP-T).

It can be observed that at step *(iii),* the a_0^* values obtained for longitudinal mechanisms (AL, AA-L, AP-L), related to fixed values of *s/L*, are almost independent by the absolute value of *L,* thus they can be approximated by the same linear regression law, and the procedure is further simplified (see. Fig. 5.16, Fig. 5.17, Fig. 5.20 and Fig. 5.21).

Linear regression is usually adopted at step *(iii)*; only for the AP-T mechanism power functions were adopted, as they better approximate the numerical results obtained by kinematic analysis.

In the following sub-sections, the parametric study of each masonry bridge class and subclass is summarised as follows:

- a table gives ranges and values of geometric factors used for defining the bridge sample and carrying out the analyses;
- regression laws approximating a_0^* values calculated by limit analysis are presented;
- for each collapse mechanism, iso-acceleration curves are plotted.

The obtained graphs can be directly used for a preliminary seismic verification of masonry bridges, once simple geometric measures of the structure under exam are known. Interpolation of results can be done, when iso-acceleration graphs are given for fixed values of reference parameters (e.g. for (AP-L) mechanism in relation to H/B parameter).

Iso-acceleration curves obtained for SW-T mechanism are presented in relation to bridges of SS_sa, 1.1 class. However, this local failure mechanism should be evaluated both for single- and multi-span masonry bridges, regardless of pier slenderness, thus the graph of Fig. 5.13 can be used for all classes.

It has to be highlighted that only curves obtained for multi-span bridges (MS_sl class) and two-three span bridges (TS_sl, 2.2) are herein reported for the (AP-T) mechanism (Fig. 5.22 and Fig. 5.23). In order to describe seismic vulnerability of all classes, in this chapter some results of 4.2 are reported again.

5.3.1 Single span bridges with squat abutments (SS_sa, 1.1)

BRIDGE CLASS		Single Span_ squat abutment (SS_sq, 1.1)
COLLAPSE MECHANISM		A-L (Arch-Longitudinal mechanism)
PARMETERS	L [m]	[3, 4, 5, 6, 7, 8, 9, 10, 12, 14, 16, 18, 20, 22,24,
	f/L	[0.1, 0.2, 0.3, 0.4, 0.5]
	s/L	[0.04, 0.05, 0.07, 0.10, .13, 0.15]

Tab. 5.2 Geometric ranges for parametric study of A-L mechanism

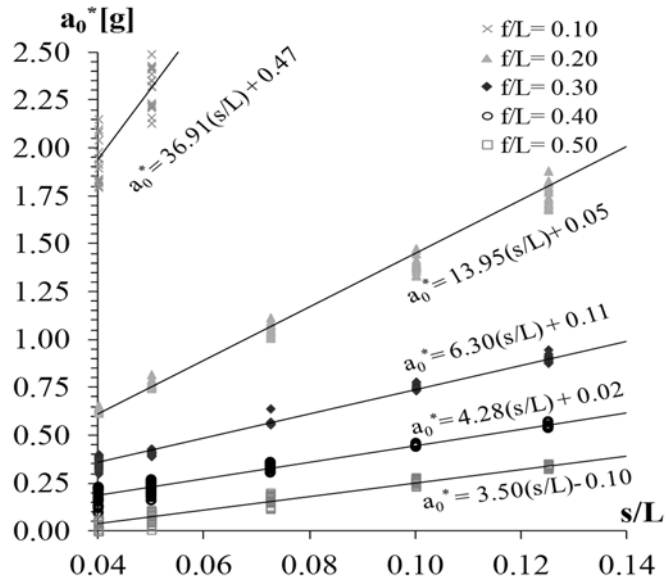

Fig. 5.10 SS_sa bridges: limit acceleration a0 and regression laws for fixed values of f/L.*

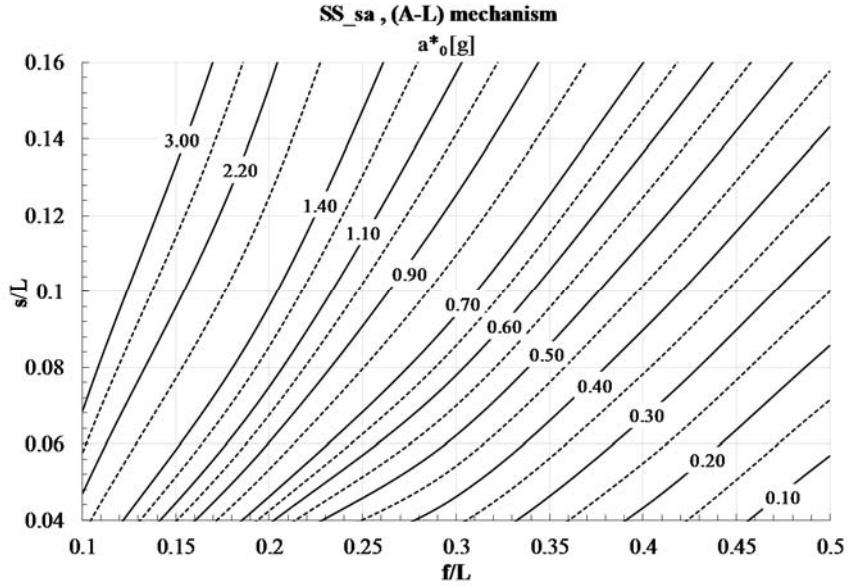

Fig. 5.11 SS_sa bridges: iso-acceleration curves for A-L mechanism.

BRIDGE CLASS		Single Span_ squat abutment (SS_sq, 1.1)**
COLLAPSE MECHANISM		SW-T (local spandrel wall out-of plane
PARMETERS	t[m]	[0.5, 0.75, 1.00, 1.25, 1.50,1.75,
	Z[m]	[1.0, 1.5, 2.0, 2.5, 3.0, 3.5, 4.0]

Tab. 5.3 Geometric ranges for parametric study of SW-T mechanism

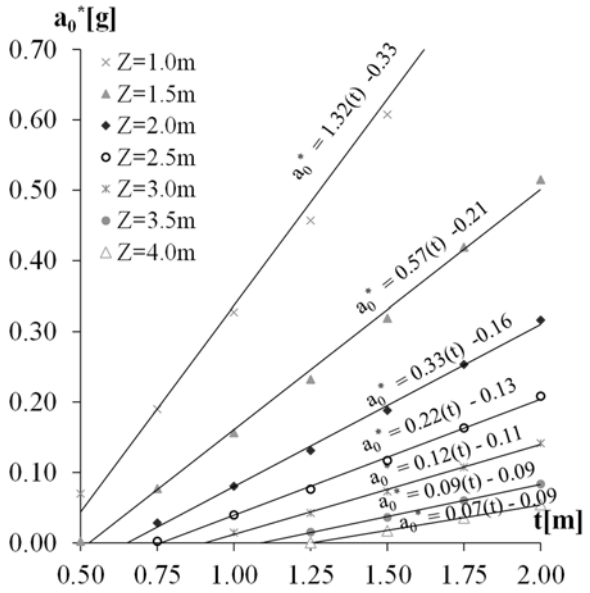

Fig. 5.12 SW-T mechanism: limit acceleration a_0^*, and regression laws for fixed values of Z.

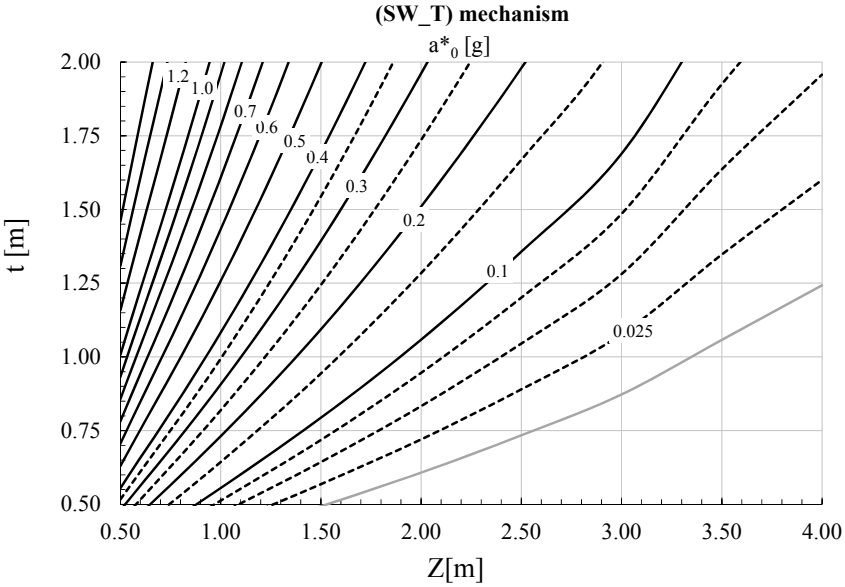

Fig. 5.13 Iso-acceleration curves for SW-T mechanism.

5.3.2 Single span bridges with high abutments (SS_ha, 1.2)

BRIDGE CLASS		Single Span_ high abutment (SS_ha, 1.1)
COLLAPSE MECHANISM		AA-L (global arch-abutment longitudinal
PARMETERS	L [m]	[3, 4, 5, 6]
	f/L	[0.5]
	s/L	[0.08, 0.10, 0.12, 0.14]
	H/B	[2.5, 3.0, 4.0, 6.0]

Tab. 5.4 Geometric ranges for parametric study of AA-L mechanism

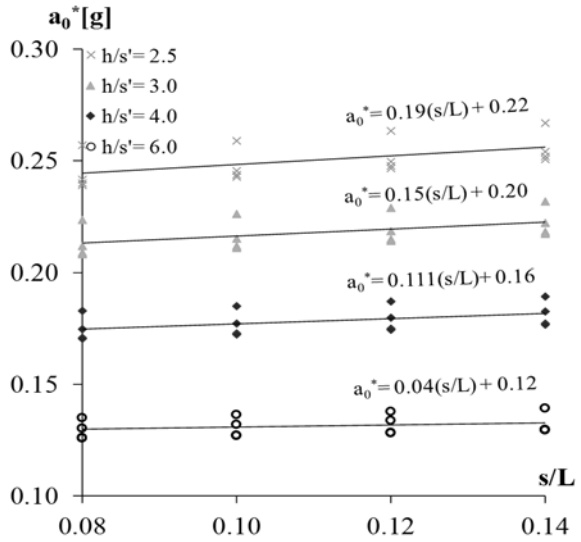

Fig. 5.14 SS_ha bridges: limit acceleration a_0^* and regression laws for fixed values of h/s'.

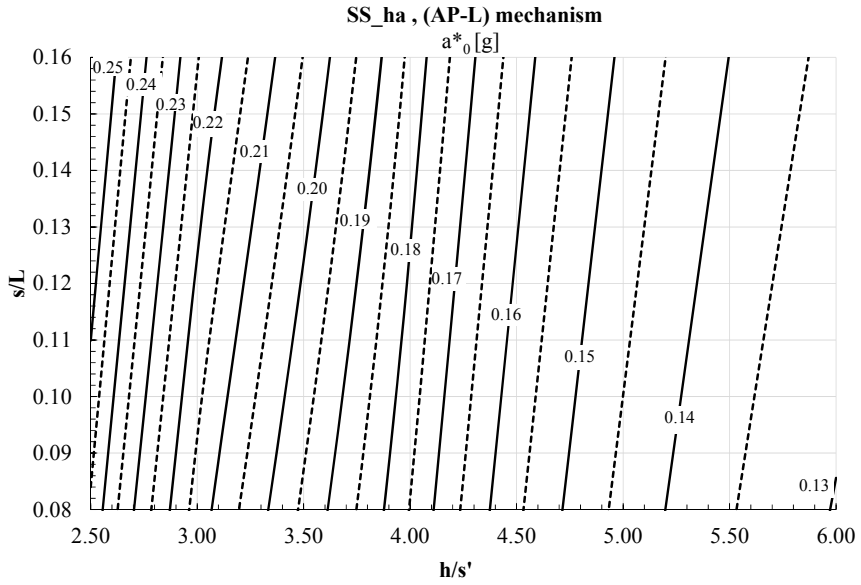

Fig. 5.15 SS_ha bridges: iso-acceleration curves for AP-L mechanism.

5.3.3 *Two-Three span (TS_sl, 2.2) and multi-span (MS_sl, 3.2) bridges with slender piers*

BRIDGE CLASS		Two , Three span_ slender piers, Multi-Span _slender piers
COLLAPSE MECHANISM		AP-L (global arch-piers longitudinal mechanism)
PARMETERS	No. of spans	[3, 5]
	L [m]	[6, 12, 18]
	f/L	[0.15, 0.3, 0.4, 0.5]
	s/L	[0.04, 0.08, 0.10, 0.12, 0.14]
	H/B	[1.5, 2.0, 4.0]

Tab. 5.5 Geometric ranges for parametric study of AP-L mechanism for TS_sl and MS_sl bridges.

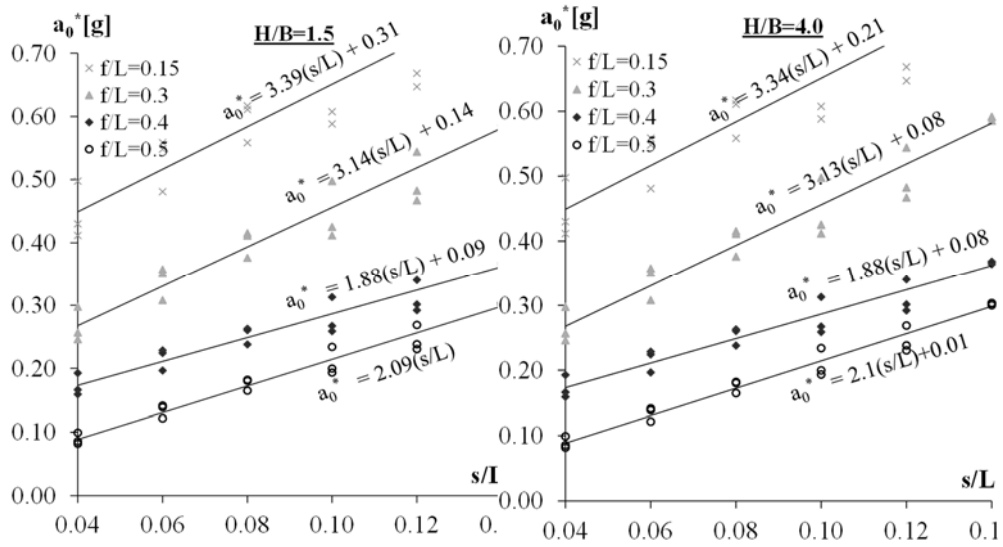

Fig. 5.16 TS_sl bridges: limit acceleration a_0^* and regression laws for fixed values of pier slenderness a) H/B=1.5, b) H/B=4.0, and various f/L ratio.

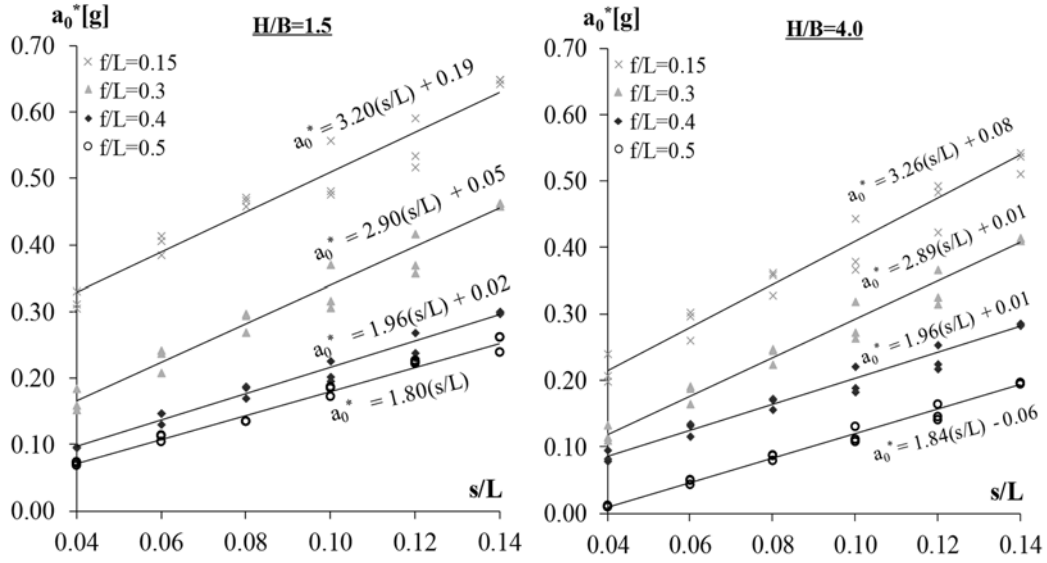

a) b)

Fig. 5.17 MS_sl bridges: limit acceleration a_0^* and regression laws for fixed values of pier slenderness a) H/B=1.5, b) H/B=4.0, and various f/L ratio.

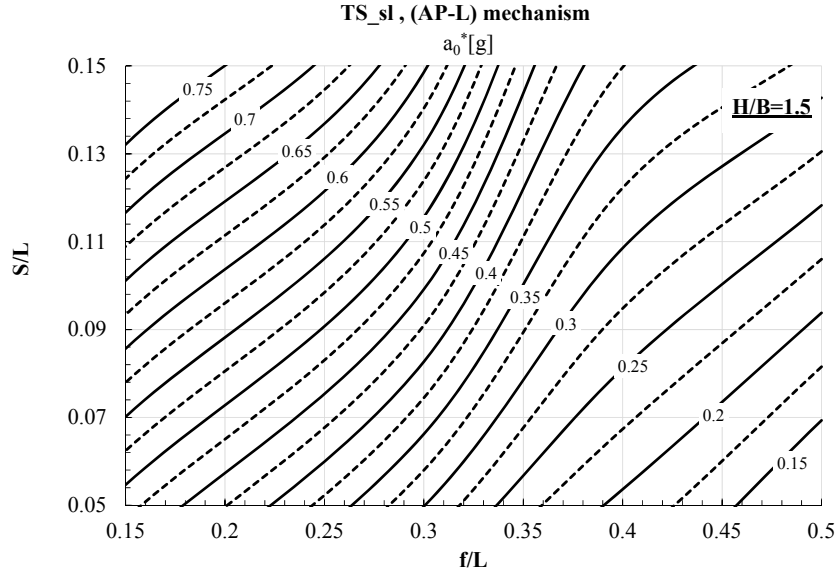

a)

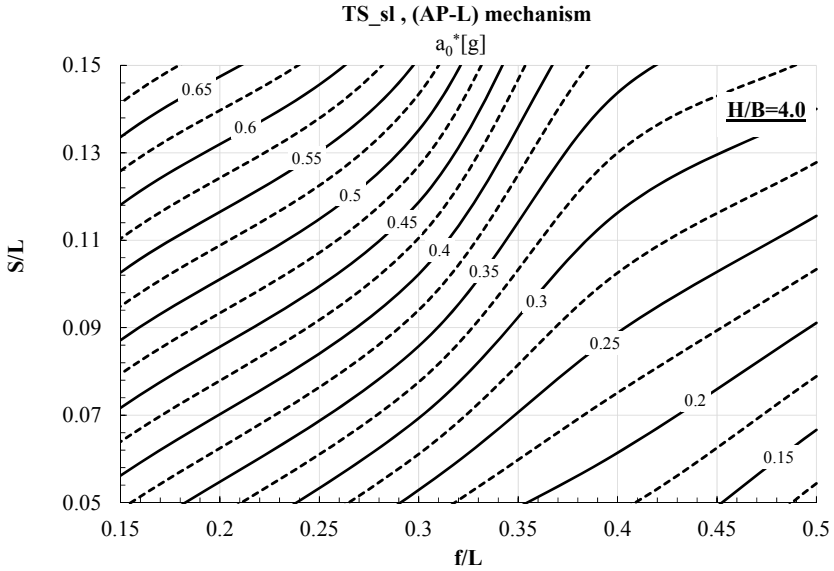

b)

Fig. 5.18 TS_sl bridges: iso-acceleration curves for AP-L mechanism for fixed value of slenderness a) H/B=1.5, b) H/B=4.0.

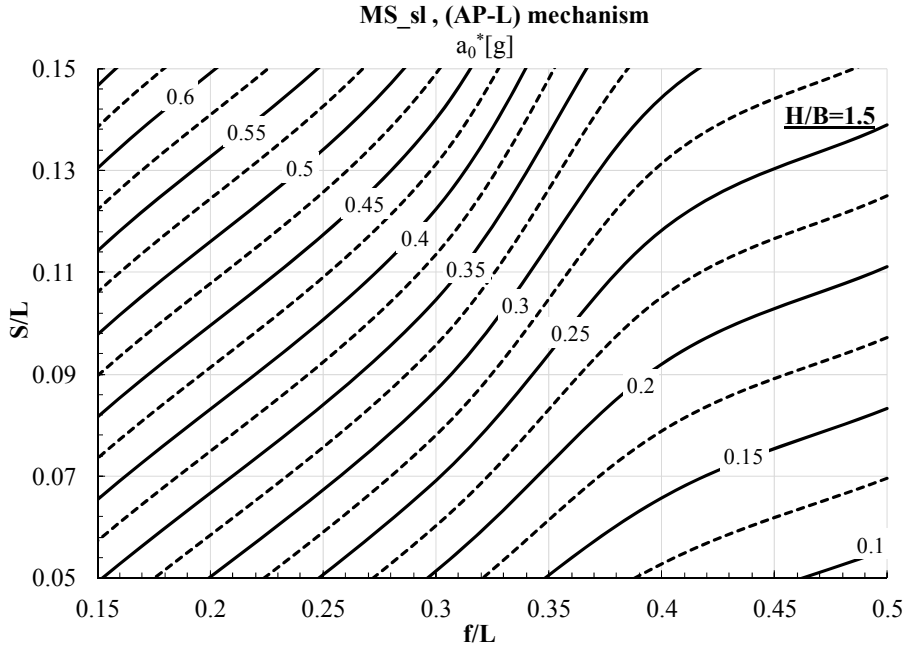

a)

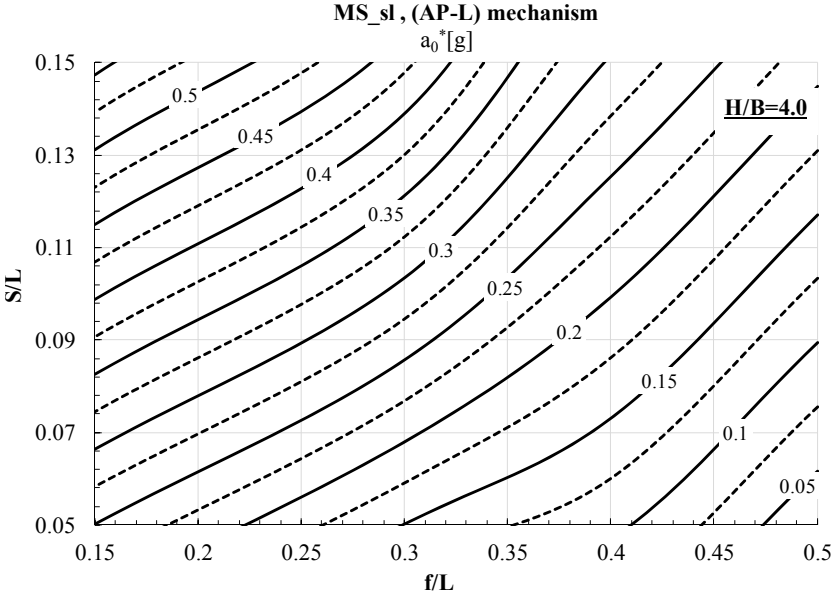

b)

Fig. 5.19 MS_sl bridges: iso-acceleration curves for AP-L mechanism, for pre-fixed values of pier slenderness a) H/B=1.5, b) H/B=4.0

BRIDGE CLASS		Multi Span_ slender piers (MS_sl, 3.2)
COLLAPSE MECHANISM		AP-T (global arch-piers transverse mechanism)
PARMETERS	No. of spans	5
	L [m]	[4,6,8,10,12,14,16,18]
	f/L	[0.1, 0.5]
	s/L	[0.08]
	H/B	[1.0, 2.0, 4.0, 6.0]
	p[m]	[5.0]

Tab. 5.6 Geometric ranges for parametric study of AP-T mechanism for MS_sl class.

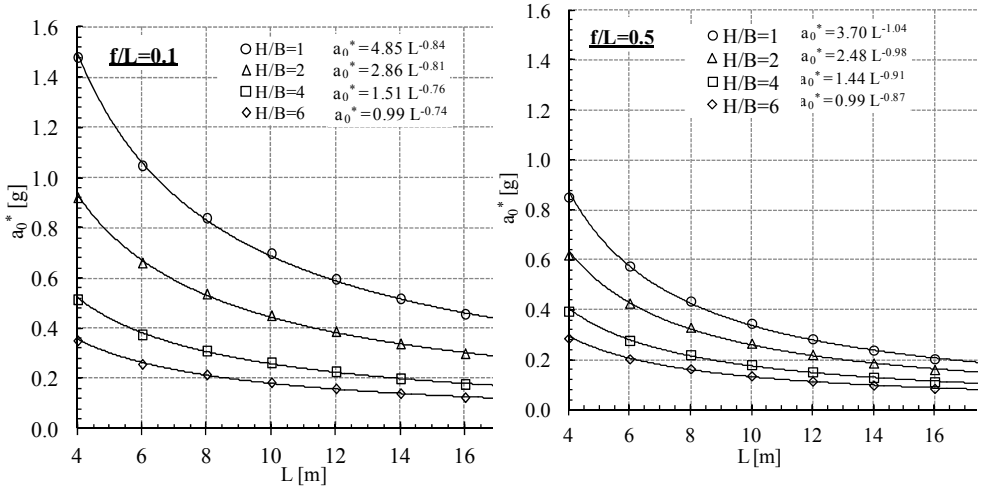

Fig. 5.20 MS_sl bridges: limit acceleration a_0^* and non-linear regression laws for fixed values of f/L ratio a) f/L=0.1, b) f/L=0.5.

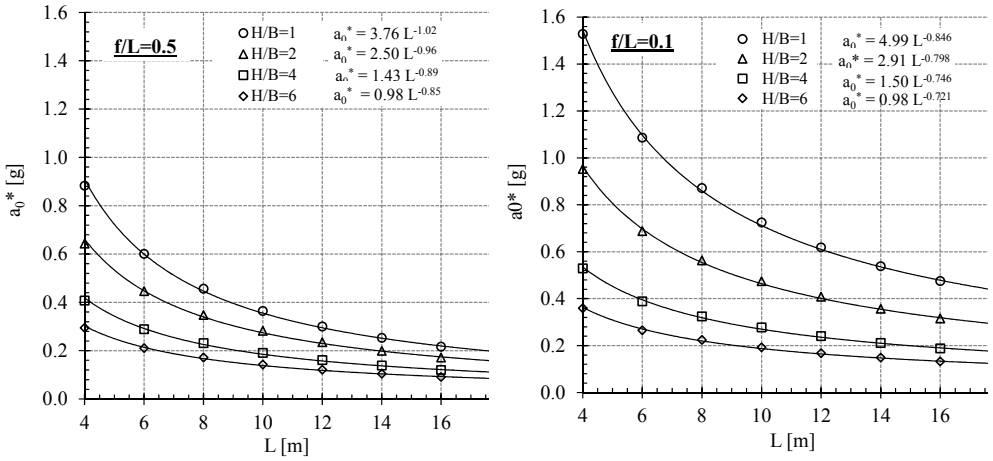

Fig. 5.21 TS_sl bridges: limit acceleration a_0^* and non-linear regression laws for fixed values of f/L ratio a) f/L=0.1, b) f/L=0.5.

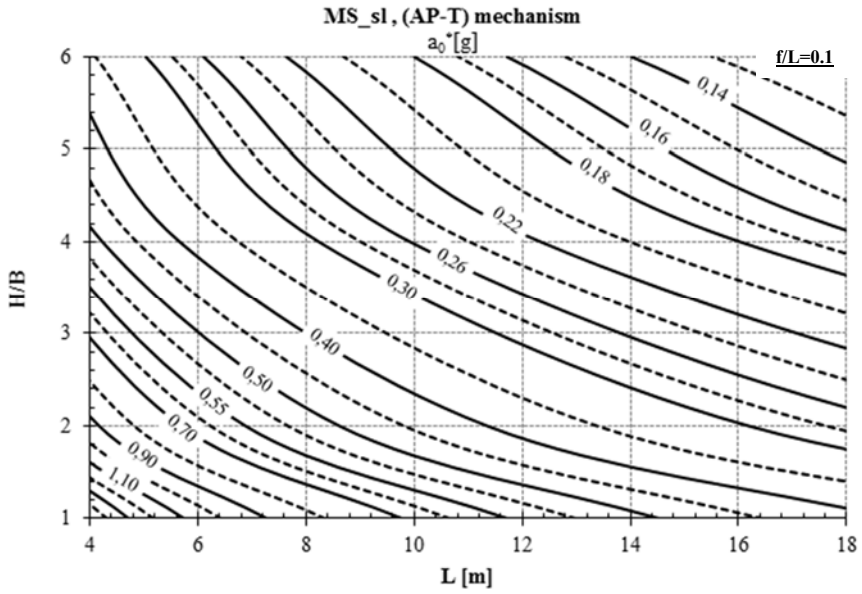

a)

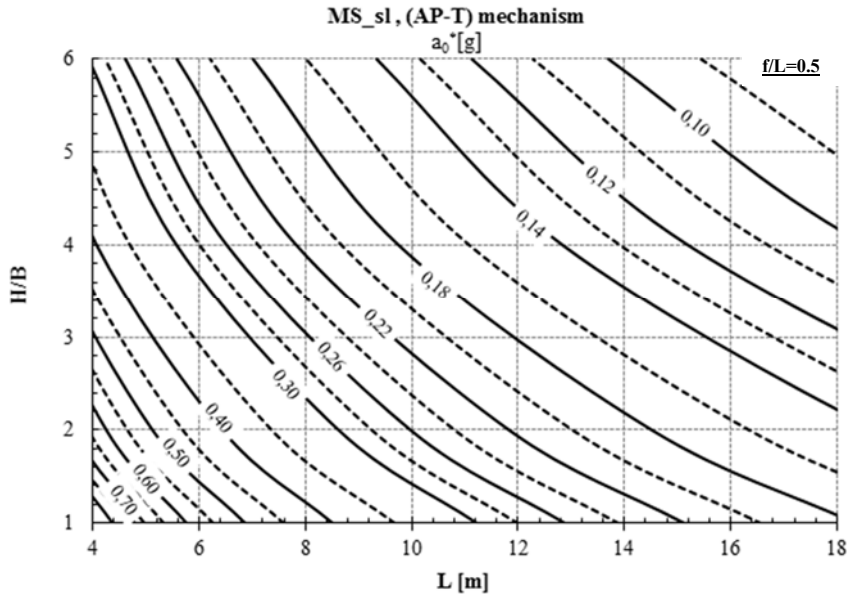

b)

Fig. 5.22 MS_sl bridges: iso-acceleration curves for AP-T mechanism, for fixed values of f/L ratio,: a) f/L=0.1, b) f/L=0.5.

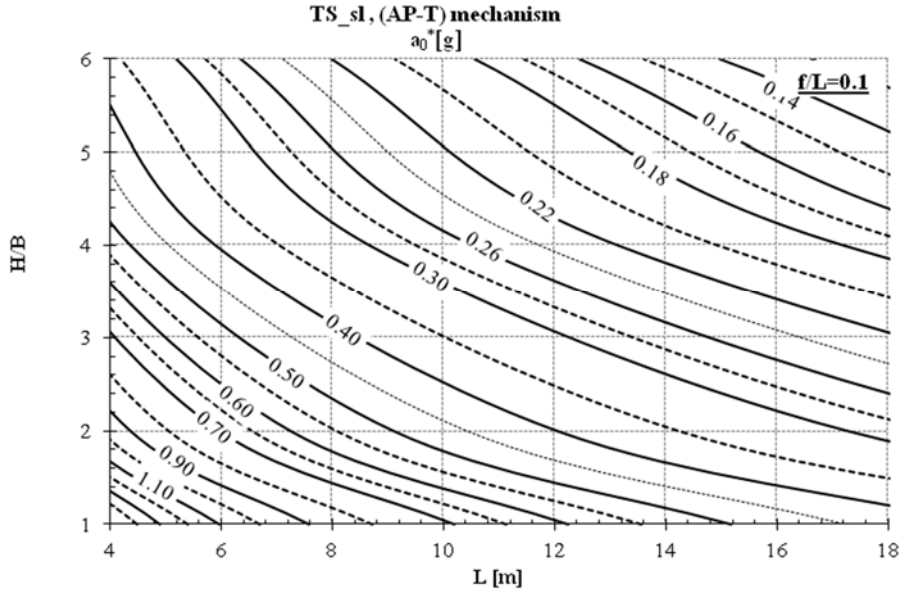

a)

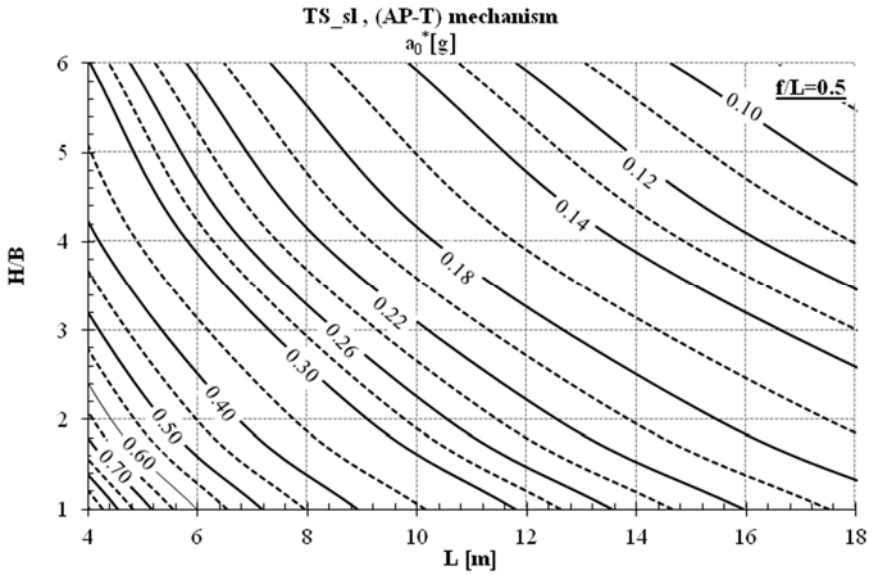

b)

Fig. 5.23 TS_sl bridges: iso-acceleration curves for AP-T mechanism, for fixed values of f/L ratio,: a) f/L=0.1, b) f/L=0.5.

5.4 Simplified seismic verification procedure

The seismic verification of a masonry arch bridge can be performed by comparing the expected Peak Ground Acceleration (PGA) at the site, with the limit acceleration that is necessary to turn the structure into a mechanism (Clemente, 1998). This approach can be adopted for all significant mechanisms in longitudinal and transverse direction, with a discrete 'rigid block' analysis procedure.

Simplified seismic safety check of local mechanisms in masonry structures can be done with linear kinematic analysis, according to current codes (NTC, 2008).

The procedure should be repeated for all possible mechanisms. The bridge global safety factor (GSF) is taken as the minimum safety coefficient deriving form the verified kinematic mechanisms.

Hence, the above presented iso-acceleration graphs can be directly used for a preliminary seismic safety check of existing masonry bridges, and for prioritizing seismic retrofitting interventions. An example of tabular verification procedure is applied below, considering two railway masonry bridges, the first with a single span (named RB1) structure and the latter being a five-span bridge (RB2).

5.4.1 Example of Single-Span, high abutments bridge

The RB1 bridge belongs to the subclass SS_ha, 1.2. The collapse mechanisms taken into account are Arch-Abutment in longitudinal direction and Spandrel-Wall rotation in transverse direction. The spectral acceleration values are computed for a rock soil with a probability of being exceeded equal to 10% in 50 years at Ultimate Limit State (ULS), and 63% in 50 years at Serviceability Limit State (SLS). a_{01}^*, a_{02}^* are limit horizontal accelerations for AA-L and SW-T mechanisms, and SF1, SF2 are the related safety factors. The limit values of horizontal acceleration were derived from the iso-acceleration curves of Fig. 5.13 and Fig. 5.15, 24, using the geometric parameters reported in Tab. 5.7.

RB1 Bridge	**ULS**	**SLS**
a_g [g]	0.239	0.102
S	1.616	1.800
a_gS [g]	0.386	0.184
q	2	1
a_gS/q	0.193	0.184
AA-L mechanism		
a_{01}^* [g]	0.203	0.203
SF1	1.05	1.10
SW-T mechanism		
a_{02}^* [g]	0.074	0.074
SF2	0.38	0.40
GSF=min(SF1,SF2)	0.38	0.40

Tab. 5.7 RB1 Bridge. No. of spans=1; L=5m; f=2.5m; s=0.5m; h=3.9m; s'=1.5m. S/L=0.1; h/s'=3.33, t=0.83m Z=2.25m.

5.4.2 Example of Multi-Span, slender piers bridge

The RB2 bridge belongs to the subclass MS_sl, 2.2. The geometric data used for seismic verifications are reported in Tab. 5.8. The safety factor is evaluated in longitudinal direction for Arch-Pier mechanism, and in transverse direction for overall Arch-Pier mechanism and local Spandrel-Wall rotation.

RB2 Bridge	**ULS**	**SLS**
a_g [g]	0.265	0.105
S	1.310	1.500
a_gS [g]	0.347	0.158
q	2	1
a_gS/q	0.173	0.158
AP-L mechanism		
a_{01}^* [g]	0.185	0.185
SF1	1.07	1.17
AP-T mechanism		
a_{02}^* [g]	0.252	0.252
SF2	1.46	1.59
SW-T mechanism		
a_{03}^* [g]	0.118	0.118
SF3	0.68	0.75
GSF=min(SF1,SF2, SF3)	0.68	0.75

Tab. 5.8 RB2 Bridge. No. of spans=5; L=8.7m; f=3.40m; S=0.75m; H=14.0m; B=3.65m; f/L=0.39, H/B=3.97, s/L=0.086, p=5.5m, t=0.94m, Z=1.70m

5.5 Consideration about seismic vulnerability in the formulation of judgement of structures state of maintenance.

Civil infrastructures belonging to railway or road transport networks are generally subjected to periodic control visual inspections.
The procedures and methodology for the execution of visual inspections for civil infrastructures are regulated in Europe by FICHE UIC Code 778-2 and by FICHE UIC Code 778-3.
During these inspections, the operator expresses a judgment about the state of maintenance of the structure through specific informatics systems of damage detection. In Italy the system used is called DOMUS (Diagnostica Opere d'arte Manutenzione Unificata Standard).

Judgment Type	Structure condition	J
A	The structure is safe for traffic allowing.	10-50
B	The structure is safe for traffic allowing after interventions	60-90
C	The structure is not safe for traffic allowing.	90-110

Tab. 5.9 Hypothetical scale of judgment of state of structure's maintenance.

If the hypothetical scale (A, B, C) reported in Tab. 5.9 is representative of the maintenance states of a structure, then a calibration of judgment values about the state of maintenance (J) can be calculated with the following formula:

$$J^* = (J + \Delta S) \leq 110 \tag{5.12}$$

The coefficient ΔS (Seismic judgment increment) takes into account seismic vulnerability of the structure and the seismicity of the structure location. This value is related to Seismic Coefficient SC (of the masonry bridge), expressed as:

$$SC = \frac{a_0^*}{a_g} \tag{5.13}$$

In this formula a_{0^*} derives from iso-acceleration curves and a_g is the pick ground acceleration, which refers to ground type A (rock).
A Seismic weight coefficient ΔS value is associated to SCs, as reported in Tab. 5.10.

Seismic coefficient SC	Seismic weight coefficient ΔS
SC>0.9	ΔS: 0
0.9≥SC≥0.5	ΔS: 30
SC< 0.5	ΔS: 50

Tab. 5.10 Seismic weight coefficient.

5.6 Conclusions

Assessment of the condition of old masonry arch bridges has become an ongoing problem for public network authorities, partly due to the seismic vulnerability of strategic railway lines. Growing interest in simplified procedures for seismic assessment has thus emerged, and limit analysis has proved to be a conceptually simple and robust method.

Based on a statistical survey of about 750 Italian railway masonry bridges, a typological classification, taking into account geometry and expected seismic collapse mechanisms in these structures is proposed here. Limit ground acceleration a_0^*, i.e., the seismic capacity of the bridge in the case of various collapse mechanisms, is calculated with the limit analysis method, and a comprehensive parametric analysis for each bridge class is carried out, evaluating the influence of geometric parameters on seismic capacity. The final result is a series of iso-acceleration curves, providing the values of horizontal limit acceleration a_0^* of bridge structures according to easily detectable geometric parameters only.

In addition, the parametric analysis carried out allows drawing some conclusion on the seismic behaviour of these structures. This study showed that, in general, masonry bridges have good resistance to seismic action, as a result of precautionary design. They are able to withstand earthquake of medium intensity without significant damages to the main structural elements.

The most vulnerable element, particularly in case of out-of-plane actions, is the spandrel wall. Damage or overturning of this secondary element does not generally involve the structural safety of the structure, but it does compromise ballast support and rail tracks. Therefore, simple interventions to prevent overturning can be very useful not only for reducing vulnerability and damage, but also to keep the network in use after a seismic event.

Taking into account overall collapse mechanisms related to the structural safety of the bridge, the class of multi-span arch bridges with slender piers is the most vulnerable. The most probable collapse mechanism is the overall longitudinal mechanism, although in case of high pier slenderness, the overall transverse mechanism becomes dangerous, as well. In any case, for the most common bridge geometries, the values of limit acceleration are high.

Single-span bridges with high abutments are vulnerable to medium-high seismic action in longitudinal direction, and the overall arch-abutment longitudinal mechanism is generally more vulnerable than the local arch mechanism typical of squat single-span bridges. In the latter class, the local arch longitudinal mechanism is vulnerable in case of semicircular arches only, particularly when they have small thickness, whereas depressed arches are very resistant to seismic action.

The cataloguing and study of the various collapse mechanisms of masonry arch bridges has thus allowed improving knowledge to guide the assessment and design of intervention for this type of bridges. On the other hand, this study allowed

constituting a tool to carry out quick simplified vulnerability assessment of complex networks, where thousands of masonry bridges are found, in order to prioritise more detailed analyses and execution of interventions.

6 SEMPLIFIED SEISMIC FRAGILITY CURVES FOR SINGLE-SPAN MASONRY BRIDGES CLASS

6.1 Introduction

Italy is globally recognised to be one of the most earthquake-prone countries in the Mediterranean area, because of the frequency of ground shakings that have historically characterised its territory and the intensity that some of them have achieved, causing significant social and economic impacts.
In this context, for a whole range of civil and strategic structures, the need of a preliminary seismic vulnerability assessment is becoming increasingly important, such as to identify those considered more exposed to seismic risk. These evaluations are fundamental to determine which structures need further investigations and afterwards retrofit interventions, with the aim of making them able to reach defined performance levels (Brime 2001; Hawk and Small 1998). In the field of infrastructures management, due to the ancientness of Italian infrastructure heritage, characterised by a remarkable expansion after the IInd World War, the need to rationally allocate the resources for structural improvement is now emerging, in order to minimise the damage risk of the most vulnerable bridges that, once damaged, would involve significant economical and social losses. These requirements are evident in both road and railway transport networks (SB-ICA 2007).
In Italy, one of the most common road and railway bridge is represented by the single-span masonry arch bridge typology. This type can reach in some Italian areas approximately the 80% of whole bridge structures in railway network.
In literature, many studies focused on local and global assessment methods of existing masonry bridges (Hughes and Blacker 1995; Boothby 1995; Brencich and De Francesco, 2004; Rota et al, 2005; Pelà et al., 2009) without using a probabilistic approach aimed to the evaluation of their seismic fragility. Several studies analysed spandrel wall collapse, as this is the most vulnerable out-of plane local collapse mechanism (Fanning and Boothby 2001; Boothby and Roberts 2001; Rota et al. 2005; Junzhe W. et al. 2013): this collapse may affect structure functionality, but rarely involves bridge global failure. For single-span masonry bridges the other possible collapse mechanism is the in-plane arch failure mechanism, whereas for

multi-span bridges also transversal behaviour has to be analysed in relation to the longitudinal and transversal slenderness of the piers.
A new simplified approach for the fast seismic vulnerability assessment of numerous masonry arch bridge clusters is proposed. The aim of this proposal is to provide useful information for the fast seismic vulnerability of single-span masonry arch bridges in the context of territorial scale analyses, through the grouping in bridge classes characterised by similar structural features. Such indications allow to quickly estimate the seismic vulnerability of extended roadway and railway bridge networks in emergency, given the high percentage of bridges characterised by this structural typology in European transportation infrastructural networks, and to optimize the retrofit intervention priorities.

6.2 Non-linear Kinematic analysis of masonry arch bridges

The non-linear kinematic seismic analysis of Masonry Bridge allows to design the capacity curve of the structure, with the centroid of the keystone of the arch assumed as a control point.
In the non-linear kinematic analysis, the principle of virtual work is applied to a deformed shape of the structure:

$$\alpha_0(\theta)\sum_i \left(P_i + Q_i\right)\delta_{x,i}(\theta) - \sum_j Q_i\delta_{y,j}(\theta) - \sum_i P_i\delta_{y,i}(\theta) = 0 \qquad (6.1)$$

All the parameters used in equation 4.1 have just been explain in 3, and $\theta=\theta_{AB}$ is the rotation of the arch segment AB and it represents the finite rotation of the structure and it identifies the unknown deformed configuration.
The deformed shape of the structure is obtained by incremental steps of rotation:

$$\theta_{k+1} = \theta_k + \Delta\theta \qquad (6.2)$$

In other words, the procedure is repeated until the arch configuration does not have any residual capacity to the seismic action.

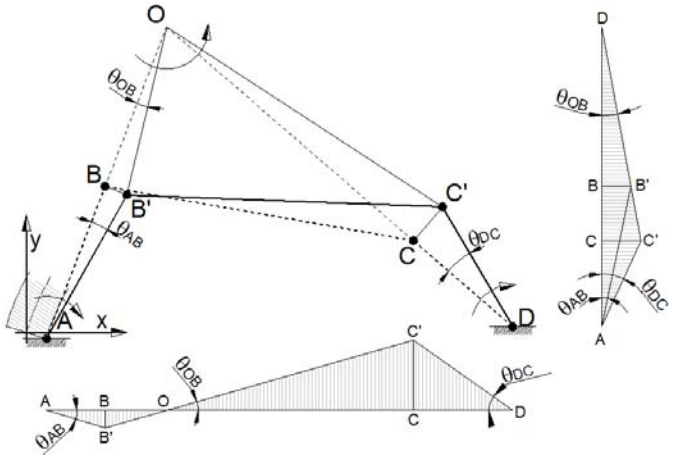

Fig. 6.1 In-plane arch mechanism.

The equations that characterised the problem can be described as a unique Lagrangian variable: the rotation of the first rigid arch segment θ.
With the application of PVW, we can obtain the collapse multiplier α(θ) and the associated displacement d(θ). The procedure ends with the derivation of a displacement zeroing the collapse multiplier. In this case, the equation of PVW become:

$$\sum_j P_j \delta_{y,j}(\theta) + \sum_i P_i \delta_{y,i}(\theta) = 0 \tag{6.3}$$

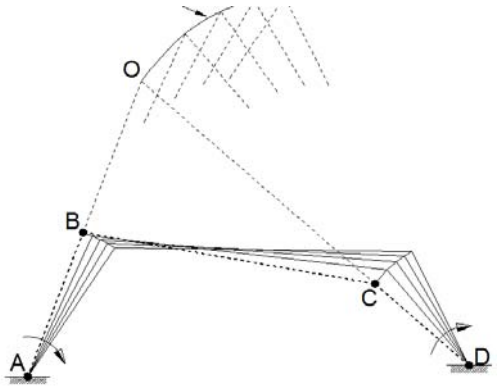

Fig. 6.2 Deformation shape of the in-plane arch mechanism.

The zeroing of the collapse multiplier coincides with an unstable equilibrium of the mechanism. This condition corresponds to the local maximum of the potential energy. It corresponds also at the zeroing of virtual work of the vertical force.

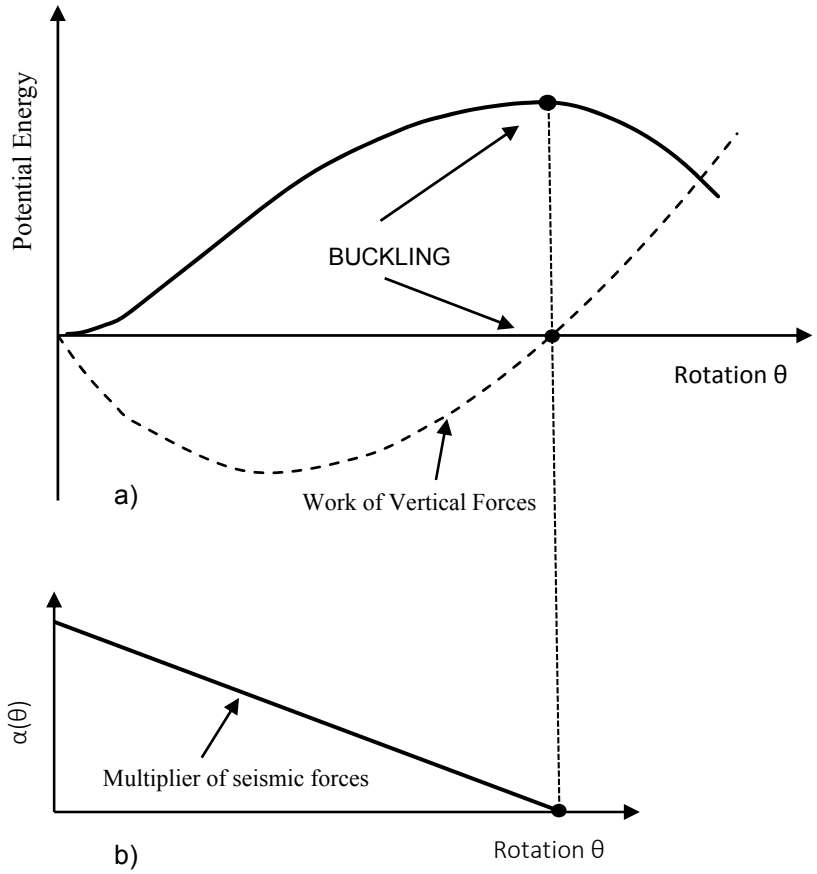

Fig. 6.3 a) Local maximum of the potential energy that corresponds also at the zeroing of virtual work of the vertical force.

In the non-linear seismic analysis, the capacity curve of the structure must be transformed in to equivalent SDOF system. The spectral acceleration a* and the spectral displacement d* of equivalent SDOF system are computed as follows.

$$a^*(\theta) = \alpha(\theta)\frac{\sum_i \left(P_i + Q_i\right)}{M^*} \tag{6.4}$$

$$d^*(\theta) = d_{x,k}(\theta)\frac{\sum_i \left(P_i + Q_i\right)\delta_{x,i}^2(\theta)}{\delta_{x,k}\sum_i \left(P_i + Q_i\right)\delta_{x,i}} \tag{6.5}$$

P_i is the resultant of weight forces directly applied in the i-th block (e.g. weight of the block);

Q_i is the resultant of weight forces not directly applied in the block but transmitted by the structure and which generate a horizontal seismic force;

θ is the generalized displacement (e.g. a rotation) assumed as reference;

$\delta_{x,i}$ is the horizontal virtual displacement of the centroid of the i-th block calculated with reference to the initial configuration of the system;

$d_{x,k}$ is the finite horizontal displacement of the generic point P of the system (that assumed as representative to plot the pushover curve) and $\delta_{x,k}$ is its virtual horizontal displacement;

M* is the mass of the structure participating to the mechanism computed as:

$$M^* = \frac{\left(\sum_i \left(P_i + Q_i\right)\delta_{x,i}^2(\theta)\right)^2}{g\sum_i \left(P_i + Q_i\right)\delta_{x,i}(\theta)} \tag{6.6}$$

6.3 Seismic Performance levels of masonry bridges

In the case of nonlinear kinematic analyses performed by rigid block model of masonry bridges, the i-damage level is basically related to the displacement where the horizontal load multiplier of the capacity curve becomes 0 (d^*_0).
The yielding condition (dy) in the kinematic capacity curve corresponds to the point in which the secant period intersects the capacity curve. In the Italian code (NTC08) the secant period Ts is conventionally assumed fixed the value of the secant displacement as d_s=0.16 d^*_0.

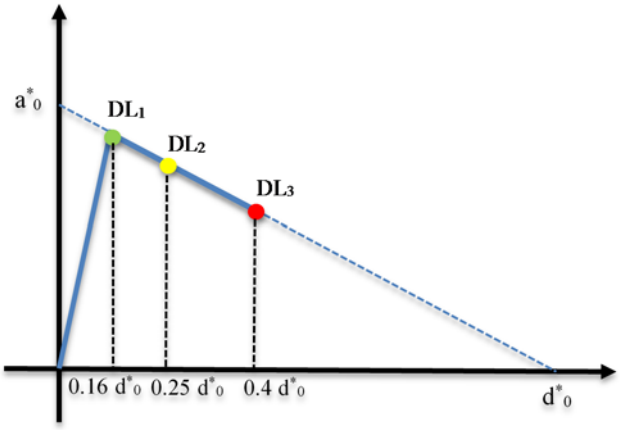

Fig. 6.4 Kinematic capacity curve and Damage levels.

The proposed limit values of damage levels 1,2 and 3 are show in Tab..

Damage Level (DL_i)	**Corresponding Displacement**
1	0.16 d^*_0
2	0.25 d^*_0
3	0.40 d^*_0

Tab. 6.1 Damage Levels.

6.4 Fragility curves construction

The use of probabilistic approaches is nowadays commonly diffused in the seismic risk estimation of structural systems, to take into account the uncertainties related to the characterisation of the main mechanical and geometrical parameters of the structure to be assessed. In this field, fragility curves are the most useful tools to describe the conditional probabilities of a structure to meet or exceed certain damage levels for a given ground motion intensity. In the case of existing masonry structures a probabilistic approach is necessary for the evaluation of the seismic demand intensity and for a realistic evaluation of the overall capacity. For these variables it is generally recognised the impossibility to attribute exact values, therefore they must be associated to probability density functions.

With regard to seismic demand, ground motion actions can be characterised by different intensities, frequency contents and durations. Materials and structures characteristics, which define the overall bridge capacity, and factors site conditions, which affect seismic demand, are so uncertain that a probabilistic approach is required for seismic vulnerability estimation. Consequently, seismic demand is defined by an interval of values, instead of a single value as provided by deterministic analysis. In this work, 7 artificial accelerograms were considered; related elastic spectra were calculated, and subsequently the elastic mean spectrum (Shinozuka et al. 2000) and the relative standard deviation were derived.

First of all, it is necessary to identify an appropriate set of performance levels (*PL*), associated with service and collapse limit states. Subsequently, correlations are formulated between a seismic intensity measure (usually defined by *PGA* or *PGV*) represented in the X-axis coordinate, and the exceedance probability for the *PL* to which the curve is referred, in the Y-axis coordinate.

Hence, a probabilistic approach has to be followed to consider the intrinsic variability of seismic demand and structural capacity parameters. The use of an analytical approach is required when data of post-earthquake damage on existing structures are not available. Generation of “analytical” fragility curves is usually carried out in three steps: in principle, seismic action is simulated on the basis of recorded or generated earthquakes. Bridge is then represented with a numerical model taking into account the uncertainty of structural properties; finally, fragility curves are generated from response data obtained from the numerical model.

Results of the analytical approach may be obtained through analyses of differing complexity such as probabilistic response spectra in conjunction with bridge inventory data (Dutta & Mander, 1998), elastic spectral analysis (Hwang et al., 2000), non-linear static analysis (Shinozuka et al., 2000), simplified methods based on

regression analysis (Karim & Yamakazi, 2003); non-linear time history analysis (i.e. Karim & Yamakazi, 2001; Choi, 2004). With regard to masonry/stone structures, other different methodologies can be also used for the structural analysis: since Heyman (Heyman 1966; Heyman 1972) pointed out that the plastic theory could be applied to masonry gravity structures (Gilbert 2007), many studies have been developed over the years on limit analyses for the assessment of masonry arches. According to Heyman's assumptions, iterative methods to find the geometric factor of safety (related to the minimum thickness of the arch) under vertical dead and live loads were proposed by Clemente et al. 1995. Extensions to the basic rigid block method for the limit safety analysis of the arch were subsequently introduced (Gilbert and Melbourne 1994; Gilbert 1998; Cavicchi and Gambarotta 2007; Clemente et al. 2010).

Although the most reliable method is based on NLDA, this type of analysis on complex models is so time-consuming that it is not useful for large-scale application In this work, fragility curves were constructed following the method proposed in Shinozuka et al., 2000, by means of non-linear static analyses based on CSM.

Generation of fragility curves requires the definition of a damage function. In earthquake engineering, damage measures proposed in scientific literature are numerous and various, and can be defined for each structural element or sub-elements (local indexes), or related to the entire global structure (global indexes). An excellent review has been made in Cosenza and Manfredi, 2000a, 2000b. The most commonly used parameters for the evaluation of structural damage are ductility (which can be defined in terms of rotation, curvature or displacements) and plastic energy dissipation.

The choice of using kinematic or cyclic ductility as a damage measure is equivalent to assume that the collapse is expected under maximum plastic displacement, independently from the number of plastic cycles and the amount of dissipated energy. Ultimate ductility corresponding to structure collapse can be determined with a monotonic test.

When energy is considered as the parameter associated to the damage function, the structure is considered to have a set amount of energy that can be plastically dissipated (Uang & Bertero, 1990). Consequently, collapse occurs when that value of dissipated energy is achieved by means of cyclic loads. In the evaluation of energy dissipation in a structure, energy-based indexes are appealing for their simplicity, but experimental assessment of the supplied energy dissipation capacity is very difficult. Other indexes are based on a combination of ductility and dissipated energy demand. The most widely used is the Park&Ang index (Park & Ang, 1985), which is defined as a linear combination of maximum displacement and dissipated energy. This index is

closely correlated with observed damage. However, the parameter that defines the weight to be associated with dissipated energy is difficult to be experimentally defined.

In scientific literature, ductility is therefore the most widely used parameter to define the damage index.

The procedure used to calculate a fragility curve for a set performance level d_{PL} is summarised below:

1) a parameter a identifying seismic intensity is set;
2) the elastic spectra referring to the accelerograms used for the set parameter a are calculated;
3) the average spectrum *m* and the average spectrum ± standard deviation □ are calculated and then represented in *AD* format;
4) a pushover analysis is carried out to calculate the capacity curve for each *j*-th bridge (i.e., of a set bridge with *j*-th characteristics of random parameters);
5) the demand curves of the three elastic spectra calculated in the previous step are determined with one of the simplified analysis methods based on CSM. Intersection with *j*-th bridge capacity curve determines three displacement values (Figure 1). $\bar{S}_{d,j}(a)$ is defined through the intersection of the capacity diagram with the mean demand curve *m.* $\bar{S}_{d,j}(a)+\sigma^{+}_{d,j}(a)$ and $\bar{S}_{d,j}(a)-\sigma^{-}_{d,j}(a)$ derive from the intersection of demand curves *m+σ* and *m-σ* respectively. Values $\sigma^{+}_{d',j}(a)$ and $\sigma^{-}_{d,j}(a)$ usually do not coincide, so that geometric mean is carried out to have only one value of standard deviation to be used for the definition of probabilistic distribution of seismic demand, as reported in (1).

$$\sigma_{d,j}(a)=\sqrt{\sigma^{+}_{d,j}(a)\cdot\sigma^{-}_{d,j}(a)} \tag{6.7}$$

6) the log-normal distribution of the damage function for the *j*-th bridge is generated by the mean $c_j(a)$ and standard deviation $\zeta_j(a)$ parameters. These parameters are obtained by the inversion of the system and their association with $\bar{S}_{d,i}(a)$ and $\sigma_{d,j}(a)$. The system is shown below

$$\bar{S}_{d,j}(a)=c_j(a)\cdot\exp\left[\left\{\zeta_j(a)\right\}^2/2\right] \tag{6.8}$$

$$\left\{\sigma_{d,j}(a)\right\}^2=\left\{\bar{S}_{d,j}(a)\right\}^2\left[\exp\left(\left\{\zeta_j(a)\right\}^2\right)-1\right] \tag{6.9}$$

7) once $c_j(a)$ and $\zeta_j(a)$ are determined for the *j*-th bridge, the probability of exceeding the damage level set as:

$$P_j\left[S_d(a) \geq d_{PL}\right] = P_j(a, d_{PL}) = 1 - \Phi\left[\frac{\ln\left(\frac{d_{PL}}{c_j(a)}\right)}{\zeta_j(a)}\right] \tag{6.10}$$

is calculated, where $\Phi[\bullet]$ is a standard normal distribution function;

8) the previous steps are then iterated for each of the other statistically different *k* bridges so as to obtain the final fragility value by the following arithmetic mean:

$$P(a, d_{PL}) = \frac{\sum_{j=1}^{K} P_j(a, d_{PL})}{k} \tag{6.11}$$

where k is the total number of random parameter combinations (and therefore the total number of statistically different bridges in terms of capacity). If each of the k bridges is characterised by a different weight, $P(a, d_{PL})$ is obtained through a weighted mean.

The procedure is repeated for all the values of seismic intensity considered.

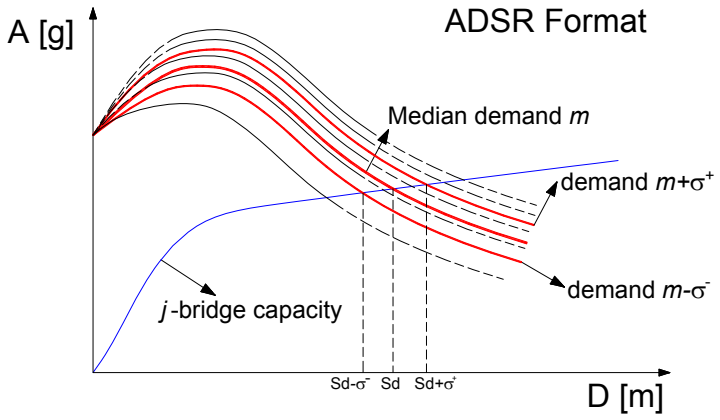

Fig. 6.5 Assessment of seismic capacity relative to the three demand curves analysed.

6.4.1 Reduction of Demand Spectrum

In this work, the function adopted for reducing the elastic response spectra is mainly based on the definition of a linear equivalent system with a proper damping and the procedure refers to the overdamped approach.
The equivalent damping is calculated by the formulation proposed by Calvi (1999) that relates the dissipated energy to the ductility reached by the structure:

$$\xi_{equ} = \xi_{el} + \alpha\left(1 - \frac{1}{\mu^{\beta}}\right) \tag{6.12}$$

Where the coefficients α and β are function of the hysteretic model assumed, μ is the ductility value and ξ_{el} is usually assumed equal to 0.05.
Ductility, that can be defined as $\mu i = d_{PLi}/d_{PL1}$, increases quite rapidly in the nonlinear range, just after DL1, exactly as damping.
The coefficient β modifies the rate of increase of hysteretic damping with ductility, and it is adopted equal to 1. The values of α, as Perpetuate D35 suggests, is equal to 0.2 for the out-plane mechanism and 0.15 for in-plane arch mechanism.
The relationships based on the damping coefficient are aimed to reduce the elastic spectrum and the expression proposed in Eurocode 8 is assumed as reference:

$$\eta_{PLi} = \sqrt{\frac{10}{5 + \xi_{PLi}}} \tag{6.13}$$

The spectral reduced acceleration for $T<T_B$ is computed as follows:

$$S_{a,red} = \frac{\eta S_{a,\max} - a_g}{T_B} + a_g \tag{6.14}$$

Moreover, for $T>T_B$ is computed as:

$$S_{a,red} = \eta S_{a,e} \quad (6.15)$$

6.5 Simplified fragility curves for single-span masonry arch bridges

The non-linear static or dynamic procedures allow to estimate the seismic vulnerability of a specific case study with accuracy. It is characterised by a defined geometry, and all the uncertainties related to the definition of the main physical and mechanical characteristics are taken into account. This approach represents the exhaustive resolution for a specific masonry arch bridge, which has been subjected of a detailed analysis of its seismic fragility.

This meticulous procedure has a limited application especially when it is necessary to quickly assess the effects of an earthquake, for example for the characterisation of the seismic fragility of large stocks of masonry arch bridges in transport networks. The proposed procedure is useful to calculate the mean fragility curve for each subclass of single span masonry bridges with squat abutment.

As illustrated in 3.1.1, the macro-class of single span masonry bridges represents the 81% of the entire masonry bridges stock and the single span masonry bridges with squat abutment are the 88% of all the single-span masonry bridges. As a consequence, the design of the fragility curve was done for this class.

The SS_sa was divided into 17 subclasses based on the geometrical parameters: L, S/L, f/L. (as reported in Tab. 6.2).

For each subclass 8 bridges with different geometric elements were generated. This was possible by means of the use of the values of L, S/L and f/l reported in Tab. 6.2.

Subclass	L [m]	f/L	s/L
1	3-6	0.2-0.3	0.075-0.1
2	3-6	0.2-0.3	0.1-0.15
3	3-6	0.3-0.4	0.075-0.1
4	3-6	0.3-0.4	0.1-0.15
5	3-6	0.4-0.5	0.075-0.1
6	3-6	0.4-0.5	0.1-0.15
7	6-10	0.2-0.3	0.075-0.1
8	6-10	0.2-0.3	0.1-0.15
9	6-10	0.3-0.4	0.075-0.1
10	6-10	0.3-0.4	0.1-0.15
11	6-10	0.4-0.5	0.075-0.1

12	6-10	0.4-0.5	0.1-0.15
13	10-20	0.2-0.3	0.05-0.1
14	10-20	0.3-0.4	0.05-0.1
15	10-20	0.4-0.5	0.05-0.1
16	20-30	0.3-0.4	0.05-0.1
17	20-30	0.4-0.5	0.05-0.1

Tab. 6.2 Geometrical parameters of single-span masonry bridges subclasses.

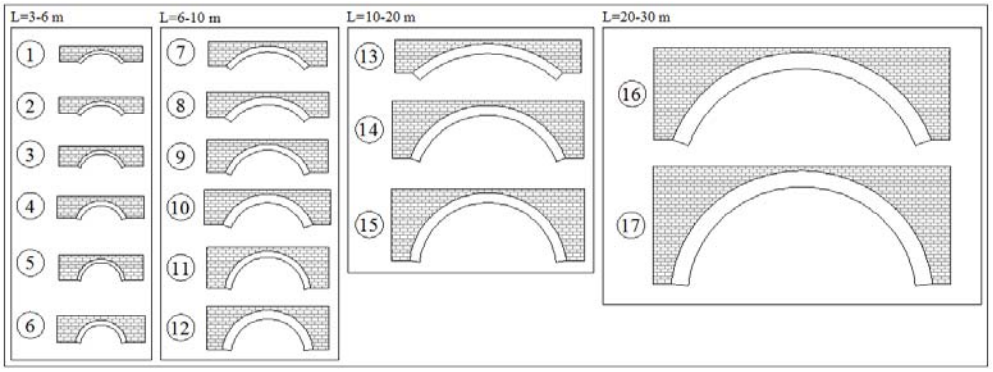

Fig. 6.6 Representation of the single span masonry bridge subclasses considered (the 16 bridges illustrated refers to the mean values of the L, S/L and f/L present in Tab. 6.2)

For each of these 8 bridges three fragility curves (PL1, PL2 and PL3) were calculated with non-linear kinematic simulations and CMS method. They were defined by means of the use of two different aleatory mechanical variables: the masonry compressive strength and the specific weight of the infill material.

As suggested by de Felice (de Felice et al 2006) a normal distribution is assigned to the masonry compressive strength (mean: 7.5 and standard deviation: 2.25). In this study, the infill material specific weight was also accounted (mean: 20 and standard deviation: 2.5).

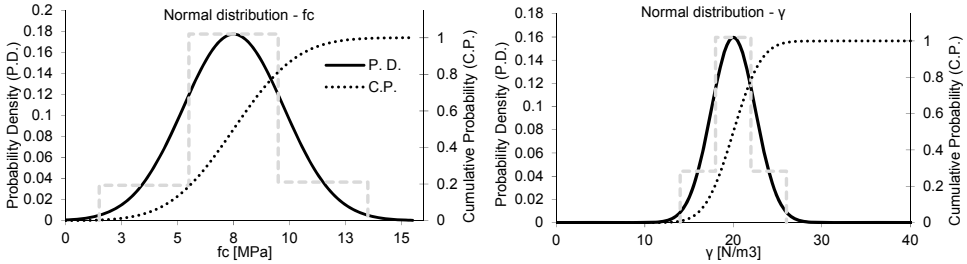

Fig. 6.7 Normal distribution of compressive strength and infill material's specific weight.

The masonry compressive strength distribution was subdivided in three homogeneous intervals of 4 MPa, characterised by their central values equal to: 3.5MPa, 7.5MPa and 11.5MPa. Also the weight of infill material was subdivided in three intervals of 4 kN/m^3 which have the following central values: 16 kN/m^3, 20 kN/m^3 and 24 kN/m^3. Nine bridge samples are obtained combining these values: their mechanical characteristics and probabilities of occurrence are presented in Tab. 6.2.

Bridge Sample	γ [kN/m^3]	Prob. (γ)	f_c [MPa]	Prob. (f_c)	Prob. (γ; f_c)
1	16	0.17747	3.5	0.13482	0.0239
2	20	0.63831	3.5	0.13482	0.0861
3	24	0.17747	3.5	0.13482	0.0239
4	16	0.17747	7.5	0.70923	0.1259
5	20	0.63831	7.5	0.70923	0.4527
6	24	0.17747	7.5	0.70923	0.1259
7	16	0.17747	11.5	0.14605	0.0259
8	20	0.63831	11.5	0.14605	0.0932
9	24	0.17747	11.5	0.14605	0.0259

Tab. 6.3 Characteristics of the 9 considered bridge samples for each of the 8 bridges of each 17 subclass.

For the calculation of the fragility curve with CSM it was necessary to define the mean spectrum that was carried out from the generation of spectrum compatible accelerograms. The spectra type adopted in this work refer to the elastic spectra type 2 (Ground type A) as referred in Eurocode 8 for the ultimate limit state (10% exceedance probability during 50 years).

In summary, three fragility curves were calculated per each of the 8 bridges, each one for three different performance levels (PL1, PL2 and PL3). Each fragility curve was obtained through the combination of the results from 9 bridge samples with their probabilities of occurrence. The three fragility curves (PL1, PL2 and PL3) of each subclass were calculated as the mean value of 8 different curves (Fig. 6.13).

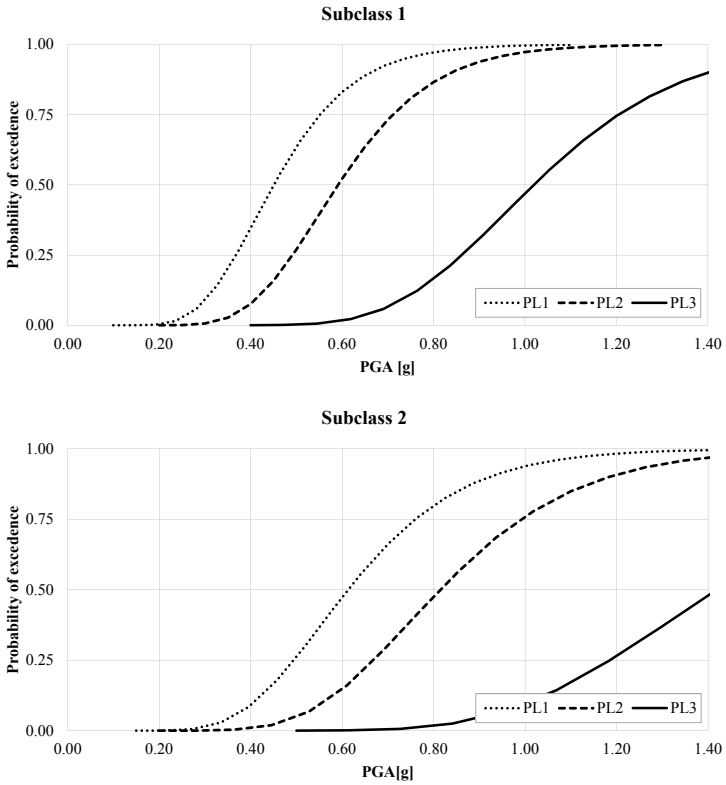

Fig. 6.8 The three fragility curves (PL1, PL2 and PL3) of subclasses 1-2.

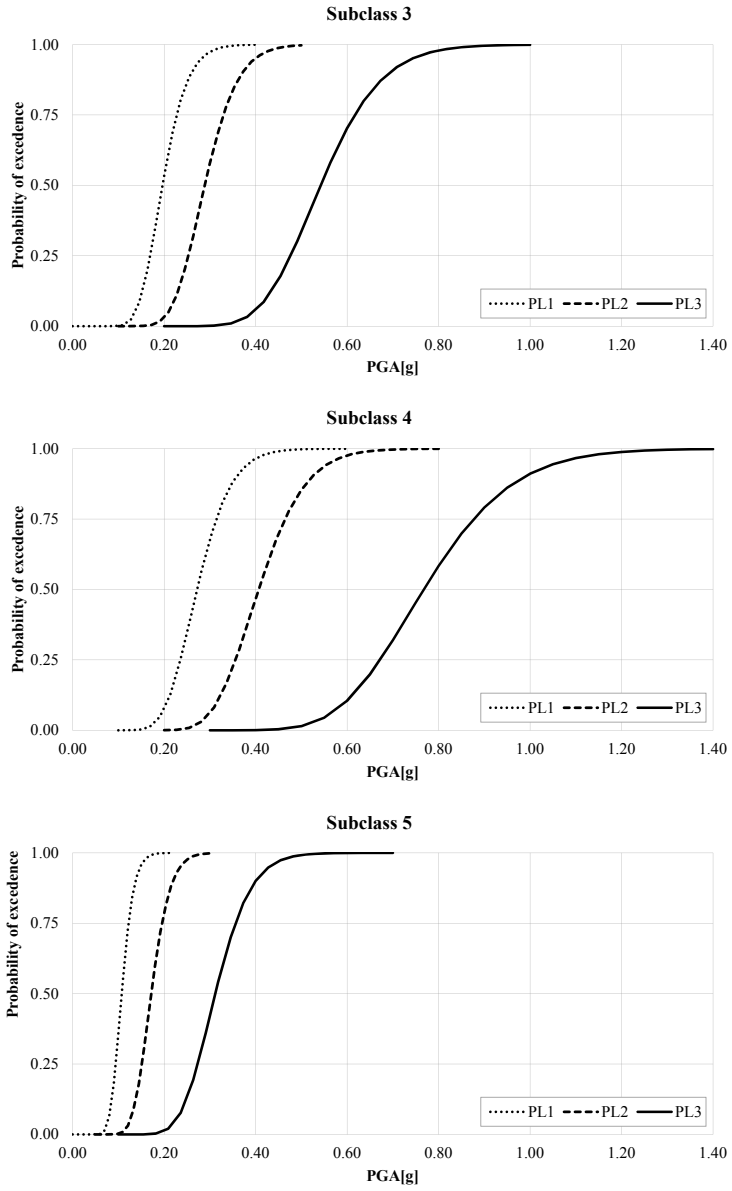

Fig. 6.9 The three fragility curves (PL1, PL2 and PL3) of subclasses 3-4-5.

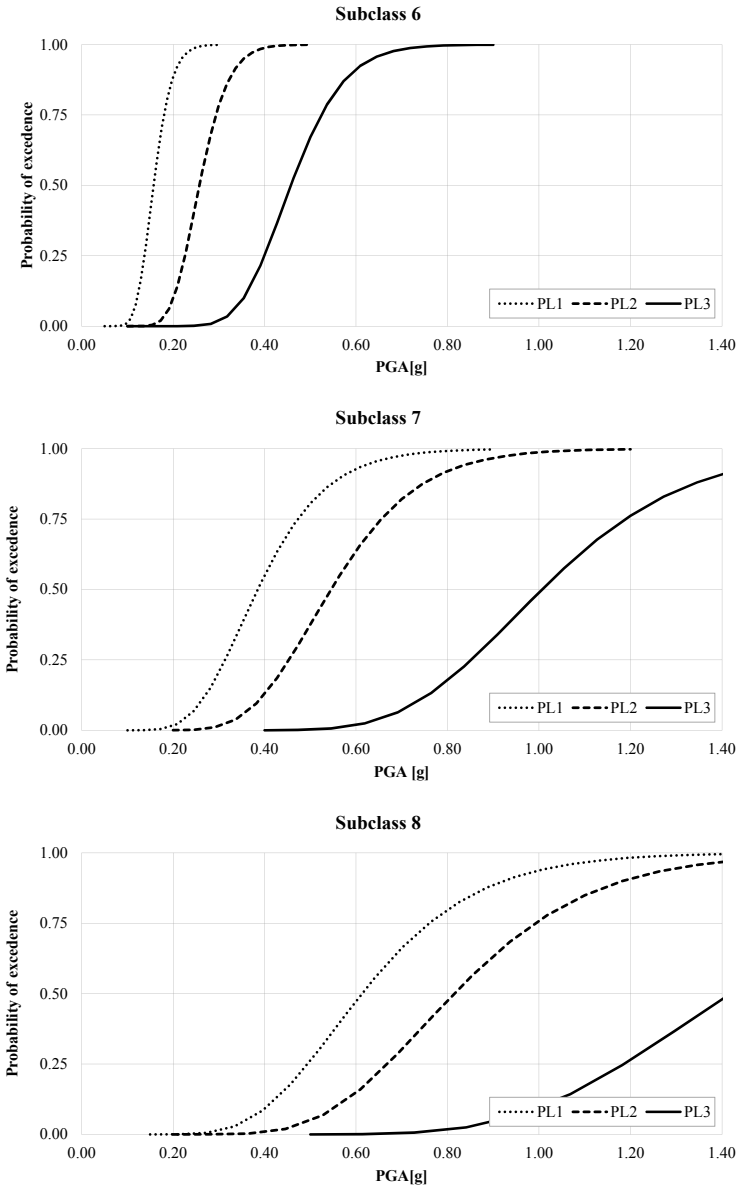

Fig. 6.10 The three fragility curves (PL1, PL2 and PL3) of subclasses 6-7-8.

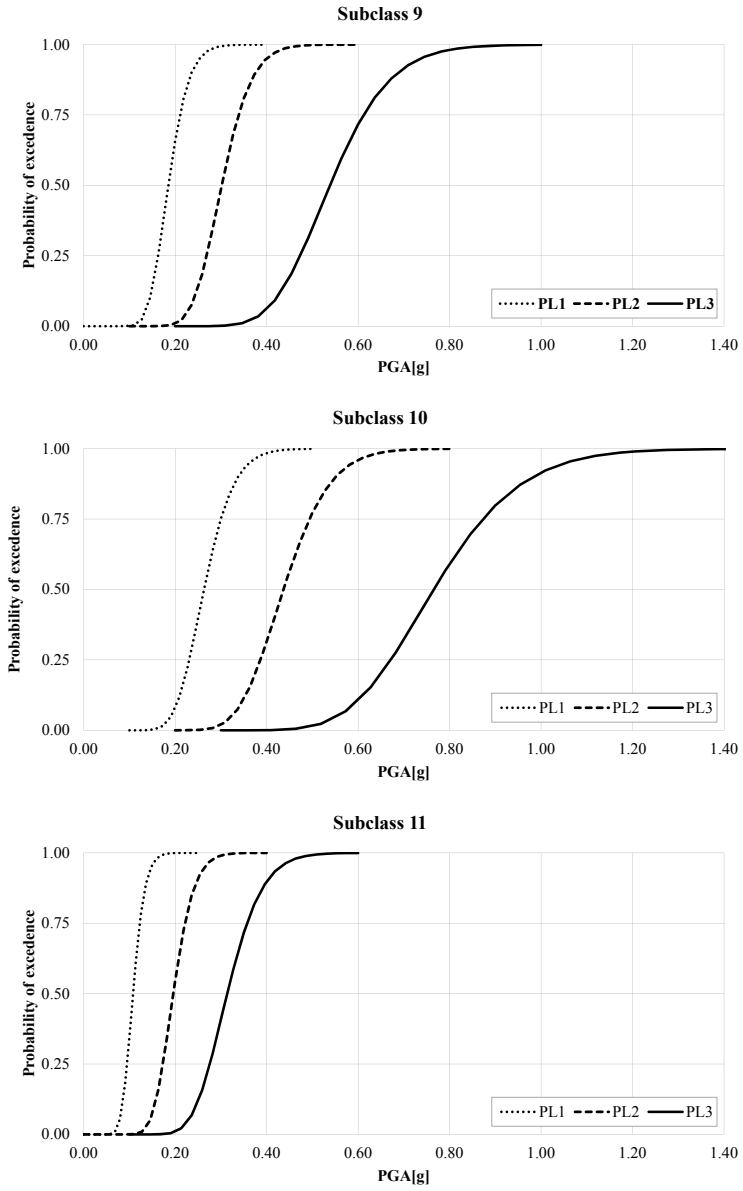

Fig. 6.11 The three fragility curves (PL1, PL2 and PL3) of subclasses 9-10-11.

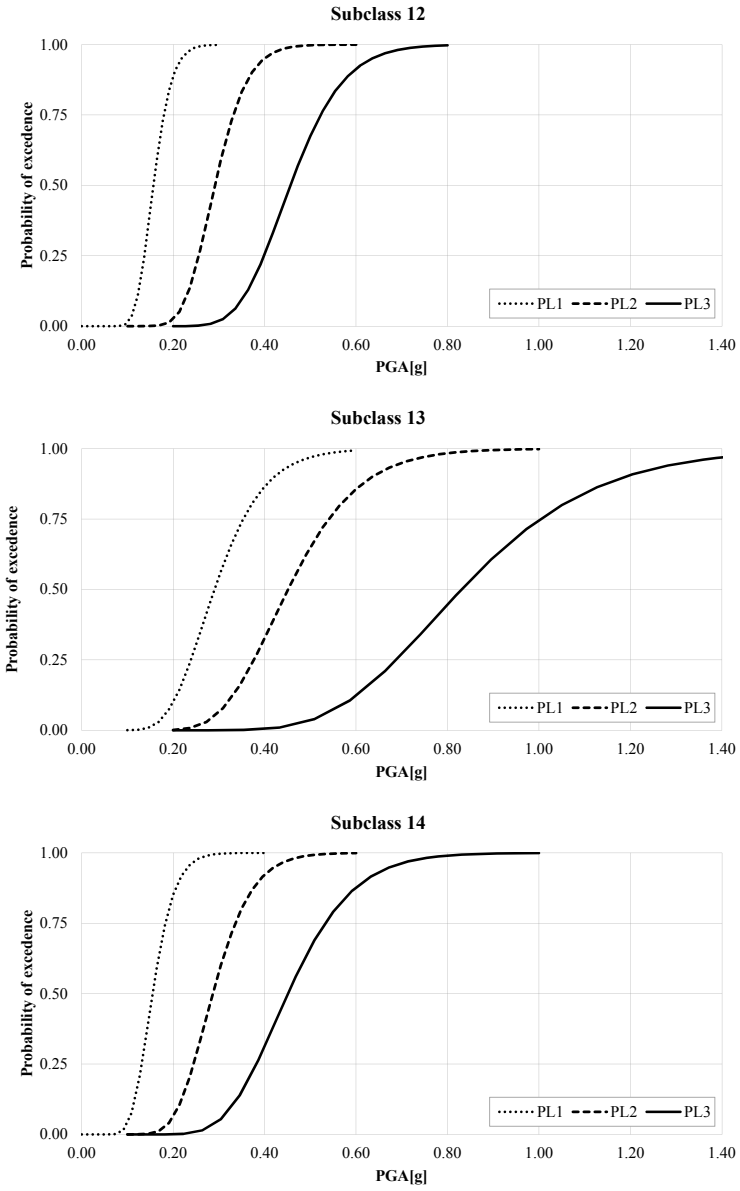

Fig. 6.12 The three fragility curves (PL1, PL2 and PL3) of subclasses 12-13-14.

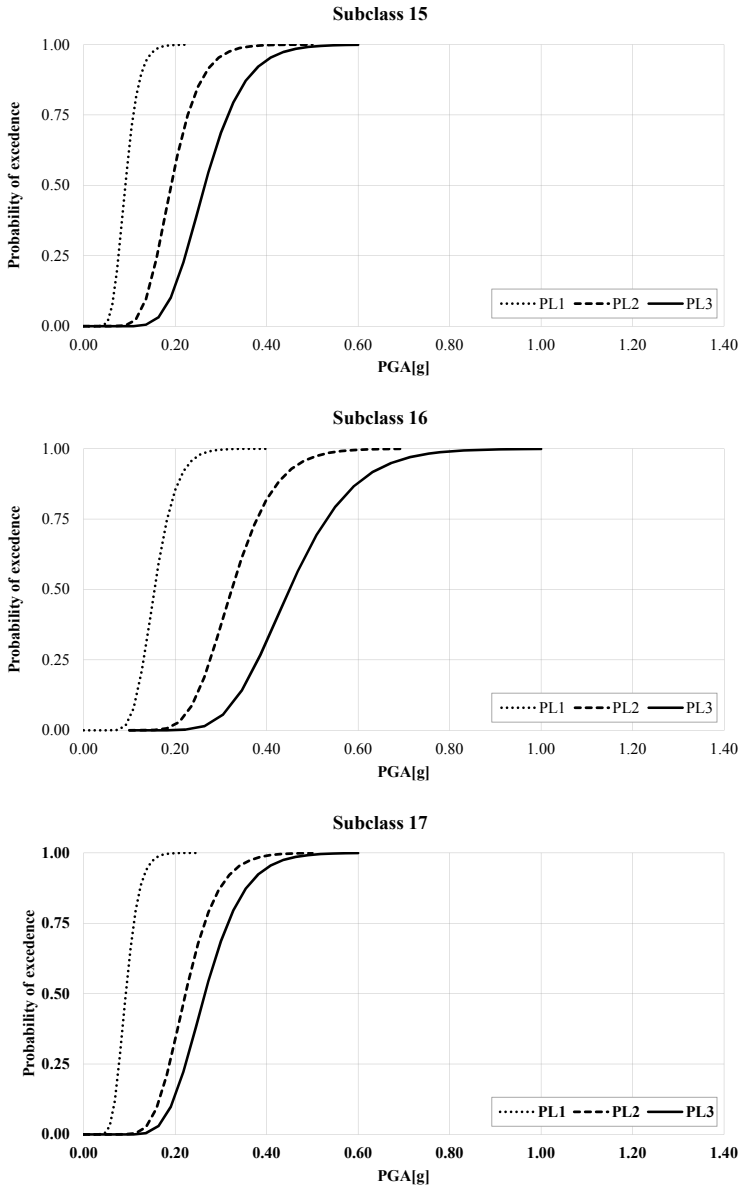

Fig. 6.13 The three fragility curves (PL1, PL2 and PL3) of subclasses 15-16-17.

As results from Fig. 6.8 to Fig. 6.13, some subclasses are characterised from an equal fragility value. This is possible because bridges with different value of L but

constant value of f/L and S/L have the same seismic vulnerability. As a consequence, of these results the subclasses began 9 and not 17 as in Tab. 6.3. has been reported.

Subclass		L [m]	f/L	s/L
SC1	(ex 1-7)	3-10	0.2-0.3	0.075-0.1
SC2	(ex 2-8)	3-10	0.2-0.3	0.1-0.15
SC3	(ex 3-9)	3-10	0.3-0.4	0.075-0.1
SC4	(ex 4-10)	3-10	0.3-0.4	0.1-0.15
SC5	(ex 5-11)	3-10	0.4-0.5	0.075-0.1
SC6	(ex 6-12)	3-10	0.4-0.5	0.1-0.15
SC7	(ex 13)	10-30	0.2-0.3	0.05-0.1
SC8	(ex 14-16)	10-30	0.3-0.4	0.05-0.1
SC9	(ex 15-17)	10-30	0.4-0.5	0.05-0.1

Tab. 6.4 Characteristics of the 9 considered bridge samples for each of the 8 bridges of each 17 subclass.

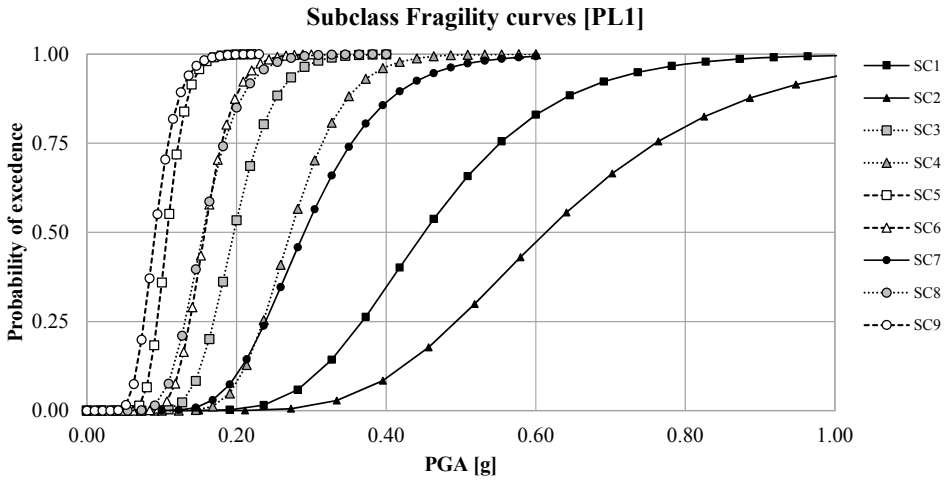

Fig. 6.14 The fragility curves (PL1) of each 17 subclasses

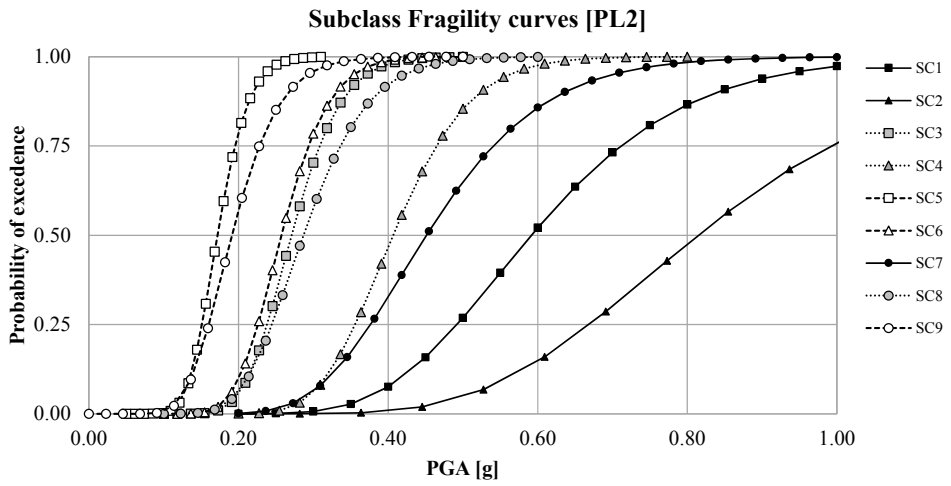

Fig. 6.15 The fragility curves (PL2) of each 17 subclasses

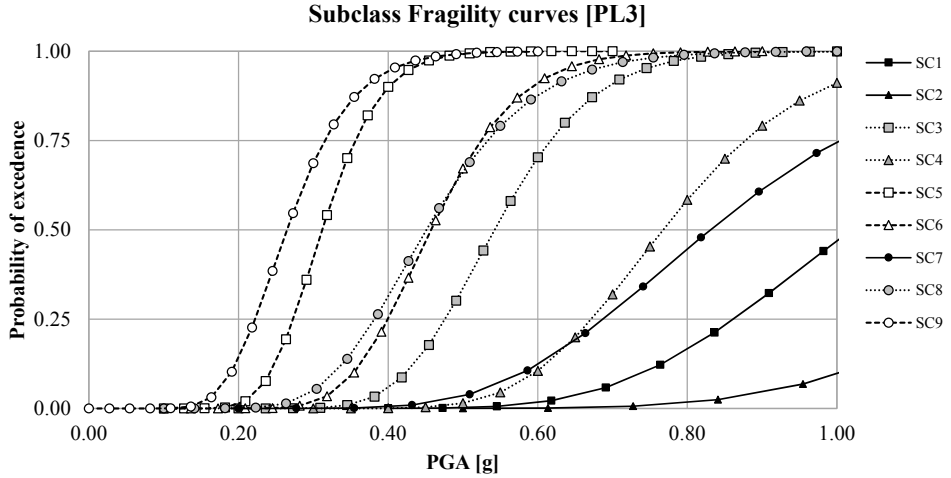

Fig. 6.16 The fragility curves (PL3) of each 17 subclasses

6.6 Conclusions

In this study the procedure for the evaluation of seismic vulnerability of a single span masonry arch bridge class is described.
This work was been carried out with a new simplified approach for a quickly seismic vulnerability assessment of masonry arch bridge clusters. Bridges were divided in classes with similar seismic vulnerability which, as guessed, have also similar geometrical configuration.

The procedure allows to calculate the fragility mean curve for each subclass; it takes into account the uncertainties referred to masonry compressive strength, infill material specific weight and seismic input.
The proposed approach allows to quickly estimate the fragility of extend road and railway bridge networks and to identify the structural retrofit intervention priorities. Future developments of this methodology should be its application at regional level for the seismic vulnerability assessment of transportation networks with regard to the specific scenario earthquakes.
Moreover, the study of the time-evolution of masonry bridges seismic vulnerability considering also materials deterioration can be a possible future outline.

7 CONCLUSION

The appraisal of condition of old masonry arch bridges has become a standing problem for public network authorities, also in relation to seismic vulnerability of strategic railway lines. A growing interest in using simplified procedures for seismic assessment has emerged and limit analysis has proved to be a conceptually simple and robust method.

In this work a typological classification of about 750 Italian railway masonry bridges is proposed, taking into account geometry and expected seismic collapse mechanisms. Limit ground acceleration a_0*, i.e. bridge seismic capacity for various collapse mechanisms, is calculated by limit analysis method and a comprehensive parametric analysis for each bridge class is carried out, evaluating the influence of geometric parameters on the seismic capacity.

The final result is a series of iso-acceleration curves, which provide the value of horizontal limit acceleration a_0* of bridge structures on the basis of easily detectable geometric parameters only. It is important to underline that these curves can be used easily at the same time of BMS during the periodical bridge visual inspections, for a quickly judgment on seismic vulnerability. Otherwise they can be used to modify the judgment obtained by BMS. The new judgment considers the intrinsic seismic vulnerability of some masonry bridges located in high seismic risk area in addition to the conservation state of the construction.

The procedure for the evaluation of seismic vulnerability of a single span masonry arch bridge class is here described. It was carried out using a new simplified approach for a quickly seismic vulnerability assessment of masonry arch bridge clusters. Bridges were divided into classes with similar seismic vulnerability which, as guessed, have also similar geometrical configuration.

The procedure allows the evaluation of the fragility mean curve for each subclass, and the uncertainties referred to masonry compressive strength, infill material specific weight and seismic input are considered.

Hence the proposed approach allows to quickly evaluate the fragility of extend road and railway bridge networks and to identify the structural retrofit intervention priorities.

7.1 Future development

Future studies should aim to account degradation phenomena of masonry bridges.
The representation of temporal evolution of deterioration and the analysis of its causes can be a starting point. Then it will be possible to correlate the deterioration evolution with the decrease of structures mechanical properties.
In this way new structural models should be studied in order to considered also the deterioration in the seismic vulnerability.
The models produced will be useful to increase the knowledge regarding the increase of vulnerability according to deterioration progress.
Moreover, the application of the subclasses fragility curves here presented can be applied in a large scale for seismic vulnerability assessment.

REFERENCES

Beconcini, M. L., Buratti, G., Croce, P., Mengozzi, M., Orsini, P., & Luise, M. (2007). *Dynamic characterization of a five spans historical masonry arch bridge.* In Proc.of ARCH'07, 5th International Conference on Arch Bridges.

Binda, L., & Tiraboschi, C. (1999*). Flat-jack test as a slightly destructive technique for the diagnosis of brick and stone masonry structures*. Int. Journal for Restoration of Buildings and Monuments, 449, 472.

Block F., DeJong M., Ochsendorf J., (2006). *As Hangs the Flexible Line: Equilibrium of Masonry Arches*. Nexus Network Journal, 8, 2. 9-18.

Boothby T. (1995) *Collapse modes of masonry arch bridges*. Journal of Bridge Masonry Society, 9, 2. 62–69.

Boothby T.E., Roberts B.J. (2001). *Transverse behaviour of masonry arch bridges*. Structural Engineer, 79, 9. 21–26.

Brencich A., De Francesco U. (2004) *Assessment of multi-span masonry Arch bridges. Part I: A simplified approach, Part II: Examples and applications*. Journal of Bridge Engineering ASCE, 582–598.

Brencich, A., Gambarotta, L., & Sterpi, E. (2007). *Stochastic distribution of compressive strength: effects on the load carrying capacity of masonry arches*. ARCH'07: 5th International Conference on Arch Bridges.

Brencich A, Sabia D. (2008). *Experimental identification of a multi-span masonry bridge: The Tanaro Bridge*. Construction and Building Materials, 22: 2087-2099.

BRIME, (2001). *Bridge management in Europe*, Final Report D14, IV Framework Programme, Brussels.

Cavicchi A, Gambarotta L., (2005). *Collapse analysis of masonry bridges taking into account arch-fill interaction*. Engineering Structures, 27. 605–15.

Cavicchi A, Gambarotta L., (2007). *Lower bound limit analysis of masonry bridges including arch–fill interaction*. Engineering Structures, 29: 3002–3014.

Calvi G.M. (1999). *A displacement-based approach for vulnerability evaluation of classes of buildings*. Journal of Earthquake Engineering. 3, 3. 411–438.

Cattari, S. and Lagomarsino, S. PERPETUATE, Deliverable D7, *Definition of seismic safety verification procedures for historical buildings*, December, 2012.

Choi E.S., DesRoches R., Nielson B. (2004) *Seismic fragility of typical bridges in moderate seismic zones*. Engineering Structures; 26, 2. 187-199.

Clemente P., Occhiuzzi A., Raithel A., (1995). *Limit behaviour of stone arch bridges. Journal of Structural Engineering*, ASCE, 121, 7. 1045-1050.

Clemente P., (1998). *Introduction to dynamics of stone arches*. Earthquake Engineering and Structural Dynamics, John Wiley & Sons, 27: 513-522.

Clemente P., (1997). *Verifica degli archi a conci lapidei*. RT/AMB/97/10, ENEA, Roma (in Italian).

Clemente P., Buffarini G., Rinaldis D. (2010). *Application of limit analysis to stone arch bridges*. Proc. 6th Int. Conference on Arch Bridges, ARCH'010, October 11-13, 2010, Fuzhou, Fujian, China.

Cocciaglia D., Mosca L., (1998). *Capacità portante dei ponti ad arco ferroviari*, La Tecnica Professionale, November 1998, (in Italian).

Cosenza E., Manfredi G. (2000a) *Damage indices and damage measures*. Progress in Structural Engineering and Materials, 2, 1. 50-59.

Cosenza E., Manfredi G. (2000b) *Indici e misure di danno nella progettazione sismica*. GNDT-Gruppo Nazionale Difesa Terremoti, ISBN 88-88151-01-X (in Italian).

Cundal, P. A. (1971). *A computer model for simulating progressive large scale movements in blocky rock systems*. In Proceedings of the symposium of the International Society of Rock Mechanics, Vol.1, Paper II-8.

Gharib M., (2002). *The Bridge Management System DANBRO*, Proceedings of the 1st Int. Conference on Bridge Mainenance, Safety and Management of Bridges, IABMAS 2002, Barcelona,14-17 July 2002.

da Porto F., Franchetti P., Grendene M., Valluzzi M.R and Modena C. (2007). *Structural capacity of masonry arch bridges to horizontal loads*, Proc., 6th Int. Conference on Arch Bridges, ARCH'07, September 12-14, 2007, Madeira, Portugal.

de Felice G., Carbone I., Clemente P. (2006) *Assessment of multi-span masonry bridges under in-plane seismic actions*. Proc. 8th National Conference on Earthquake Engineering, 8NCEE, San Francisco, April 18-22, Paper n° 1267.

de Felice, G. (2009). *Assessment of the load-carrying capacity of multi-span masonry arch bridges using fibre beam elements*. Engineering Structures, 31, 1634-1647.

De Luca A., Giordano A., Mele E., (2004). *A simplified procedure for assessing the seismic capacity of masonry arches*, Engineering Structures, 26. 1915-1929.

De Lorenzis L., DeJong M. and Oschendorf J. (2007). *Failure of masonry arches under impulse base motion*. Earthquake and Structural Dynamics, 6:2119–2136.

Dìaz J., Romera L., Hernandez S. (2012) *A case study on the influence of mechanical properties on the collapse load of stone arch bridges*. WIT Transactions on the Built Environment; 109: 267-277.

Drucker, D. C. (1954). *Coulomb friction, plasticity and limit loads*. Journal of Applied Mechanics, 21, 1. 71-74.

Eurocode 8 - Part 1-1 (2005), *Design provisions for earthquake resistance of structures*. Part 1-1:General rules – Seismic actions and general requirements for structures. ENV 1998-1, CEN: Brussels, 2005.

Eurocode 8- Part 3 (2005), *Design of structures for earthquake resistance*. Part 3: Assessment andretrofitting of buildings. ENV 1998-3, CEN: Brussels, 2005.

Dutta A., Mander J.B. (1998) *Seismic fragility analysis of highway bridges*. INCEDE-MCEER Center-to-Center Workshop on Earthquake Engineering Frontiers in Transportation Systems, Tokyo, Japan, June.

Fajfar P. (1999) *Capacity spectrum method based on inelastic spectra*. Earthquake Engineering and Structural Dynamics 28,9. 979-993.

Fajfar, P. (2000). *A nonlinear analysis method for performance-based seismic design*. Earthq Spectra , 16, 3. 573-92.

Fanning, P. F., & Boothby, T. E. (2001). *Three-dimensional modelling and full-scale testing of stone arch bridges*. Computers and Structures, 79:2645-2662.

FEMA 356 (2000). "*Prestandard and commentary for the seismic rehabilitation of buildings*". ATC: Washington.

FEMA 440 (2005). "*Improvement of nonlinear static seismic analysis procedures*". ATC: Washington.

FICHE UIC Code 778-4 2nd edition, April 2011 "Defects in tailway bridges and procedures for maintenance".

FICHE UIC Code 778 3 2r,à edition, April 2011 "Recommendation fot the inspection, assessment and maintenance of masonry arch bridges".

Gilbert M. and Melbourne C. (1994). Rigid-block of masonry structures. The Structure Engineer, 72, 21. 356-361.

Gilbert M. (1998). *On the analysis of multi-ring brickwork arch bridges*. Proc. 2nd Int. Conference on Arch Bridges, Arch Bridges, October 6-9, 1998, Venice, Italy.
Gilbert M. (2001). *RING: 2-D rigid-block analysis program for masonry arch bridges*, Proc, 3rd Int. Conference on Arch Bridges, ARCH'01, September 19-21, 2001, Paris, France.
Gilbert M. (2007). *Limit analysis applied to masonry arch bridges: state-of-the-art and recent developments*, Proc. 6th Int. Conference on Arch Bridges, ARCH'07, September 12-14, 2007, Madeira, Portugal.
Gilbert, M., Nguyen, D., & Smith, C. C. (2007). *Computational limit analysis of soil-arch interaction in masonry arch bridges*. ARCH'07: 5th International Arch Bridges Conference, 633-640.
Hawk, H. and Small, E.P. (1998). *The BRIDGIT bridge management system*, Structural Engineering International, IABSE, **8**: 309-14.
Harvey, W. J., Maunder, E. A., & Ramsay, A. C. (2007). *The influence of spandrel wall construction on arch bridge behaviour*. ARCH'07: 5th International Arch Bridges Conference.
Hughes, T. G., & Blackler, M. J. (1997). *A review of the UK masonry arch assessment methods*. Proceeding of the Institution of Civil Engineers, 122, 305-315.
Hughes, T. G., & Pritchard, R. (1998). *In situ measurement of dead and live load stressesin a masonry arch*. Engineering Structures, 20, 5-13.
Heyman J. (1966). *The stone skeleton*. International Journal of Solids and Structures, 2. 249-279.
Heyman J. (1972). *Coulomb's Memoirs on Statics*, Cambridge: Cambridge University Press.
Heyman J. (1982). *The Masonry Arch*, Ellis Horwood Ltd.
HAZUS 99 (2001) *Direct Physical Damage to Lifelines-Transportation Systems*.
Hughes T.G., Blackler M.J. (1995). *A review of the UK masonry assessment methods*. Proceedings of the Institution of Civil Engineers: Structures and Buildings, 110, 4. 373–382.
Hwang H., Jernigan J.B., Lin Y.W. (2000). *Evaluation of Seismic Damage to Memphis Bridges and Highway Systems*. Journal of Bridge Engineering; 5 (4): 322-330.
Italian Ministry of Infrastructure, 2008. *Technical standards for construction*, NTC '08, (in Italian).

Italian State Railways, (1907). *Modalità da adottarsi per la compilazione dei progetti dei manufatti*, Torino, Italy, (in Italian).

Italian State Railways, (1924). *Ponti in muratura: norme disegni schematici e dati relativi ai ponti eseguiti, esempi*, (in Italian).

Italian State Railways, (2013). Istruzioni 44C, Visite di controllo ai ponti alle gallerie e alle altre opere d'arte dell'infrastruttura ferroviaria (in Italian).

Islami, K., Betti, R., Zampieri P., *Structural assessment outcomes from the demolition of an arch bridge with cluster modal analysis*. International Bridge Conference. June 2-6, 2013, in Pittsburgh, Pennsylvania.

Junzhe W., Heath A., Walker P. (2013) *Transverse behaviour of masonry arch bridge – Investigation of spandrel wall failure*. Proceedings of 7th International Conference on Arch Bridges – Maintenance, Assessment and Repair, 2-4 October 2013, Trogir-Split, Croatia.

Karim K.R., Yamazaki F. (2001). *Effect of earthquake ground motions on fragility curves of highway bridge piers based on numerical simulations*. Earthquake Engineering and Structural Dynamics; 30: 1839-1856.

Karim K.R., Yamazaki F. (2003). *A simplified method of constructing fragility curves for highway bridges*. Earthquake Engineering and Structural Dynamics; 32(10): 1603-1626.

Kooharian, A. (1952). *Limit analysis of voussoir (segmental) and concrete arches*. Journal American Concrete Institute, 24, 317-328.

Lemos, J. V. (2007). *Discrete element modelling of masonry structures*. International Journal of Architectural Heritage, 190-213.

LimitState, L. (2011). LimitState: RING Manual - Version 3.0.

Livesley, R. K. (1978). *Limit analysis of structures formed from rigid blocks*. Int. J. for Numerical Methods in Engineering, 12, 1853-1871

Lourenço P.B. (1994). *Analysis of masonry structures with interface elements: theory and applications*. Report 03-21-22-0-01, Delft University of Technology, Delft, Netherlands.

Melbourne C., Wang J. (2007). *A new masonry arch assessment strategy* (SMART), Proc. 5th Int. Conference on Arch Bridges ARCH'07, September 12-14, 2007, Madeira, Portugal.

Melbourne, C., Wang, J., Gilbert, M., & Smith, C. (2009). *Review of assessment methods for masonry arch highway bridges*. CSS Masonry Arch Research Project Final Draft Report.

Midas FEA v2.9.6 (2009). *Nonlinear and detail FE Analysis System for Civil Structures*. Midas Information Technology Co. Ltd.

Modena, C., Tecchio, G., Pellegrino, C., da Porto, F., Donà, M., Zampieri, P., Zanini, M.A. (2014), *Typical deficiencies and strategies for retrofitting rc and masonry arch bridges in seismic areas*, Structure and Infrastructure Engineering. (in press).

Ordinance of the Presidency of the Council of Ministers 3431 (May, 2005). Initial elements on the general criteria for classifying national seismic zones and technical standards for construction. Official Gazette of the Italian Republic (in Italian).

Oliveira D., Lourenco P.B., Lemos C. (2010. *Geometric issues and ultimate load capacity of masonry arch bridges from the nortwest Iberian Peninsula*. Engineering Structures; 32, 12. 3955-3965.

Oliveira, D. V., Maruccio, C., & Lourenço, P. B. (2007). *Numerical modelling of a load test on a masonry arch bridge*. ARCH'07: 5th International Conference on Arch Bridges, 577-584.

Orbàn, Z. (2004). *Assessment, reliability and maintenance of masonry arch railway bridges in Europe*. In: Proc. of ARCH'04: 4th Iinternational Confference on Arch Bridges.

Orbán, Z., & Gutermann, M. (2009). *Assessment of masonry arch railway bridges using non-destructive in-situ testing methods*. Engineering Structures, 31, 2287-2298.

Park Y.-J., Ang A. H.-S. (1985). *Mechanistic seismic damage model for reinforced concrete*. Journal of Structural Engineering, 111(4):722-739.

Pelà L., Aprile A., Benedetti, A., (2009). Seismic assessment of masonry arch *bridges*. Engineering Structures, 31, 8. 1777-1778.

Pelà L., Aprile A., Benedetti, A., (2013). *Comparison of seismic assessment procedures for masonry arch bridges*. Construction and Building Materials, 38: 381-394.

Pellegrino, C., Zanini, M., Zampieri P., Modena C., (2013). *Il ruolo del livello di conoscenza nella verifica sismica di tipologie ricorrenti di ponti in c.a. e in muratura*. Proceedings of the 15th Italian Conference on Earthquake Engineering-ANIDIS , June 30- 2July 4 2013, Padova, (In Italian).

Pellegrino C., Zanini M.A., Zampieri, P., Modena C (2013*). L'utilizzo delle indagini in situ e in laboratorio per la valutazione della vulnerabilità sismica dei ponti esistenti*. Progettazione Sismica. 4, 3. 67-81

Resemini S. And Lagomarsino S., (2004). *Sulla vulnerabilità sismica di ponti ad arco in muratura*, Proc. 11th Italian Conference on Earthquake Engineering-ANIDIS, L'ingegneria sismica in Italia, 25-29 January 2004, Genova, Italy.

Rota M., Pecker A., Bolognini D., Pinho R. (2005). *A methodology for seismic vulnerability of masonry arch bridge walls*. Journal of Earthquake Engineering. 9, 2. 331–353.

SB-ICA (2007). *Guideline for Inspection and Condition Assessment of Railway Bridges*. Prepared by Sustainable Bridges - a project within EU FP6. (Available from http://www.sustainablebridges.net).

Sejourne P. (1916). Grandes Voutes Tome 1-VI. Imprimerie Vve Tardy, Bourges.

Selby R.G. and Vecchio, F.J (1993).*Three-dimensional constitutive relations for reinforced concrete*. Tech. Rep. 93-02, Univ. Toronto, Dept. Civil Eng., Toronto, Canada.

Schlegel, R., & Will, J. (2007). *Sensitivity analysis and parameter identification on historical masonry arch bridges*. ARCH'07: 5th International Conference on Arch Bridges, 507-514.

Shinozuka M., Feng M.Q., Kim H.K., Kim S.H. (2000). *Non linear static procedure for fragility curves development*. Journal of Engineering Mechanics-Asce; 126, 12. 1287-1295.

Sinopoli, A., Corradi, M., & Foce, F. (1998). *Lower and upper bound theorems for masonry arches as rigid system with unilateral contacts*. Arch Bridges, 99-108.

Tecchio G., Zampieri P., da Porto F., Modena C., Prota A. and Manfredi, G. (2012). Simplified assessment of railway masonry bridges seismic capacity. Proc. 15th World Conference on Earthquake Engineering (WCEE), September 24-28, Lisbon, Portugal.

Tecchio, G., da Porto, F., Zampieri, P., Modena, C., Bettio, C. (2012). *Static and seismic retrofit of masonry arch bridges*: case studies. 6th International Conference on Bridge Maintenance and Safety (IABMAS 2012), July 8-12, Stresa, Lake Maggiore, Italy.

Thompson P.D., Small E.P., Johnson M. and Marshall A.R.,(1998). *The Pontis bridge management system, Structural Engineering International*, IABSE, **8**: 303-8.

Towler, K. D., & Sawko, F. (1982). *Limit state behaviour of brickwork arches*. Proceeding 6th Internaional Brick Masonry Conference.

Uang C.M., Bertero V.V. (1990). *Evaluation of seismic energy in structures. Earthquake Engineering and Structural Dynamics*. 19: 77-90.

University of Padova, (2006). I.Br.I.D. *Italian Bridge Interactive Database Project*. [Online] Available from: http://ibrid.dic.unipd.it.

Vecchio F.J. and M.P. Collins (1986). *The modified compression field theory for reinforced concrete elements subjected to shear*. ACI Journal 83, 22. 219-231.

Wang, J., & Melbourne, C. (2007). *Finite element analyses of soil-structure interaction in masonry arch bridges*. ARCH'07: 5th International Arch Bridges Conference.

Zampieri, P., Tecchio, G., da Porto, F., Modena C.. *Assessment and retrofit of masonry arch bridges*. International Conference on Rehabilitation and Restoration of Structures 2013. February 13-16, 2013 Indian Institute of Technology Madras.

Zampieri, P., Tecchio, G., da Porto F., Fuser S., Modena C., (2013). *Analisi limite per la valutazione della capacità sismica trasversale di ponti multi-campata in muratura con pile snelle*. Proceedings of the 15th Italian Conference on Earthquake Engineering-ANIDIS , June 30-2 July 4 2013, Padova, (In Italian).

Zampieri, P., Tecchio, G., da Porto F., Modena C., (2013). *Limit analysis of transverse seismic capacity of multi-span masonry arch bridges*. Bulletin of Earthquake Engineering. (Tentatively accept)

Zucchini, A., & Lourenço, P. (2004). *A coupled homogenisation - damage model for masonry cracking.* Computers and Structures, 82, 917-929.